

THE UNIAXIAL MECHANICAL RESPONSE OF MULTI-RIDGE ICE

**VOLUME I
SUMMARY REPORT**

J. F. DORRIS

J. S. AUSTIN

**TECHNICAL
PROGRESS
REPORT**

**BRC 45-85
OCTOBER 1985**

SHELL DEVELOPMENT COMPANY

A DIVISION OF SHELL OIL COMPANY

**BELLAIRE RESEARCH CENTER
HOUSTON, TEXAS**



PROPERTY OF SHELL DEVELOPMENT COMPANY.
The information contained herein is considered confidential
by SHELL DEVELOPMENT COMPANY.
Exportation of this document is subject to license under
the Export Administration Act of 1969.

THE UNIAXIAL MECHANICAL RESPONSE OF MULTI-RIDGE ICE

VOLUME I
SUMMARY REPORT

BY

J. F. DORRIS AND J. S. AUSTIN

TECHNICAL PROGRESS REPORT

BRC 45-85
OCTOBER 1985

Project No. 327-27802.34
Mechanical Properties of Sea Ice

SHARED - Under the Research Agreement between SIRM,
and Shell Oil Company dated January 1, 1960,
as amended.

Reviewed by: E.G. Ward
E.N. Earle
Participant: C.A. Gutierrez
Released by: J.H. Lybarger
Reference: Based on work through December 1983.

TABLE OF CONTENTS

Page

Volume I

Abstract.....	ix
Introduction.....	1
Mechanical Properties and Statistical Summary.....	4
Comparison with CRREL's Results.....	6
Temperature and Strain Rate Effects on the Mechanical Properties.....	22
Linear Regression Models Based on Total Dissipated Energy.....	28
Linear Regression Models Based on Energy Dissipated at Peak Strength.....	32
Idealized Stress-Strain Response.....	51
Energy Components.....	52
Stress-Energy Pairs.....	54
A Parameter for Characterizing the Stress-Strain Response of Multi-Year Ridge Ice.....	63
"Average" Stress-Strain Curves.....	66
Physical Properties.....	83
Summary.....	103
Recommendations for Future Work.....	105
References.....	107

Volume II

Appendix A - Procedure for Smoothing MPSI Stress-Strain Curves.....	A-1
---------------------------------------------------------------------	-----

Volume III

Appendix B - Cubic Splines for Force-Time Histories.....	B-1
----------------------------------------------------------	-----

Volume IV

Appendix C - Stress-Strain Curves.....	C-1
----------------------------------------	-----

LIST OF ILLUSTRATIONS

Figure Number		Page
	Volume I	
1	Maximum stress as a function of strain at maximum stress for $T = -5^{\circ}\text{C}$	33
2	Maximum stress as a function of strain at maximum stress for $T = -20^{\circ}\text{C}$	34
3	Maximum stress as a function of stress at 4.5% strain for $T = -5^{\circ}\text{C}$	35
4	Maximum stress as a function of stress at 4.5% strain for $T = -20^{\circ}\text{C}$	36
5	Maximum stress as a function of the initial tangent modulus for $T = -5^{\circ}\text{C}$	37
6	Maximum stress as a function of the initial tangent modulus for $T = -20^{\circ}\text{C}$	38
7	Maximum stress as a function of the total energy for $T = -5^{\circ}\text{C}$	39
8	Maximum stress as a function of the total energy for $T = -20^{\circ}\text{C}$	40
9	Stress at 4.5% strain as a function of the total energy for $T = -5^{\circ}\text{C}$	41
10	Stress at 4.5% strain as a function of the total energy for $T = -20^{\circ}\text{C}$	42
11	Maximum stress as a function of the energy dissipated at maximum stress for $T = -5^{\circ}\text{C}$	44
12	Maximum stress as a function of the energy dissipated at maximum stress for $T = -20^{\circ}\text{C}$	45
13	Strain at maximum stress as a function of the energy dissipated at maximum stress for $T = -5^{\circ}\text{C}$	47
14	Strain at maximum stress as a function of the energy dissipated at maximum stress for $T = -20^{\circ}\text{C}$	48
15	Strain at maximum stress as a function of the energy dissipated at maximum stress for $\dot{\epsilon} = 10^{-5}/\text{sec}$	49
16	Strain at maximum stress as a function of the energy dissipated at maximum stress for $\dot{\epsilon} = 10^{-3}/\text{sec}$	50

Figure Number		Page
17	Schematic diagram of idealized material models.....	53
18	Schematic representation of flow energy and crushing energy...	55
19	Maximum stress as a function of the crushing energy for $T = -5^{\circ}\text{C}$	57
20	Maximum stress as a function of the crushing energy for $T = -20^{\circ}\text{C}$	58
21	Stress at 4.5% strain as a function of the flow energy for $T = -5^{\circ}\text{C}$	61
22	Stress at 4.5% strain as a function of the flow energy for $T = -20^{\circ}\text{C}$	62
23	$(\sigma_M - \sigma_R)/\sigma_R$ as a function of I_C/I_F for $T = -5^{\circ}\text{C}$	64
24	$(\sigma_M - \sigma_R)/\sigma_R$ as a function of I_C/I_F for $T = -20^{\circ}\text{C}$	65
25	Variation of the mechanical response of multi-year ridge ice for $\dot{\epsilon} = 10^{-5}/\text{sec}$ and $T = -5^{\circ}\text{C}$	67
26	Variation of the mechanical response of multi-year ridge ice for $\dot{\epsilon} = 10^{-5}/\text{sec}$ and $T = -20^{\circ}\text{C}$	68
27	Variation of the mechanical response of multi-year ridge ice for $\dot{\epsilon} = 10^{-3}/\text{sec}$ and $T = -5^{\circ}\text{C}$	69
28	Variation of the mechanical response of multi-year ridge ice for $\dot{\epsilon} = 10^{-3}/\text{sec}$ and $T = -20^{\circ}\text{C}$	70
29	Point by point "average" stress-strain curve of multi- year ridge ice for $\dot{\epsilon} = 10^{-5}/\text{sec}$ and $\dot{\epsilon} = 10^{-3}/\text{sec}$ at $T = -5^{\circ}\text{C}$	71
30	Point by point "average" stress-strain curve of multi- year ridge ice for $\dot{\epsilon} = 10^{-5}/\text{sec}$ and $\dot{\epsilon} = 10^{-3}/\text{sec}$ at $T = -20^{\circ}\text{C}$	72
31	Least squares "average" stress-strain curve of multi-year ridge ice for $\dot{\epsilon} = 10^{-5}/\text{sec}$ and $\dot{\epsilon} = 10^{-3}$ at $T = -5^{\circ}\text{C}$	80
32	Least squares "average" stress-strain curve of multi-year ridge ice for $\dot{\epsilon} = 10^{-5}/\text{sec}$ and $\dot{\epsilon} = 10^{-3}/\text{sec}$ at $T = -20^{\circ}\text{C}$	81
33	Maximum stress as a function of porosity for $\dot{\epsilon} = 10^{-5}/\text{sec}$ and $T = -5^{\circ}\text{C}$	95

Figure Number		Page
34	Maximum stress as a function of porosity for $\dot{\epsilon} = 10^{-5}/\text{sec}$ and $T = -20^{\circ}\text{C}$	96
35	Maximum stress as a function of porosity for $\dot{\epsilon} = 10^{-3}/\text{sec}$ and $T = -5^{\circ}\text{C}$	97
36	Maximum stress as a function of porosity for $\dot{\epsilon} = 10^{-3}/\text{sec}$ and $T = -20^{\circ}\text{C}$	98
37	Initial tangent modulus as a function of porosity for $\dot{\epsilon} = 10^{-5}/\text{sec}$ and $T = -5^{\circ}\text{C}$	99
38	Initial tangent modulus as a function of porosity for $\dot{\epsilon} = 10^{-5}/\text{sec}$ and $T = -20^{\circ}\text{C}$	100
39	Initial tangent modulus as a function of porosity for $\dot{\epsilon} = 10^{-3}/\text{sec}$ and $T = -5^{\circ}\text{C}$	101
40	Initial tangent modulus as a function of porosity for $\dot{\epsilon} = 10^{-3}/\text{sec}$ and $T = -20^{\circ}\text{C}$	102

Volume II

A-1	Typical spline fit to experimental data.....	A-3
A-2	Enlarged view near the origin of the strain measured by the extensometer and the two DCDTs for a $\dot{\epsilon} = 10^{-5}/\text{sec}$ test.....	A-5
A-3	Enlarged view near the origin of the strain measured by the extensometer and the two DCDTs for a $\dot{\epsilon} = 10^{-3}/\text{sec}$ test.....	A-6
A-4	Measured strain and force histories for a $\dot{\epsilon} = 10^{-5}/\text{sec}$ test.....	A-7
A-5	Measured strain and force histories for a $\dot{\epsilon} = 10^{-3}/\text{sec}$ test.....	A-8
A-6	Measured force histories for a $\dot{\epsilon} = 10^{-5}/\text{sec}$ and $\dot{\epsilon} = 10^{-3}/\text{sec}$ test on the same coordinate axes.....	A-9
A-7	Enlarged view near the origin of the force history for a $\dot{\epsilon} = 10^{-5}/\text{sec}$ test.....	A-11
A-8	Enlarged view near the origin of the strain history for a $\dot{\epsilon} = 10^{-5}/\text{sec}$ test.....	A-12
A-9	Enlarged view near the origin of the force history for a $\dot{\epsilon} = 10^{-3}/\text{sec}$ test.....	A-13
A-10	Enlarged view near the origin of the strain history for a $\dot{\epsilon} = 10^{-3}/\text{sec}$ test.....	A-14

Figure Number		Page
A-11	Primary smoothing and tangent at the inflection point for a $\dot{\epsilon} = 10^{-5}/\text{sec}$ test.....	A-16
A-12	Primary smoothing and tangent at the inflection point for a $\dot{\epsilon} = 10^{-3}/\text{sec}$ test.....	A-17
A-13	Schematic diagram of the location of the additional spline with respect to the secondary smoothing.....	A-19
A-14	Smooth curve obtained for a $\dot{\epsilon} = 10^{-5}/\text{sec}$ test using one additional knot to supplement the secondary smoothing.....	A-21
A-15	Enlarged view of Figure A-14 near the origin.....	A-22
A-16	Schematic diagram of the location of the two additional knots with respect to the secondary smoothing.....	A-23
A-17	Smooth curve obtained for a $\dot{\epsilon} = 10^{-3}/\text{sec}$ test using two additional knots to supplement the secondary smoothing.....	A-25
A-18	Enlarged view of Figure A-17 near the origin.....	A-26
A-19	Measured force history of a $\dot{\epsilon} = 10^{-3}/\text{sec}$ test with a premature failure.....	A-27
A-20	Measured strain history of a $\dot{\epsilon} = 10^{-3}/\text{sec}$ test with a premature failure.....	A-28
A-21	Schematic diagram of the procedure to smooth tests with a premature failure.....	A-30
A-22	Initial smoothing and the construction of the tangent to the inflection point for a test with a premature failure.....	A-31
A-23	Final smoothing for a test with a premature failure.....	A-32
A-24	Final stress-strain curve for a $10^{-5}/\text{sec}$ test.....	A-37
A-25	Final stress-strain curve for a $10^{-3}/\text{sec}$ test.....	A-38
A-26	Final stress-strain curve for a test with a premature failure.....	A-39

LIST OF TABLES

Table Number		Page
	Volume I	
1	Identifying Labels for Each Test Condition.....	5
2	Description of Mechanical Properties.....	5
3	Mechanical Properties for Samples Tested at $\dot{\epsilon} = 10^{-5}/\text{sec}$ and $T = -5^{\circ}\text{C}$	7
4	Mechanical Properties for Samples Tested at $\dot{\epsilon} = 10^{-5}/\text{sec}$ and $T = -20^{\circ}\text{C}$	10
5	Mechanical Properties for Samples Tested at $\dot{\epsilon} = 10^{-3}/\text{sec}$ and $T = -5^{\circ}\text{C}$	12
6	Mechanical Properties for Samples Tested at $\dot{\epsilon} = 10^{-3}/\text{sec}$ and $T = -20^{\circ}\text{C}$	15
7	Statistical Summary of Mechanical Properties for $\dot{\epsilon} = 10^{-5}/\text{sec}$ and $T = -5^{\circ}\text{C}$	17
8	Statistical Summary of Mechanical Properties for $\dot{\epsilon} = 10^{-5}/\text{sec}$ and $T = -20^{\circ}\text{C}$	18
9	Statistical Summary of Mechanical Properties for $\dot{\epsilon} = 10^{-3}/\text{sec}$ and $T = -5^{\circ}\text{C}$	19
10	Statistical Summary of Mechanical Properties for $\dot{\epsilon} = 10^{-3}/\text{sec}$ and $T = -20^{\circ}\text{C}$	20
11	Comparison of Mean Values of Selected Mechanical Properties. Numbers Indicate the Mean Values Reported Here Normalized by the Mean Values Reported in Reference 1.....	21
12	Pairwise t-Tests for the Two Levels of Constant Strain Rate...	24
13	Pairwise t-Tests for the Two Levels of Constant Temperature...	26
14	Summary of Mean Values for σ_M	29
15	Summary of Mean Values for ϵ_M	29
16	Summary of Mean Values for σ_R	30
17	Summary of Mean Values for E_T	30
18	Summary of Mean Values for I_T	31
19	Linear Regression Models Based on Total Dissipated Energy.....	31

Table Number		Page
20	Linear Regression Models Based on Energy Dissipated at Maximum Stress.....	46
21	Summary of Mean Values for I_p	46
22	Summary of Mean Values for I_F	56
23	Summary of Mean Values for I_C	56
24	Linear Regression Models Based on Crushing Energy and Flow Energy.....	60
25	Summary of Mean Values for I_C/I_F	60
26	Summary of Normalized "Errors" for $\dot{\epsilon} = 10^{-5}/\text{Sec}$ and $T = -5^\circ\text{C}$	73
27	Summary of Normalized "Errors" for $\dot{\epsilon} = 10^{-5}/\text{Sec}$ and $T = -20^\circ\text{C}$	76
28	Summary of Normalized "Errors" for $\dot{\epsilon} = 10^{-3}/\text{sec}$ and $T = -5^\circ\text{C}$	77
29	Summary of Normalized "Errors" for $\dot{\epsilon} = 10^{-3}/\text{sec}$ and $T = -20^\circ\text{C}$	79
30	Comparison of Residual Error for the Two Averaging Techniques.....	82
31	Structural Classification Schemes for Multi-Year Pressure Ridge Ice Samples According to Cox et al. ¹	82
32	Strength, Structure, and Porosity of Selected Ridge Ice Samples Tested at $\dot{\epsilon} = 10^{-5}/\text{Sec}$ and $T = -5^\circ\text{C}$ from Cox et al. ¹	85
33	Strength, Structure, and Porosity of Selected Ridge Ice Samples Tested at $\dot{\epsilon} = 10^{-3}/\text{Sec}$ and $T = -5^\circ\text{C}$ from Cox et al. ¹	86
34	Physical Properties for Samples Tested at $\dot{\epsilon} = 10^{-5}/\text{Sec}$ and $T = -5^\circ\text{C}$ from Cox et al. ¹	87
35	Physical Properties for Samples Tested at $\dot{\epsilon} = 10^{-5}/\text{Sec}$ and $T = -20^\circ\text{C}$ from Cox et al. ¹	89
36	Physical Properties for Samples Tested at $\dot{\epsilon} = 10^{-3}/\text{Sec}$ and $T = -5^\circ\text{C}$ from Cox et al. ¹	90
37	Physical Properties for Samples Tested at $\dot{\epsilon} = 10^{-3}/\text{Sec}$ and $T = -20^\circ\text{C}$ from Cox et al. ¹	92

Table Number		Page
38	Statistical Summary of Physical Properties of Ice Samples Tested at T = -5°C.....	93
39	Statistical Summary of Physical Properties of Ice Samples Tested at T = -20°C.....	94

Volume II

A-1	Spline parameters for R5A-165/191.....	A-34
A-2	Spline parameters for R4B-299/325.....	A-35
A-3	Spline parameters for R8B-483/509.....	A-36

ABSTRACT

The mechanical properties from the uniaxial compression tests conducted in Phase I of the Mechanical Properties of Sea Ice program are summarized. The tests were conducted at temperatures of -5°C and -20°C and at strain rates of 10^{-5} and $10^{-3}/\text{sec}$. The effects of temperature and strain rate on each mechanical property are investigated. Each stress-strain curve is presented and an energy based parameter is derived to characterize the mechanical response of each curve. The effects of temperature and strain-rate on this parameter are also investigated. The physical properties of each test sample are listed, and their effect on the mechanical properties is briefly discussed.

KEY WORDS: ice mechanics, ridge, ice formed feature, mechanical property, statistical analysis, compressive strength, strain, linear, regression analysis, prediction, testing, stress, load (force), energy, temperature

TECHNICAL PROGRESS REPORT BRC 45-85

THE UNIAXIAL MECHANICAL RESPONSE OF MULTI-YEAR RIDGE ICE

BY

J. F. DORRIS AND J. S. AUSTIN

INTRODUCTION

The Mechanical Properties of Sea Ice (MPSI) is a project, consisting of several phases, to determine the mechanical properties of multi-year sea ice. The project was developed and administered by Shell Development Company. Participants sponsoring Phase I of the project (MPSI-1) included Amoco Production Company, Arco Oil and Gas Company, Chevron Oil Field Research Company, Exxon Production Research Company, Gulf Research and Development Company, Minerals Management Service of the Department of Interior, Mitsui Engineering and Shipbuilding Company, Sohio Petroleum Company, and Texaco Incorporated. The field program to collect ice samples and the experimental program for ice testing were conducted by the U.S. Army Cold Regions Research and Engineering Laboratory (CRREL) at Hanover, New Hampshire.

The experimental program in MPSI-1 was designed to accomplish three goals:

1. Measure the mechanical (i.e., 1-D compressive) properties of multi-year ridge ice,
2. Determine whether there is any significant variation in the mechanical properties within and between ridges, and
3. Develop the test techniques to be used in subsequent phases of the program.

The results presented here summarize the approximately 200 uniaxial compression tests conducted in MPSI-1. These tests have already been documented by Cox et al.¹ in a CRREL report and several excerpts have been presented as technical papers by individual CRREL authors.²⁻⁴ The CRREL report¹ describes the field program and experimental program in detail and presents the mechanical and physical properties of each test sample. The

purpose of this report is to present an analysis of the digitized test data which complements and expands upon CRREL's analyses by utilizing the entire stress-strain history of each test.

The ice samples tested were extracted with a 4 1/4 in. diameter core barrel in the spring of 1981 from ten multi-year pressure ridges located in the Beaufort Sea, northwest of Reindeer Island. The ice samples were transported to the CRREL laboratories and prepared for testing. Sample preparation included cutting each sample to length, machining the samples to test geometry, and fitting the ends with synthane endcaps. The samples were then tested under uniaxial test conditions. Mellor et al.⁵ describe the details of sample preparation and testing techniques.

The mechanical properties were measured by Cox et al.¹ at two temperatures (i.e., -5°C , -20°C) and two strain rates (i.e., $10^{-5}/\text{sec}$, $10^{-3}/\text{sec}$). These temperatures and strain rates were chosen to bracket the temperature and strain rate regimes of most interest to the engineer. To characterize the ice, physical properties (e.g., brine volume, porosity, etc.) of each sample were measured. To better define the physical properties of each ice sample, Cox and Weeks⁶ developed a method of calculating the air volume of the sample. This method permits the total porosity to be calculated by knowing both the air volume and brine volume. A statistical summary of the mechanical properties shows large scatter which is attributed to the wide variation of ice types found in multi-year ridges. Richter and Cox³ developed a classification scheme for multi-year ridge ice which offers a means of reducing the scatter by grouping tests according to ice structure. This classification scheme was applied to approximately 35 test samples in Phase I, and a forthcoming report by Richter-Menge and Cox will contain additional crystallographic analyses of MPSI-1 test samples.

Weeks⁴ investigates the statistical variation of strength within and between ridges. Based on these statistics, he concludes that there is no significant variation between cores at the same site (i.e., within the same ridge) nor is there any significant differences between ridges. However, Weeks qualifies his conclusions by pointing out that the ridges used in this study represent old, well-healed ridges whose strength characteristics are probably quite different than younger, less consolidated ridges.

Subsequent phases of the program will emphasize other types of tests to give a complete picture of the mechanical response of multi-year ridge

ice. To this end, test techniques were developed for uniaxial tension, constant load compression, and conventional triaxial tests. The conventional triaxial tests are conducted by applying the confining pressure in proportion to the axial stress. These test techniques are discussed by Mellor et al.⁵

The goal here is to describe the mechanical (i.e., uniaxial compression) response as a whole by looking at the stress-strain curves. We begin by listing the mechanical properties and describing the effects of temperature and strain rate on those properties. The mechanical properties are then integrated in such a way as to yield a quantity which characterizes a particular stress-strain curve. The variation in the mechanical response at each test condition will be illustrated, and the ability to characterize each stress-strain curve will permit a discussion of changes in mechanical response with changes in temperature and strain rate.

The stress-strain curves presented here were produced by digitizing the analog records of each test and fitting splines to the digitized data. To make the splines suitable for future constitutive modeling, certain assumptions were made about the initial conditions of the force-time record which yielded different values for the mechanical properties than those reported by Cox et al.¹ These differences are small except in one case which will be noted later. The assumptions made and procedures followed in processing the data are described in Appendix A. The spline for each force-time history is printed in Appendix B and each stress-strain curve is presented according to test condition in Appendix C.

For completeness, the physical properties measured by Cox et al.¹ will be listed here. Although the large variations in mechanical properties and mechanical response of multi-year ridge ice are related to the physical properties of each test sample, discussion will be limited because of the limited amount of crystallographic data presently available. Attempts, however, will be made to establish bounds and identify trends for the dependence between mechanical and physical properties. The pending crystallographic analysis by Richter-Menge and Cox will permit a more detailed look into the effects of physical properties.

MECHANICAL PROPERTIES AND STATISTICAL SUMMARY

The uniaxial compression test samples in MPSI-1 were taken from ten multi-year pressure ridges in the Beaufort Sea. At each ridge, two sites were selected several meters apart. At a particular site, the samples were extracted from two cores several centimeters apart. Each sample was labeled with a Ridge ID, whose nomenclature identified the ridge, core (and site), and depth of the sample. The designations R1 through R10 in the Ridge ID identify the ridge and the letters A-D identify the core. The letters A, B designate the cores at one site while the letters C, D designate the cores at the second site. The depths in centimeters from the top of the ridge to the top and bottom of the ice samples are denoted in the Ridge ID by the two numbers separated by a slash. Thus a sample designated R1A-062/089 would indicate a sample taken from Ridge 1, site 1, core A, and a depth of 62 centimeters to the top and 89 centimeters to the bottom of the sample.

The uniaxial compression tests were conducted at two temperatures (i.e., $T = -5^{\circ}\text{C}$, $T = -20^{\circ}\text{C}$) and two strain rates (i.e., $\dot{\epsilon} = 10^{-5}/\text{sec}$, $\dot{\epsilon} = 10^{-3}/\text{sec}$). The four possible combinations of temperatures and strain rates give four independent test conditions. For convenience in later discussions, the test conditions are assigned labels which are listed in Table 1. In the following data summaries, all tests are grouped according to test conditions. Each test within a test condition group is identified by the Ridge ID of the test sample.

Following the procedures discussed in Appendix A, stress-strain curves were generated for each test from which the mechanical properties were calculated. The particular mechanical properties considered in the analysis of the stress-strain curves are described in Table 2. This list includes the mechanical properties commonly used by engineers to describe the mechanical response of other materials as well as additional properties not usually calculated. The additional properties include the energy dissipated at peak strength, the total energy dissipated, "flow" energy, and "crushing" energy. The flow and crushing energy terms are obtained from a decomposition of the total energy and will be defined in the next section. For completeness, the failure modes defined by Dorris⁷ are included but will not be discussed here.

In Table 2, the most important quantities used to describe the mechanical response of multi-year ridge ice are σ_M , ϵ_M , E_T , σ_R , and I_T . The quantity, I_T , is the integral of the stress-strain curve and measures the

Table 1

IDENTIFYING LABELS FOR EACH TEST CONDITION

$\dot{\epsilon}$ \ T	-5°C	-20°C
$10^{-5}/\text{sec}$	C55	C520
$10^{-3}/\text{sec}$	C35	C320

Table 2

DESCRIPTION OF MECHANICAL PROPERTIES

Mechanical Property	Description	Units
σ_M	Maximum Stress	psi
ϵ_M	Strain at Maximum Stress	%
σ_R	Residual Stress (Stress at 4.5% Strain)	psi
ϵ_E	Strain at End of Test	%
E_T	Initial Tangent Modulus	psi $\times 10^6$
E_S	Secant Modulus $E_S = \frac{\sigma_M}{\epsilon_M}$	psi $\times 10^6$
σ_R/σ_M	Stress Ratio	---
FM	Failure Mode	---
I_P	Energy to Maximum Stress $I_P = \int_0^{\epsilon_M} \sigma(\epsilon) d\epsilon$	(in-lbf)/in ³
I_T	Energy to 4.5% Strain $I_T = \int_0^{.045} \sigma(\epsilon) d\epsilon$	(in-lbf)/in ³
I_F	Flow Energy $I_F = 1/2 \left(.09 - \frac{\sigma_R}{E_T} \right) \sigma_R$	(in-lbf)/in ³
I_C	Crushing Energy ($I_C = I_T - I_F$)	(in-lbf)/in ³
I_C/I_F	Energy Ratio	---

material's ability to store or dissipate energy. The spatial distribution of I_T in the stress-strain plane characterizes the material's response as either brittle or ductile. For multi-year ridge ice, the quantities σ_M , ϵ_M , E_T and σ_R can approximate the spatial distribution of I_T by defining the initial condition, peak value, and final value of the material response. In the following, these five quantities will be referred to collectively as primary properties.

In contrast to σ_M , ϵ_M , and E_T , the primary properties σ_R and I_T are arbitrary since their value depends on the choice of strain at which they were calculated. Each test was programmed to end at 5% strain, but the procedures followed in processing the data resulted in tests with varying lengths slightly less than 5% strain. In order to make meaningful comparisons between the properties associated with the end of the test, 4.5% strain was arbitrarily chosen to be the strain at which σ_R and I_T are calculated.

The mechanical properties are tabulated for each test according to the four test conditions in Tables 3-6. Any test in these tables having missing values indicates a test which did not reach 4.5% strain due to premature failure of the test sample. All available mechanical properties are used in the following statistical summary of properties, but only those tests which reached 4.5% strain will be used in describing the stress-strain response of multi-year ridge ice.

A statistical summary of the mechanical properties for each test condition is provided in Tables 7-10. The tables list the number of samples for each property along with the standard descriptive statistics of each sample population. A measure of kurtosis and skewness is included to give an impression of the shape of each distribution of the mechanical properties.

COMPARISON WITH CRREL'S RESULTS

The mean values of selected properties from Tables 7-10 are normalized by the corresponding mean values reported by Cox et al.¹ to provide a comparison of data sets. The ratios of mean values are listed in Table 11 and show good agreement between the data sets except for the initial tangent modulus at the low strain rate.

The discrepancy in modulus values can be attributed to different measuring techniques. The instrumentation of an ice sample provided two methods of measuring the axial displacement. One method employed two DCDTs

Table 3

MECHANICAL PROPERTIES

STRAIN RATE = (10E-5)/SEC TEMPERATURE = -5°C

Ridge ID	σ_M	ϵ_M	σ_R	ϵ_E	E_T	E_S	σ_R/σ_M	FM	I_P	I_T	I_F	I_C	I_C/I_F
R1A-062/089	425.	.344	241.	4.84	0.965	0.123	0.566	31	1.20	13.0	10.8	2.19	0.202
R1B-062/089	321.	.463	205.	4.87	0.467	0.069	0.638	31	1.18	10.4	9.2	1.22	0.133
R2A-140/165	368.	.597	236.	4.85	0.493	0.062	0.643	30	1.80	12.8	10.6	2.24	0.212
R2B-094/121	167.	.142	174.	4.88	0.201	0.117	1.042	10	0.16	7.0	7.0	0.00	0.000
R3A-106/131	333.	.461	245.	4.84	0.330	0.072	0.736	30	1.26	12.4	10.9	1.47	0.134
R3B-161/187	300.	.335	201.	4.86	0.231	0.089	0.670	13	0.76	10.2	9.0	1.24	0.139
R4A-312/338	277.	.481	189.	4.86	0.482	0.058	0.681	30	1.11	9.7	8.5	1.23	0.145
R4B-328/354	244.	.497	156.	4.77	0.211	0.049	0.641	31	0.95	8.1	7.0	1.14	0.163
R5A-165/191	606.	.229	272.	4.87	1.041	0.265	0.449	13	1.00	15.3	12.2	3.10	0.254
R5B-075/101	755.	.219	241.	4.86	0.797	0.345	0.319	30	1.15	14.6	10.8	3.79	0.351
R7A-059/085	359.	.545	252.	4.86	0.488	0.066	0.702	30	1.58	12.8	11.3	1.53	0.135
R7B-126/152	239.	.452	206.	4.86	0.327	0.053	0.864	10	0.90	9.3	9.2	0.09	0.010
R8A-133/159	238.	.335	202.	4.85	0.450	0.071	0.848	13	0.66	9.2	9.0	0.16	0.017
R8B-162/189	324.	.433	224.	4.81	0.294	0.075	0.693	30	1.11	11.4	10.0	1.41	0.141
R3C-095/122	265.	.483	201.	4.87	0.177	0.055	0.759	30	1.00	9.6	8.9	0.67	0.075
R3D-159/186	201.	.841	198.	4.50	0.268	0.024	0.986	30	1.51	8.8	8.8	0.00	0.000
R5C-039/066	376.	.435	253.	4.88	0.689	0.086	0.675	30	1.39	13.1	11.3	1.76	0.155
R5D-159/186	359.	.599	230.	4.82	0.212	0.060	0.640	30	1.68	12.3	10.2	2.07	0.203
R6C-166/193	211.	.337	221.	4.88	0.314	0.063	1.045	10	0.58	9.4	9.4	0.00	0.000
R8C-048/075	228.	.234	169.	4.88	0.500	0.097	0.741	31	0.42	8.1	7.6	0.52	0.069
R8D-236/263	329.	.254	267.	4.88	0.441	0.130	0.812	30	0.65	12.0	11.9	0.07	0.006
R1A-226/252	208.	.204	113.	4.86	1.286	0.102	0.546	31	0.34	5.7	5.1	0.62	0.122
R1A-399/425	203.	.234	127.	4.88	1.056	0.087	0.625	13	0.40	6.6	5.7	0.89	0.156
R2A-205/230	403.	.461	.	2.90	0.584	0.087	.	0	1.46
R2A-314/339	313.	.257	163.	4.85	0.432	0.121	0.522	12	0.62	8.4	7.3	1.10	0.150
R2B-408/434	339.	.607	258.	4.85	0.466	0.056	0.762	13	1.73	12.8	11.5	1.26	0.109
R2B-468/494	259.	.380	194.	4.86	0.534	0.068	0.749	31	0.83	9.6	8.7	0.91	0.104

Table 3 (Cont'd.)

Ridge ID	σ_M	ϵ_M	σ_R	ϵ_E	E_T	E_S	σ_R/σ_M	FM	I_P	I_T	I_F	I_C	I_C/I_F
R3A-220/245	248.	.342	178.	4.81	0.183	0.073	0.716	31	0.64	8.6	7.9	0.68	0.085
R3A-430/456	301.	.463	208.	4.87	1.045	0.065	0.692	31	1.20	10.6	9.3	1.26	0.135
R3B-363/389	369.	.501	243.	4.86	0.499	0.074	0.658	30	1.56	12.7	10.9	1.82	0.168
R4A-426/452	318.	.312	176.	4.86	0.661	0.102	0.554	32	0.79	9.5	7.9	1.60	0.203
R4B-391/417	293.	.277	190.	4.85	0.708	0.106	0.648	31	0.67	9.4	8.5	0.88	0.103
R4B-449/475	244.	.355	166.	4.85	0.282	0.069	0.680	13	0.69	8.3	7.4	0.88	0.118
R5A-397/423	309.	.480	225.	4.80	0.135	0.064	0.729	10	1.05	11.3	9.9	1.36	0.137
R5A-442/468	451.	.253	209.	4.86	0.624	0.178	0.462	30	0.88	11.9	9.4	2.53	0.270
R5A-504/530	319.	.493	220.	4.78	0.232	0.065	0.692	30	1.25	11.0	9.8	1.20	0.123
R5B-341/367	361.	.553	.	4.13	0.469	0.065	.	31	1.62
R5B-398/423	294.	.407	229.	4.78	0.344	0.072	0.779	13	0.95	11.3	10.2	1.07	0.105
R7A-263/289	71.	.078	59.	4.86	0.234	0.091	0.841	31	0.04	2.6	2.6	0.00	0.000
R7A-342/368	553.	.218	160.	4.83	0.542	0.254	0.289	32	0.86	9.4	7.2	2.22	0.310
R7B-241/267	226.	.448	161.	4.86	0.185	0.050	0.714	30	0.80	7.8	7.2	0.63	0.087
R8A-164/190	259.	.242	176.	4.85	0.387	0.107	0.679	10	0.50	8.4	7.9	0.52	0.066
R8A-432/458	631.	.169	199.	4.84	0.866	0.372	0.315	13	0.77	11.2	8.9	2.27	0.254
R8B-333/359	335.	.253	206.	4.86	0.936	0.132	0.615	30	0.66	10.6	9.2	1.35	0.146
R8B-515/541	338.	.416	219.	4.95	0.449	0.081	0.647	30	1.14	11.5	9.8	1.70	0.173
R3C-296/323	290.	.610	.	1.23	0.412	0.048	.	30	1.51
R3C-380/407	186.	.210	127.	4.87	0.278	0.089	0.681	10	0.31	6.0	5.7	0.31	0.055
R3D-219/246	252.	.341	186.	4.87	0.316	0.074	0.739	30	0.69	8.9	8.3	0.58	0.070
R3D-287/314	334.	.659	251.	4.88	0.328	0.051	0.752	30	1.87	12.7	11.2	1.50	0.134
R5C-219/246	290.	.487	197.	4.72	0.248	0.059	0.679	30	1.13	10.2	8.8	1.41	0.161
R5C-282/309	257.	.508	189.	4.88	0.295	0.051	0.733	31	1.08	9.3	8.4	0.86	0.101
R5D-225/252	368.	.508	235.	4.88	0.387	0.072	0.640	30	1.51	12.4	10.5	1.90	0.181
R5D-294/321	325.	.498	208.	4.88	0.461	0.065	0.640	31	1.33	11.2	9.3	1.89	0.203
R6A-562/589	219.	.479	176.	4.88	0.327	0.046	0.804	30	0.89	8.4	7.9	0.53	0.067

Table 16

SUMMARY OF MEAN VALUE FOR σ_R (PSI)

$\begin{array}{c} T \\ \hline \dot{\epsilon} \end{array}$	-5°C	-20°C
$10^{-5}/\text{sec}$	200±44 61	249±72 29
$10^{-3}/\text{sec}$	42 177±57	18 255±76

Table 17

SUMMARY OF MEAN VALUE FOR E_T (PSI × 10⁶)

$\begin{array}{c} T \\ \hline \dot{\epsilon} \end{array}$	-5°C	-20°C
$10^{-5}/\text{sec}$.509±.356 67	.690±.576 37
$10^{-3}/\text{sec}$	69 1.010±.312	41 1.135±.614

Table 18

SUMMARY OF MEAN VALUE FOR I_T (in-lbf)/in³

$\dot{\epsilon}$ \ T	-5°C	-20°C
10 ⁻⁵ /sec	10.19±2.50 61	12.70±3.21 29
10 ⁻³ /sec	42 13.74±2.82	18 22.35±3.35

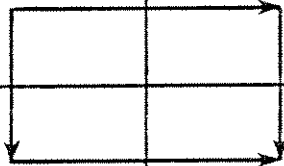


Table 19

LINEAR REGRESSION MODELS BASED ON TOTAL DISSIPATED ENERGY

Independent Variable	Dependent Variable	Test Condition	Linear Coefficient	Intercept	R ²
I_T	σ_M	C55	37.31	-62.58	.54
I_T	σ_M	C520	22.11	120.71	.47
I_T	σ_M	C35	30.70	433.61	.36
I_T	σ_M	C320	31.54	699.45	.48
I_T	σ_R	C55	16.57	31.08	.88
I_T	σ_R	C520	21.61	-25.63	.93
I_T	σ_R	C35	17.24	-59.46	.72
I_T	σ_R	C320	18.20	-151.22	.64

plotting the maximum stress as a function of the other primary mechanical properties (i.e., ϵ_M , σ_R , E_T , and I_T) in Figures 1-8. Figures 1 and 2 are of interest since they contain the loci of points for the peak value of the stress-strain curve and illustrate the large variation in the mechanical response within a particular test condition and between test conditions. Linear regression lines were calculated for each property pair at each test condition in Figures 1-8. The property pair which showed the strongest correlation (i.e., the highest R^2 value) is σ_M vs I_T . The regression lines are drawn for this pair in Figures 7 and 8 and the regression parameters are listed in Table 19. Regression models for the other property pairs had significantly lower R^2 values and for this reason they are not drawn or tabulated here.

Plots and linear regression models were also produced for all pairwise combinations of the remaining primary mechanical properties. The only property pair which showed a correlation is σ_R vs I_T . Plots for this pair together with the regression line for each test condition are shown in Figures 9 and 10. The regression parameters for this pair at each test condition are listed in Table 19.

The positive correlations for σ_M and σ_R with I_T are not surprising when one considers the general shape of the stress-strain curve for multi-year ridge ice. The interesting observation is the similarity in slopes (except possibly for σ_M vs I_T at C520) at each test condition for the two models. This suggests that the variations of σ_M with I_T and σ_R with I_T are independent of temperature and strain rate. The temperature and strain rate effects on the σ_M vs I_T and σ_R vs I_T models are accounted for by translations of the regression lines in the plane.

LINEAR REGRESSION MODELS BASED ON ENERGY DISSIPATED AT PEAK STRENGTH

Our ability to calculate ice loads would be greatly improved if a failure criteria could be formulated to predict the maximum stress. Failure or yield criteria are often formulated by appealing to energy considerations. We have already seen some correlation between the maximum stress (σ_M) and the total dissipated energy (I_T) in Figures 7 and 8. However, I_T depends on the post peak behavior of the stress-strain curve and, consequently, would not be useful in the prediction of σ_M . Instead, an energy-based failure criterion

MPSI PHASE1: UNIAXIAL COMPRESSION

TEMPERATURE = -5 DEG C

* STRAIN RATE = (10E-5)/SEC
O STRAIN RATE = (10E-3)/SEC

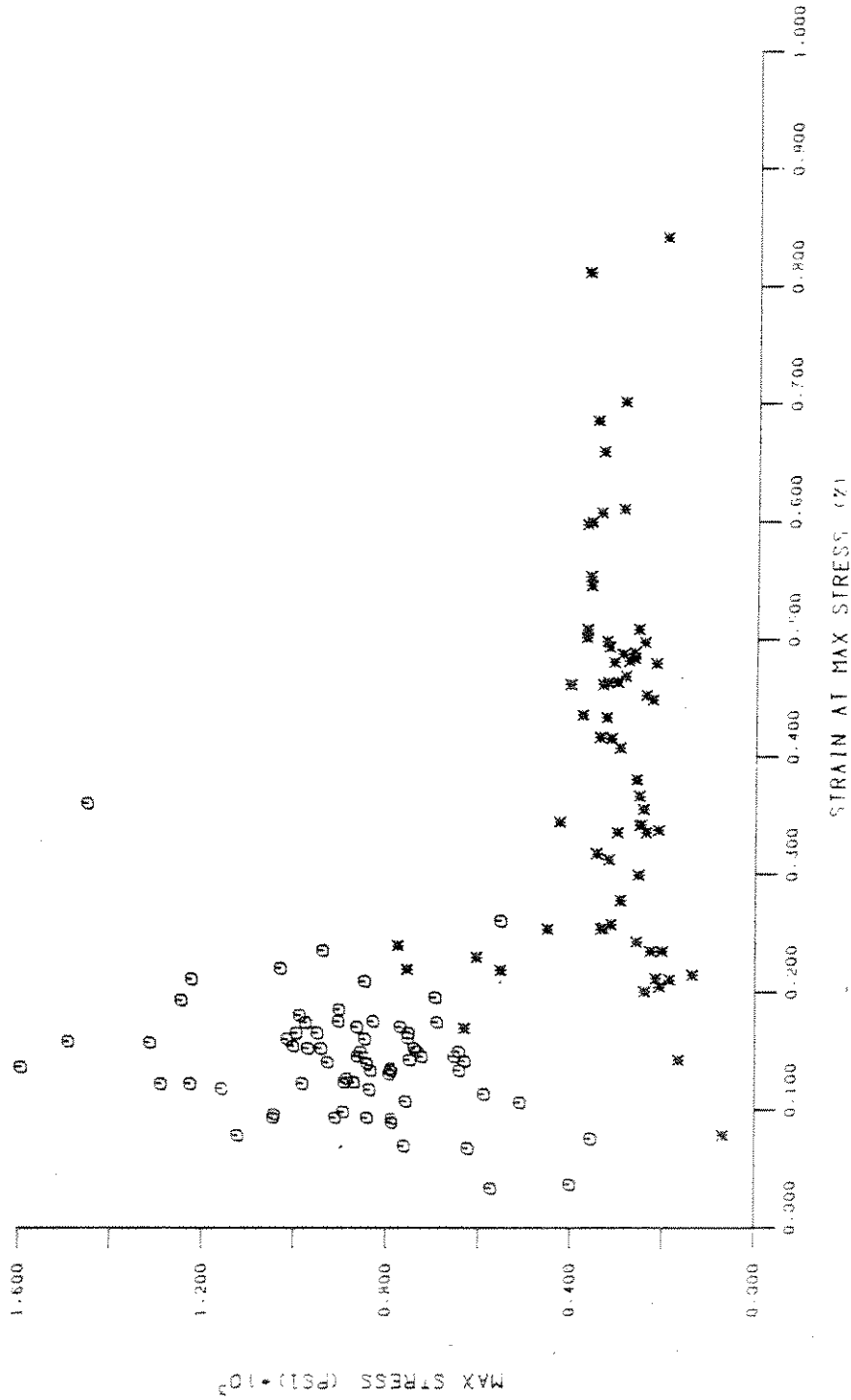


Fig. 1 - Maximum stress as a function of strain at maximum stress for
T = -5°C.

MPSI PHASE1: UNIAXIAL COMPRESSION TEMPERATURE = -20 DEG C

* STRAIN RATE = 1.0E-5/SEC
O STRAIN RATE = 1.0E-3/SEC

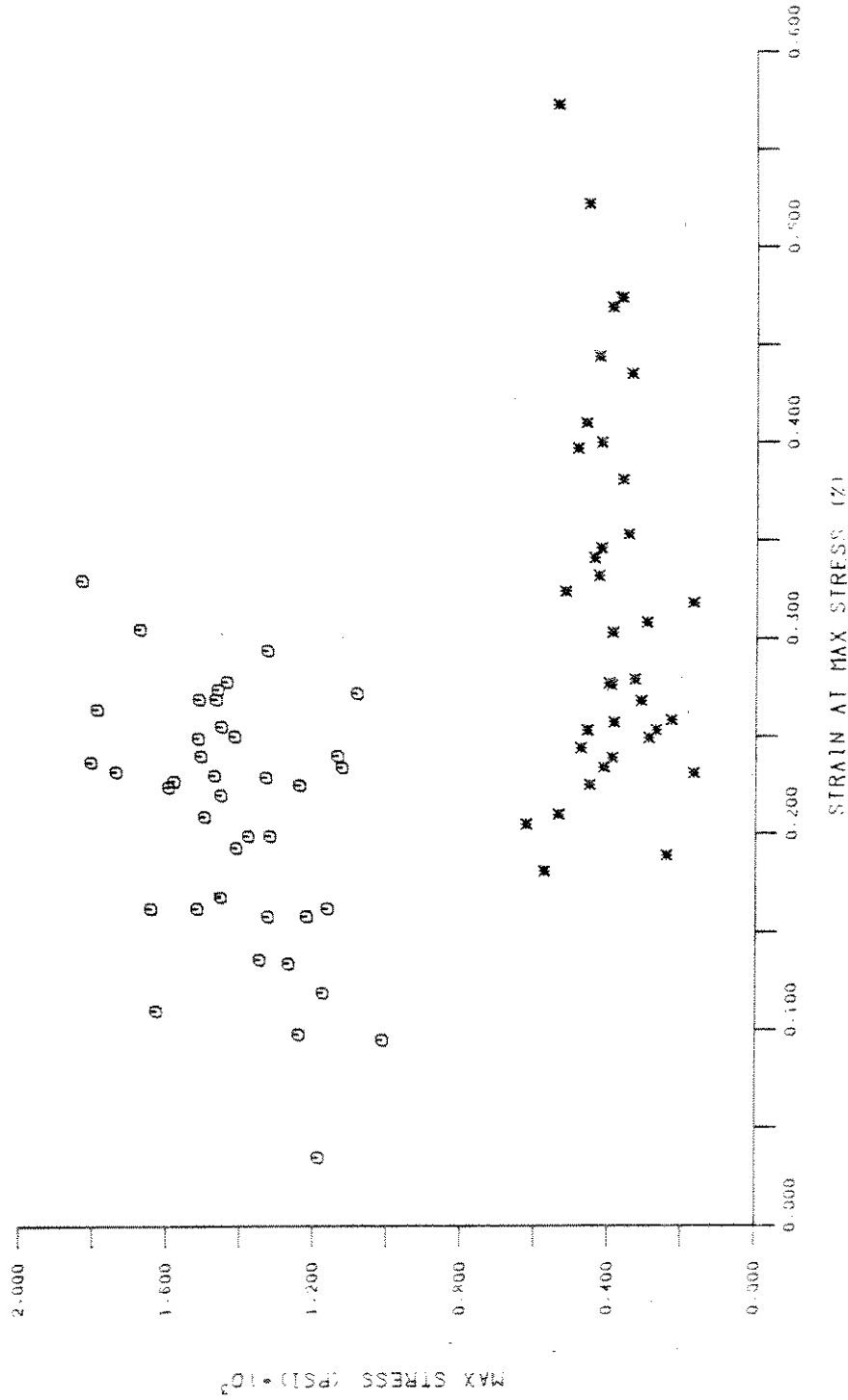


Fig. 2 - Maximum stress as a function of strain at maximum stress for
T = -20°C.

MPSI PHASE1: UNIAXIAL COMPRESSION TEMPERATURE = -5 DEG C

* STRAIN RATE = (10E-3)/SEC
O STRAIN RATE = (10E-3)/SEC

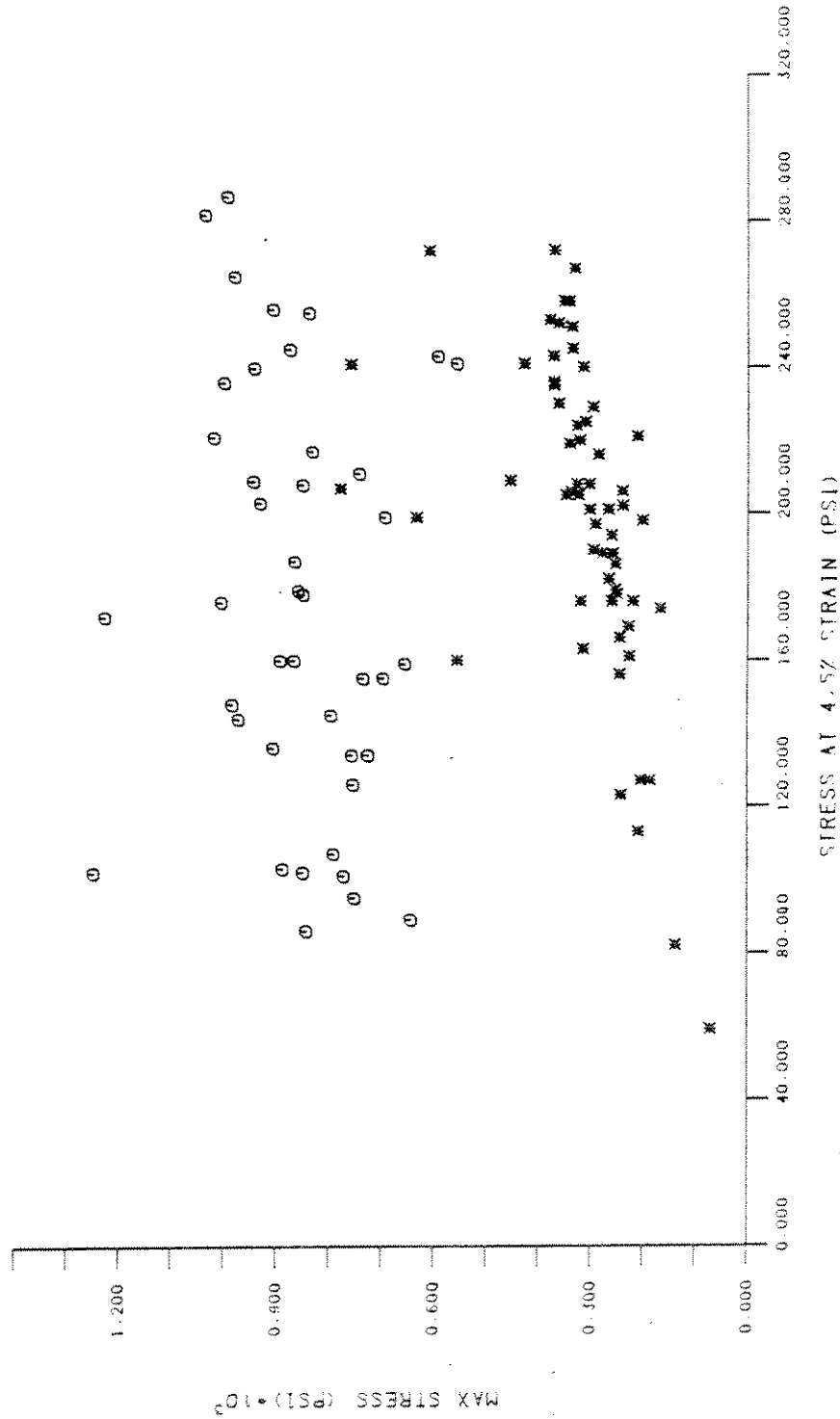


Fig. 3 - Maximum stress as a function of stress at 4.5% strain for T = -5°C.

MPSI PHASE1: UNIAXIAL COMPRESSION TEMPERATURE = -20 DEG C

* STRAIN RATE = (1.0E-5)/SEC
O STRAIN RATE = (1.0E-3)/SEC

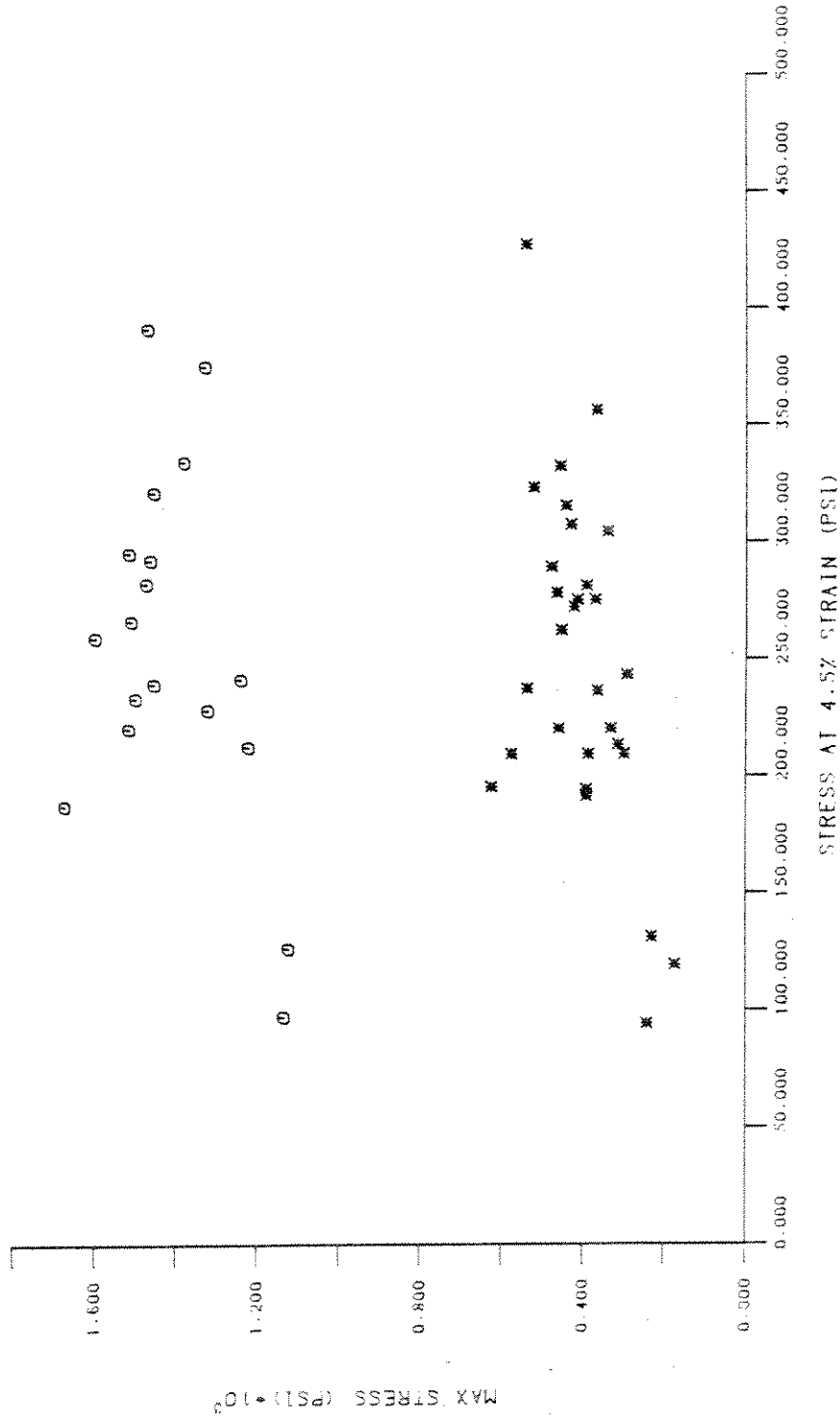


Fig. 4 - Maximum stress as a function of strain at 4.5% strain for T = -20°C.

MPSI PHASE1: UNIAXIAL COMPRESSION

TEMPERATURE = -5 DEG C

* STRAIN RATE = (10E-5)/SEC
 ○ STRAIN RATE = (10E-3)/SEC

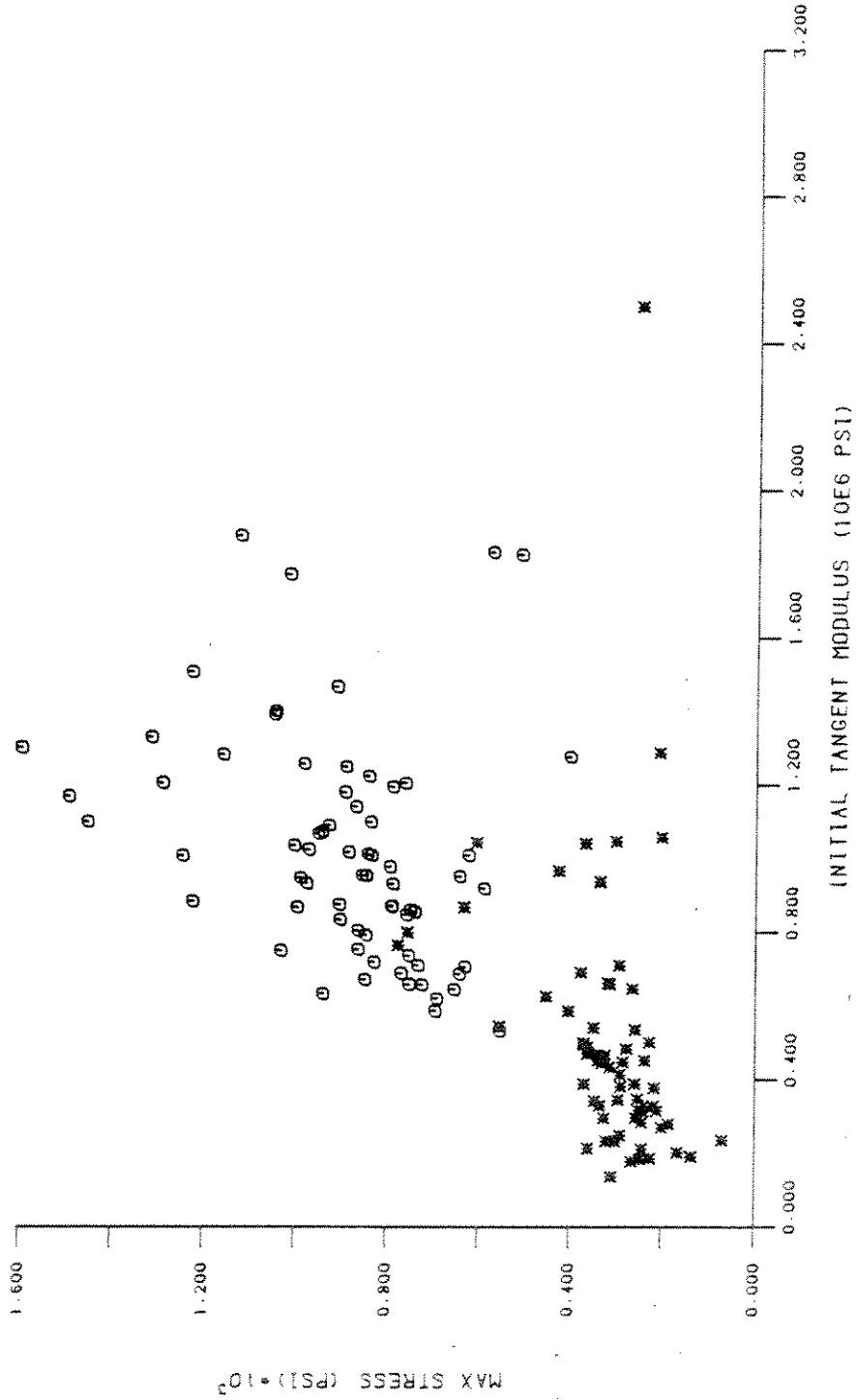


Fig. 5 - Maximum stress as a function of the initial tangent modulus for $T = -5^{\circ}\text{C}$.

MPSI PHASE1: UNIAXIAL COMPRESSION
TEMPERATURE = -20 DEG C

■ STRAIN RATE = (10E-3)/SEC
○ STRAIN RATE = (10E-3)/SEC

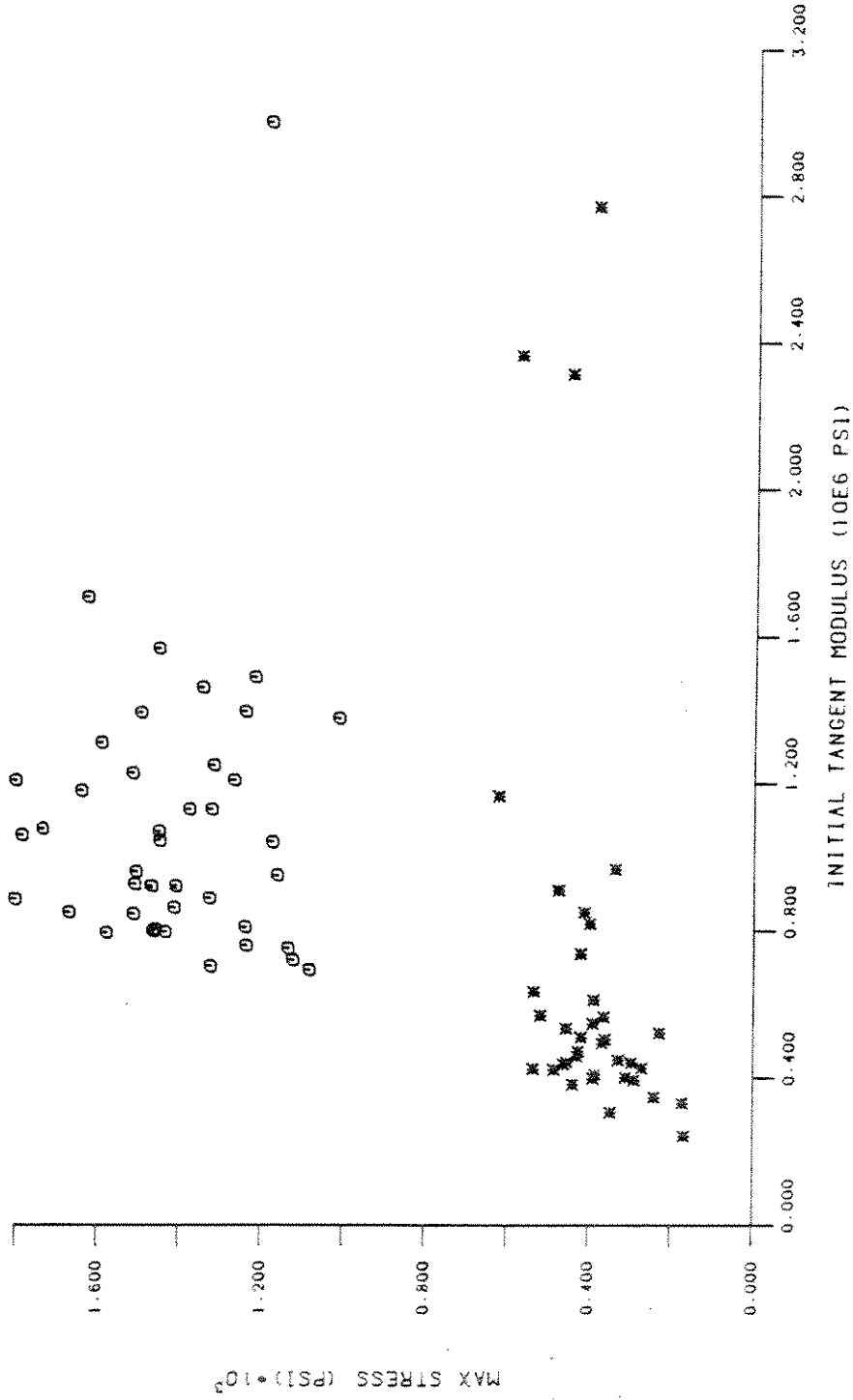


Fig. 6 - Maximum stress as a function of the initial tangent modulus for
T = -20°C.

MPSI PHASE1: UNIAXIAL COMPRESSION TEMPERATURE = -5 DEG C

* STRAIN RATE = (10E-5)/SEC
 O STRAIN RATE = (10E-3)/SEC
 --- LINEAR REGRESSION LINE STRAIN RATE = (10E-5)/SEC
 - - - LINEAR REGRESSION LINE STRAIN RATE = (10E-3)/SEC

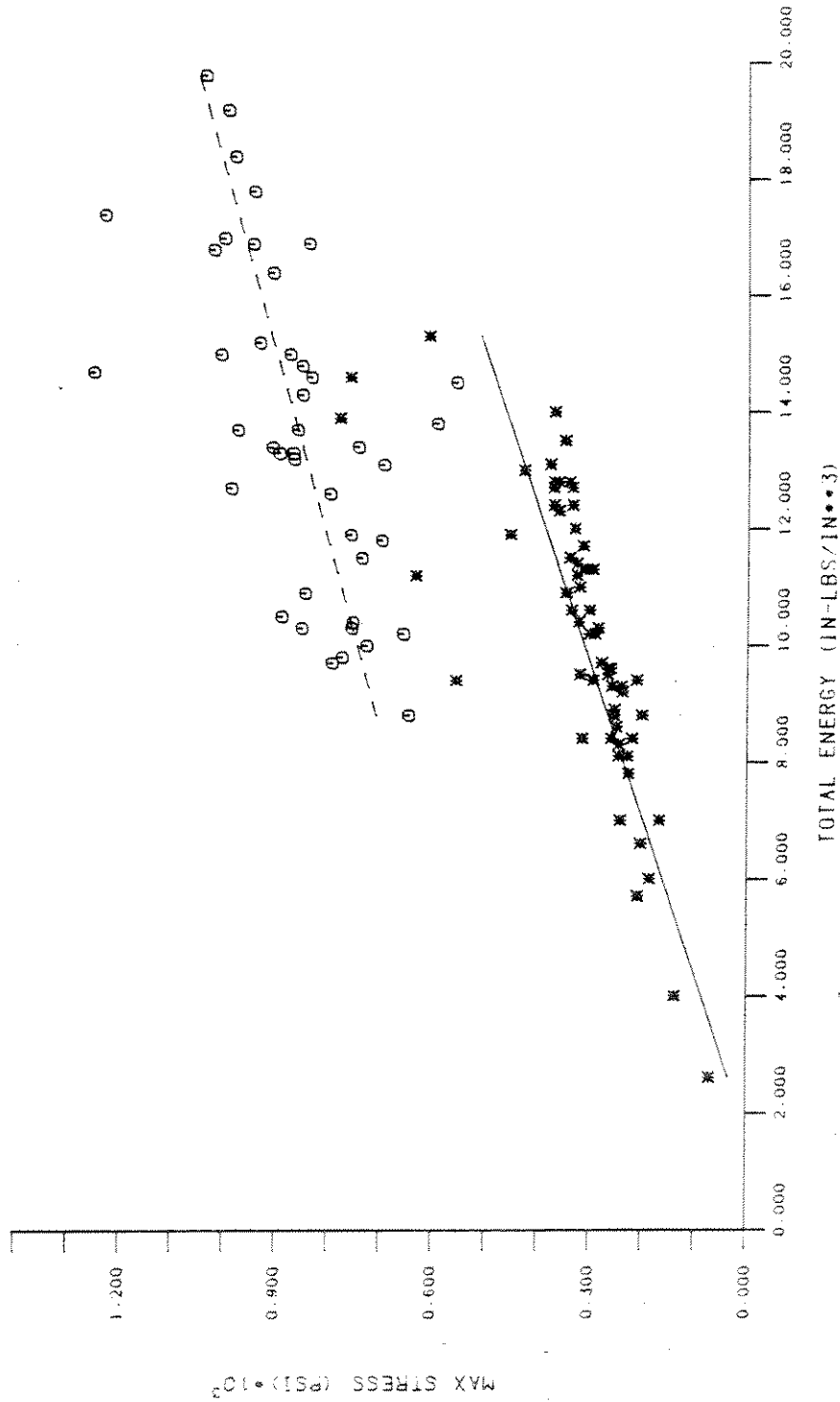


Fig. 7 - Maximum stress as a function of the total energy for T = -5°C.

MPSI PHASE1: UNIAXIAL COMPRESSION TEMPERATURE = -20 DEG C

* STRAIN RATE = (10E-5)/SEC
 O STRAIN RATE = (10E-3)/SEC
 — LINEAR REGRESSION LINE
 - - - LINEAR REGRESSION LINE

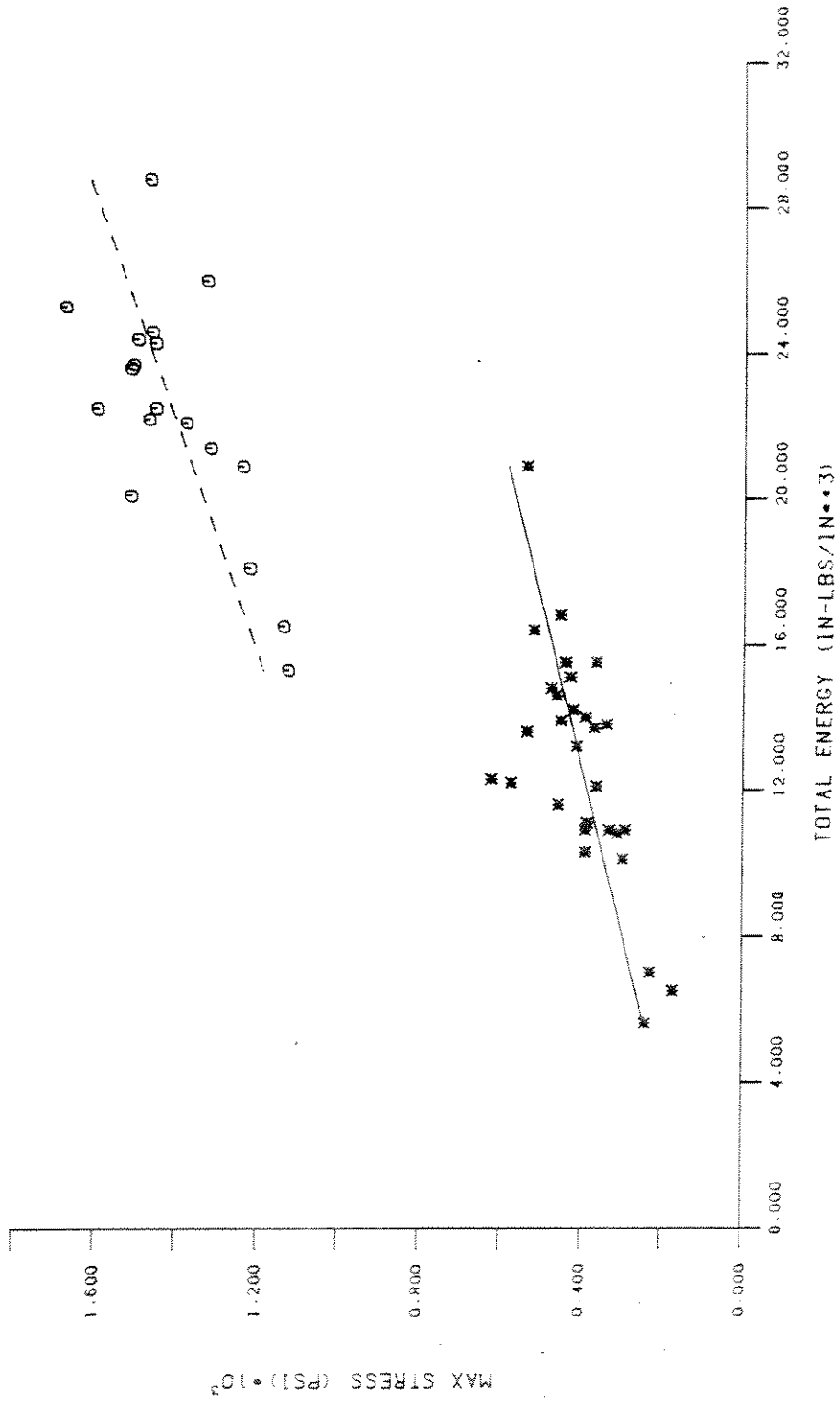


Fig. 8 - Maximum stress as a function of the total energy for T = -20°C.

MPSI PHASE1: UNIAXIAL COMPRESSION TEMPERATURE = -5 DEG C

* STRAIN RATE = (10E-3)/SEC
 O STRAIN RATE = (10E-3)/SEC
 --- LINEAR REGRESSION LINE STRAIN RATE = (10E-3)/SEC
 --- LINEAR REGRESSION LINE STRAIN RATE = (10E-3)/SEC

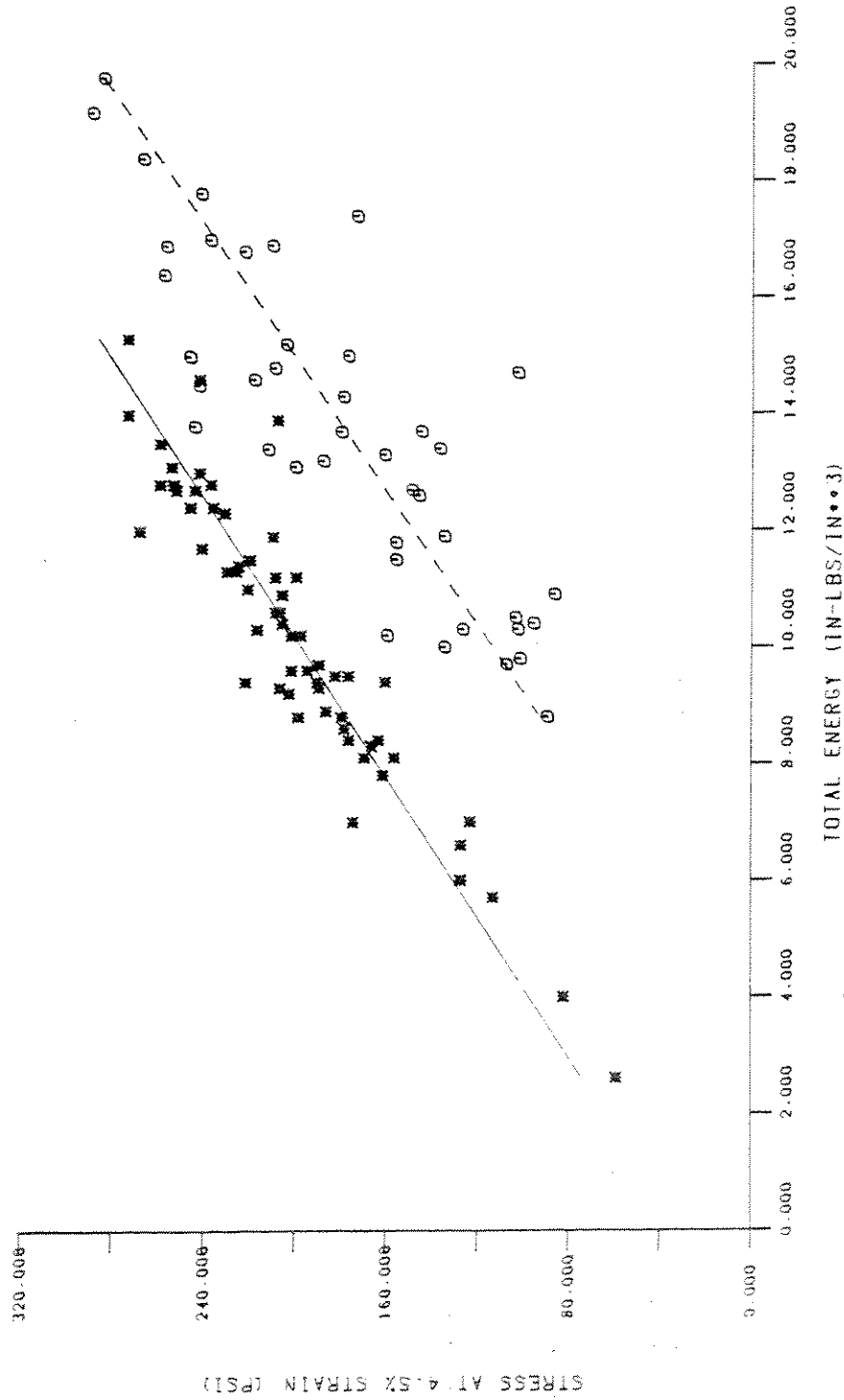


Fig. 9 - Stress at 4.5% strain as a function of the total energy for T = -5°C.

MPSI PHASE1: UNIAXIAL COMPRESSION

TEMPERATURE = -20 DEG C

* STRAIN RATE = $1.0E-5$ /SEC
 O STRAIN RATE = $1.0E-3$ /SEC
 — LINEAR REGRESSION LINE
 --- LINEAR REGRESSION LINE

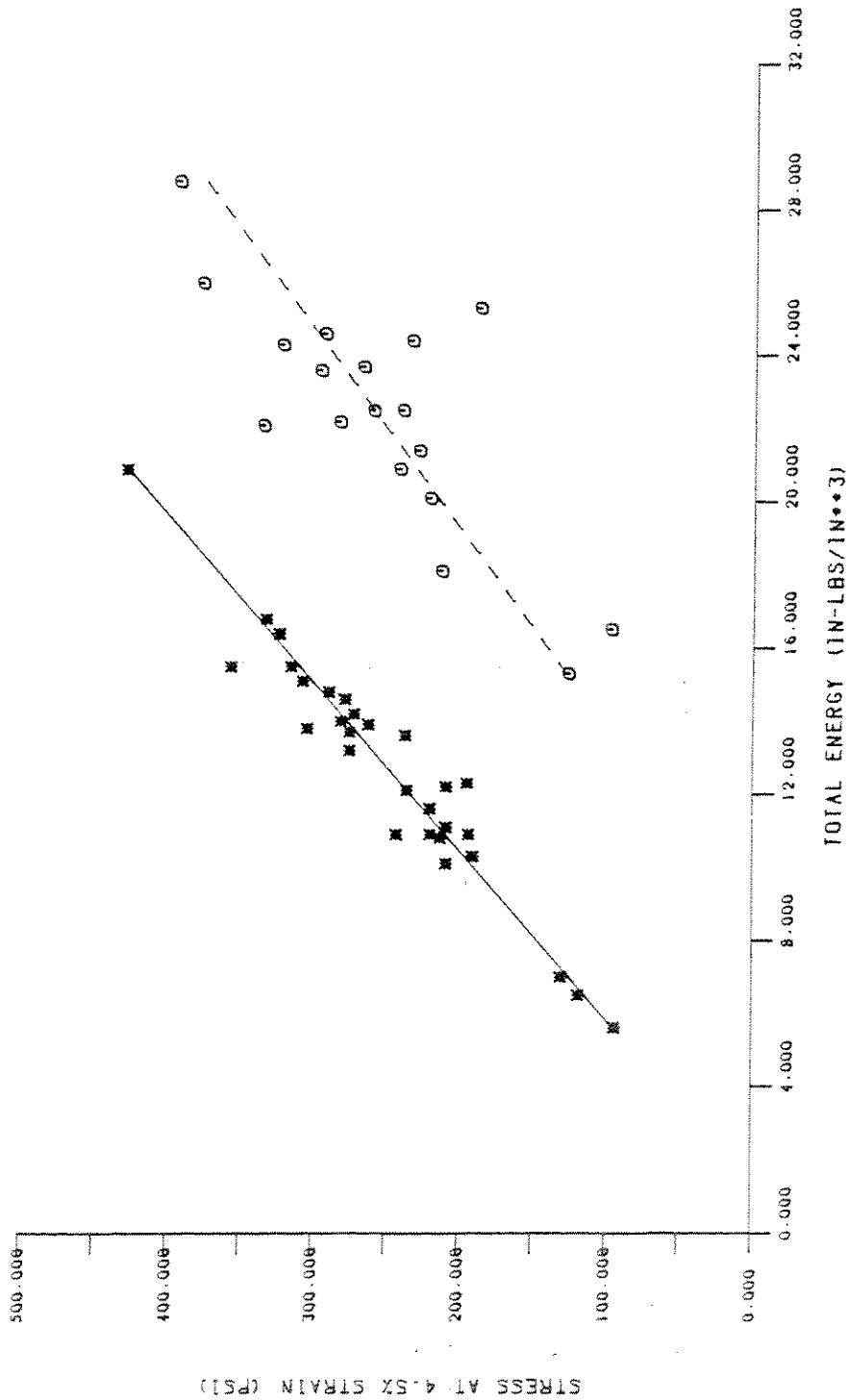


Fig. 10 - Stress at 4.5% strain as a function of the total energy for $T = -20^{\circ}\text{C}$.

for σ_M should be formulated in terms of energy dissipated up to peak strength (I_p). We investigate this possibility by plotting σ_M vs I_p in Figures 11 and 12. Regression lines are calculated for this property pair, and the regression parameters are listed in Table 20.

Comparison of the R^2 values in Table 20 shows a stronger correlation for the high strain rate test conditions (i.e., C35 and C320). The weaker correlations for the low strain rate test condition are probably a result of the flatness of the low strain rate stress-strain curve. There, the maximum stress is difficult to determine causing greater error in the calculation of I_p . Comparison of the R^2 values for σ_M in Table 20 with those in Table 19 shows a stronger correlation for the model based on I_T . In contrast to the σ_M vs I_T models, the σ_M vs I_p models show no similarity in slopes.

Failure and yield criteria have traditionally been formulated in stress space. However, some recent work in the theory of plasticity has suggested that a more natural formulation for failure criteria would be in strain space. This would be particularly true for a material such as ice which exhibits a strain-softening behavior. A stress formulation for the failure criterion of a strain-softening material would have to be double valued whereas a strain formulation would remain single-valued. Thus we seek correlations between the failure strain (i.e., strain at maximum stress), ϵ_M , and the energy dissipated at maximum stress. The ϵ_M vs I_p ordered pairs for each test condition are plotted in Figures 13 and 14. Regression lines are calculated for each test condition, and the parameters are listed in Table 20. The high R^2 values in Table 20 are to be expected since,

$$I_p = \int_0^{\epsilon_M} \sigma(\epsilon) d\epsilon = f(\epsilon_M) .$$

However, we note the similarities in slopes for the two pairs of test conditions with constant strain rate. Regression lines are recalculated by combining all data points for the two levels of constant strain rate. The combined regression lines along with the data points are shown in Figures 15 and 16, and the regression parameters are listed in Table 20. The high R^2 values for the combined data points indicate that a temperature independent model for ϵ_M vs I_p is plausible. Again we note a stronger correlation for the high strain rate than the low strain rate.

MPSI PHASE I: UNIAXIAL COMPRESSION

TEMPERATURE = -5 DEG C

* STRAIN RATE = $(1.0E-5)/\text{SEC}$
 O STRAIN RATE = $(1.0E-3)/\text{SEC}$
 — LINEAR REGRESSION LINE
 - - - LINEAR REGRESSION LINE

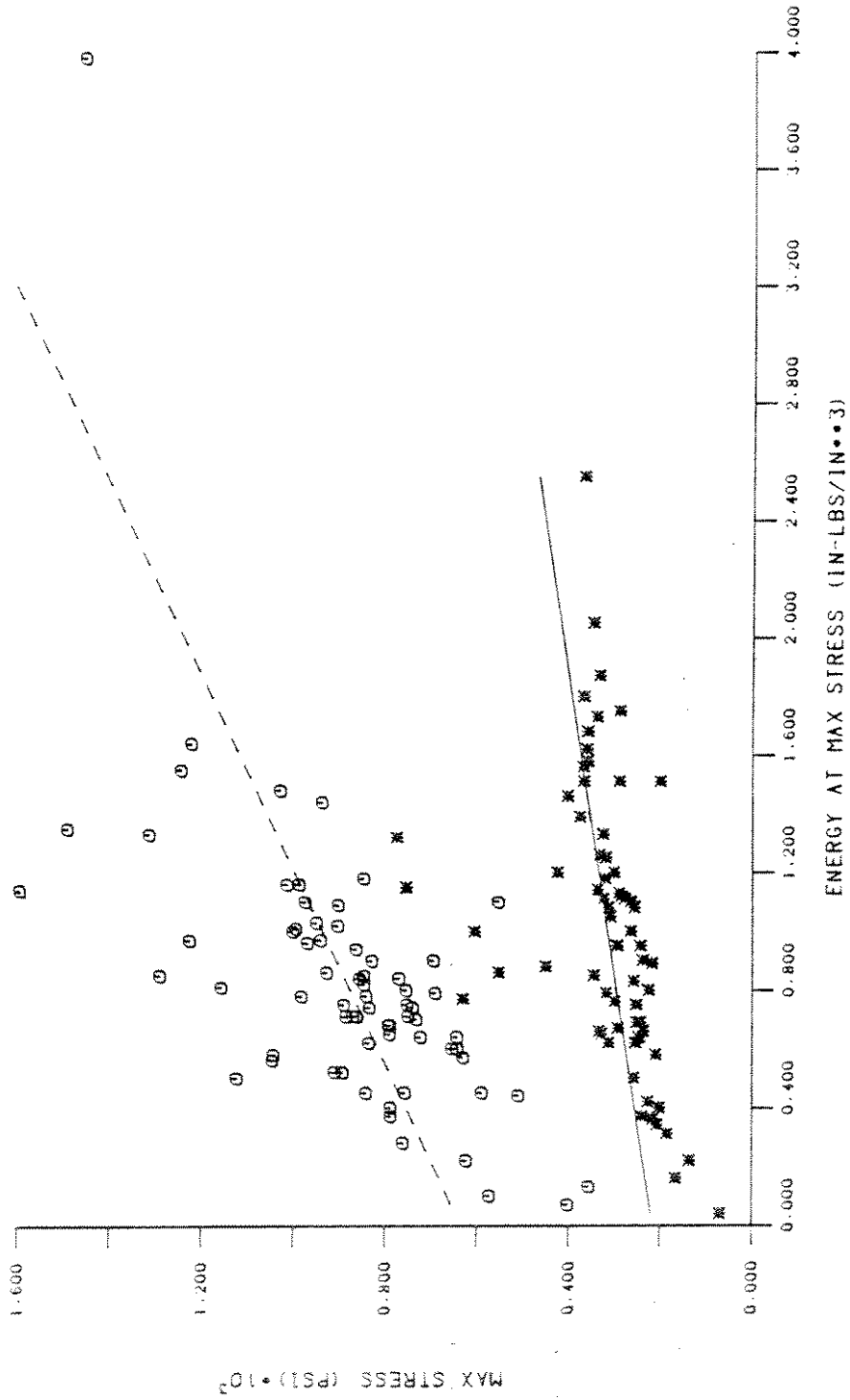


Fig. 11 - Maximum stress as a function of the energy dissipated at maximum stress for $T = -5^{\circ}\text{C}$.

MPSI PHASE1: UNIAXIAL COMPRESSION TEMPERATURE = -20 DEG C

* STRAIN RATE = (1.0E-5)/SEC
 O STRAIN RATE = (1.0E-3)/SEC
 --- LINEAR REGRESSION LINE
 --- LINEAR REGRESSION LINE
 --- LINEAR REGRESSION LINE
 --- LINEAR REGRESSION LINE

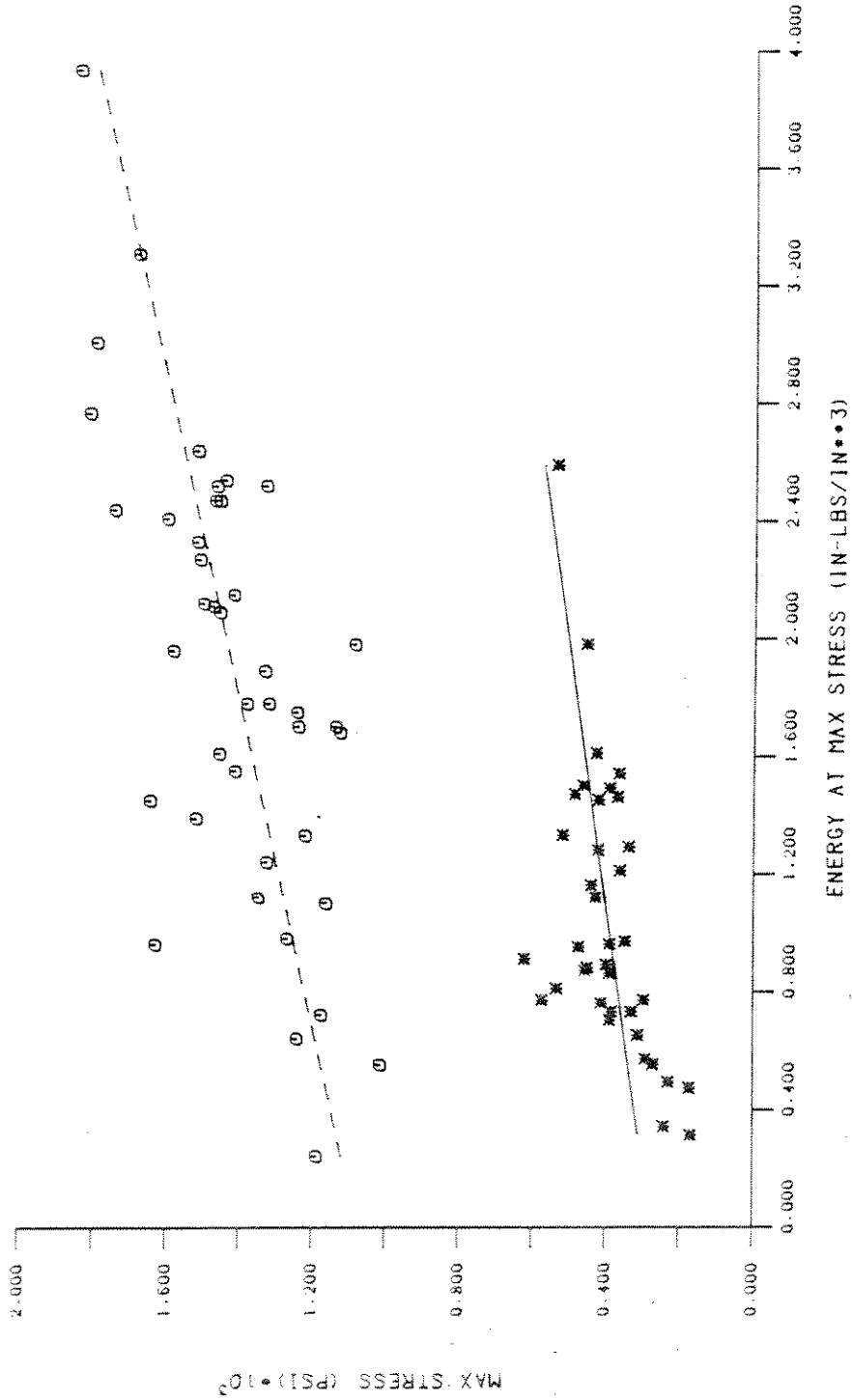


Fig. 12 - Maximum stress as a function of the energy dissipated at maximum stress for T = -20°C.

Table 20

LINEAR REGRESSION MODELS BASED ON ENERGY DISSIPATED AT MAXIMUM STRESS

Independent Variable	Dependent Variable	Test Condition	Linear Coefficient	Intercept	R ²
I _P	σ _M	C55	98.05	216.68	.15
I _P	σ _M	C520	114.25	274.68	.28
I _P	σ _M	C35	292.70	635.26	.40
I _P	σ _M	C320	178.16	1075.01	.46
I _P	ε _M	C55	0.285	0.112	.75
I _P	ε _M	C520	0.187	0.128	.79
I _P	ε _M	C35	0.086	0.071	.76
I _P	ε _M	C320	0.077	0.063	.87
I _P	ε _M	C55, C520	0.250	0.117	.67
I _P	ε _M	C35, C320	0.074	0.077	.85

Table 21

SUMMARY OF MEAN VALUES FOR I_P (in-lbf)/in³

$\begin{array}{c} T \\ \epsilon \end{array}$	-5°C	-20°C
10 ⁻⁵ /sec	1.014±.488 67	1.038±.473 37
10 ⁻³ /sec	69 .836±.507	41 1.883±.770

MPSI PHASE1: UNIAXIAL COMPRESSION

TEMPERATURE = -5 DEG C

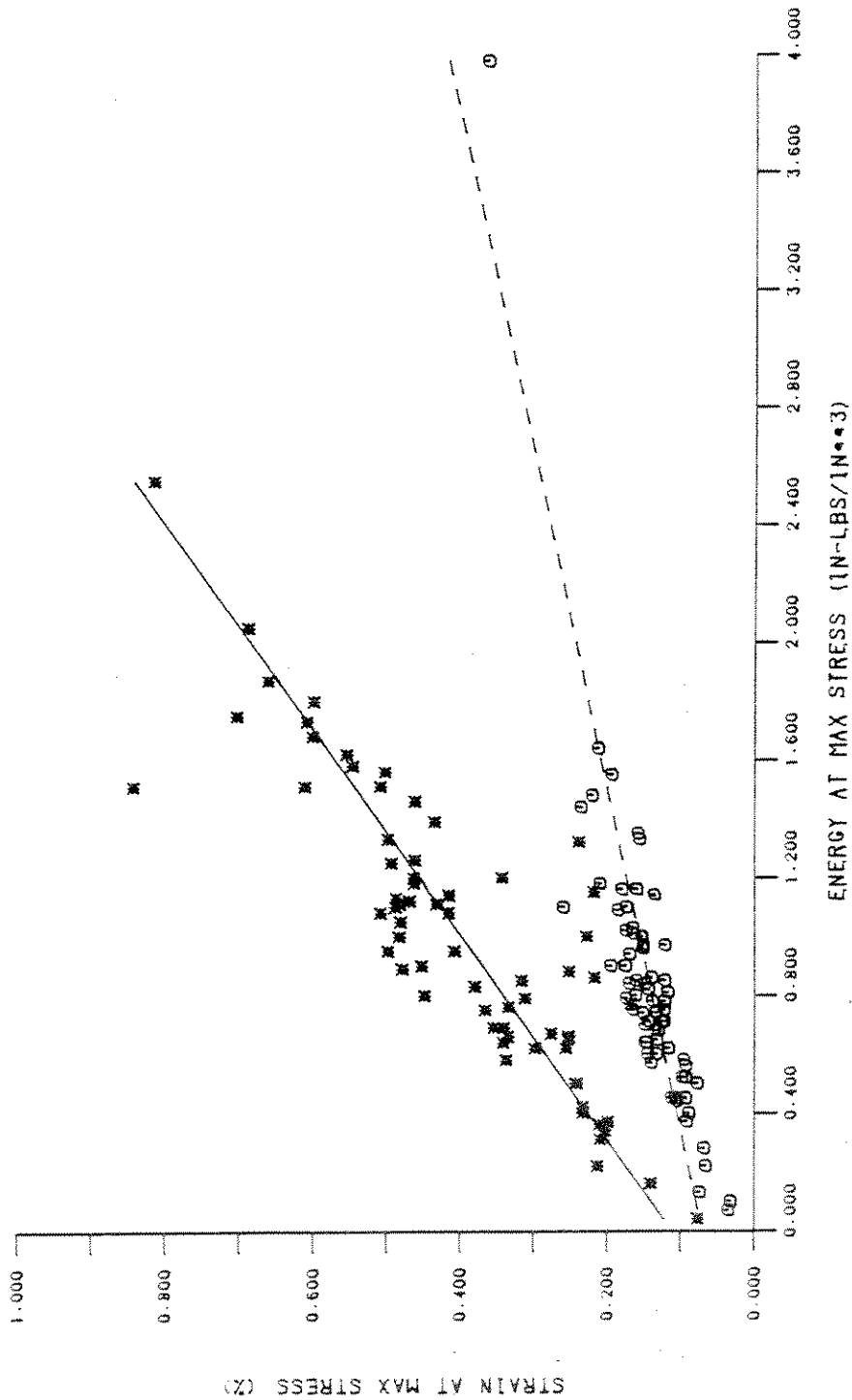


Fig. 13 - Strain at maximum stress as a function of the energy dissipated at maximum stress for $T = -5^{\circ}\text{C}$.

MPSI PHASE1: UNIAXIAL COMPRESSION
TEMPERATURE = -20 DEG C

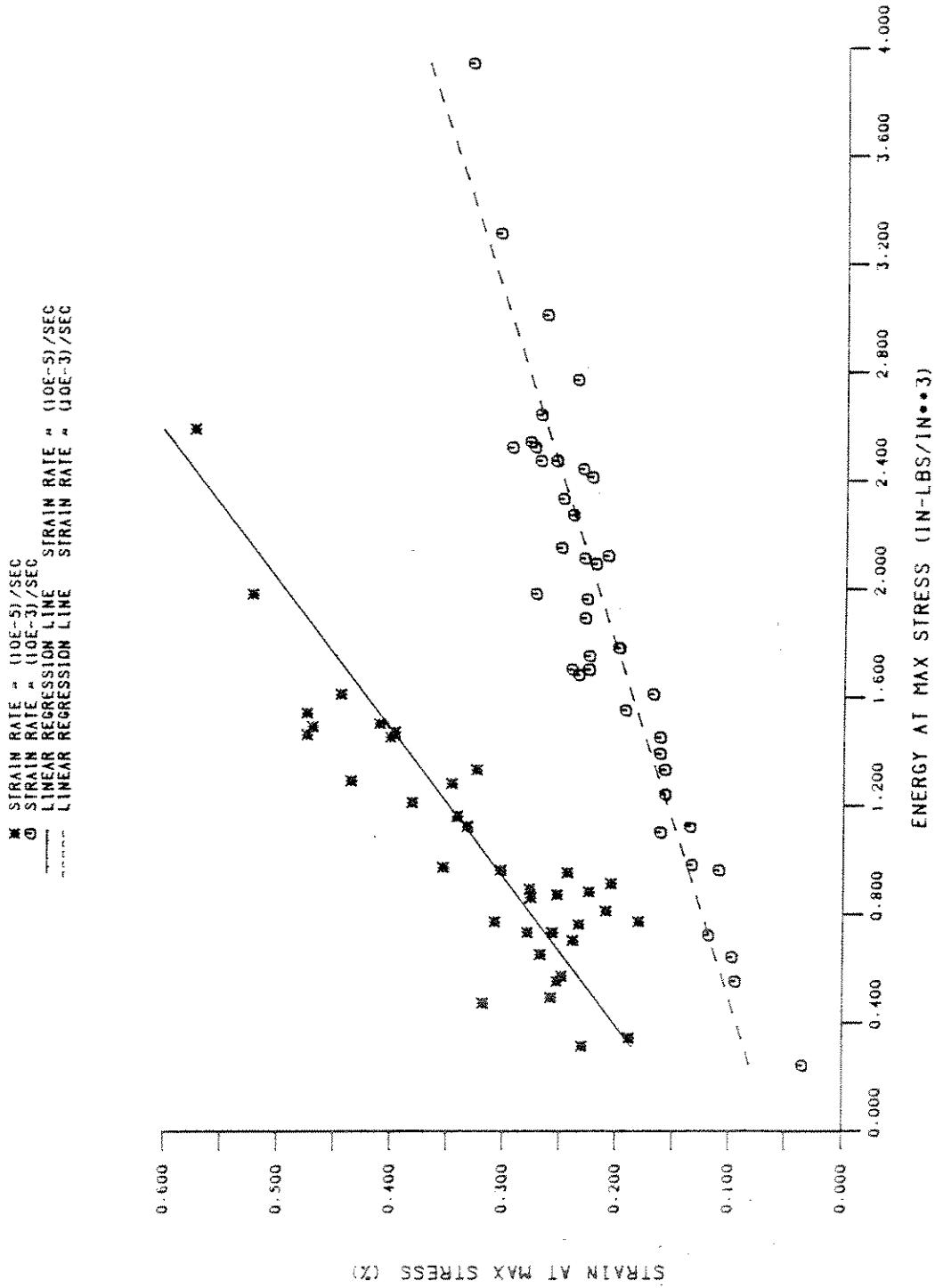


Fig. 14 - Strain at maximum stress as a function of the energy dissipated at maximum stress for T = -20°C.

MPSI PHASE1: UNIAXIAL COMPRESSION STRAIN RATE = $(10E-5)/\text{SEC}$

* TEMPERATURE = -5 DEG C
 O TEMPERATURE = -20 DEG C
 — COMMON LINEAR REGRESSION LINE

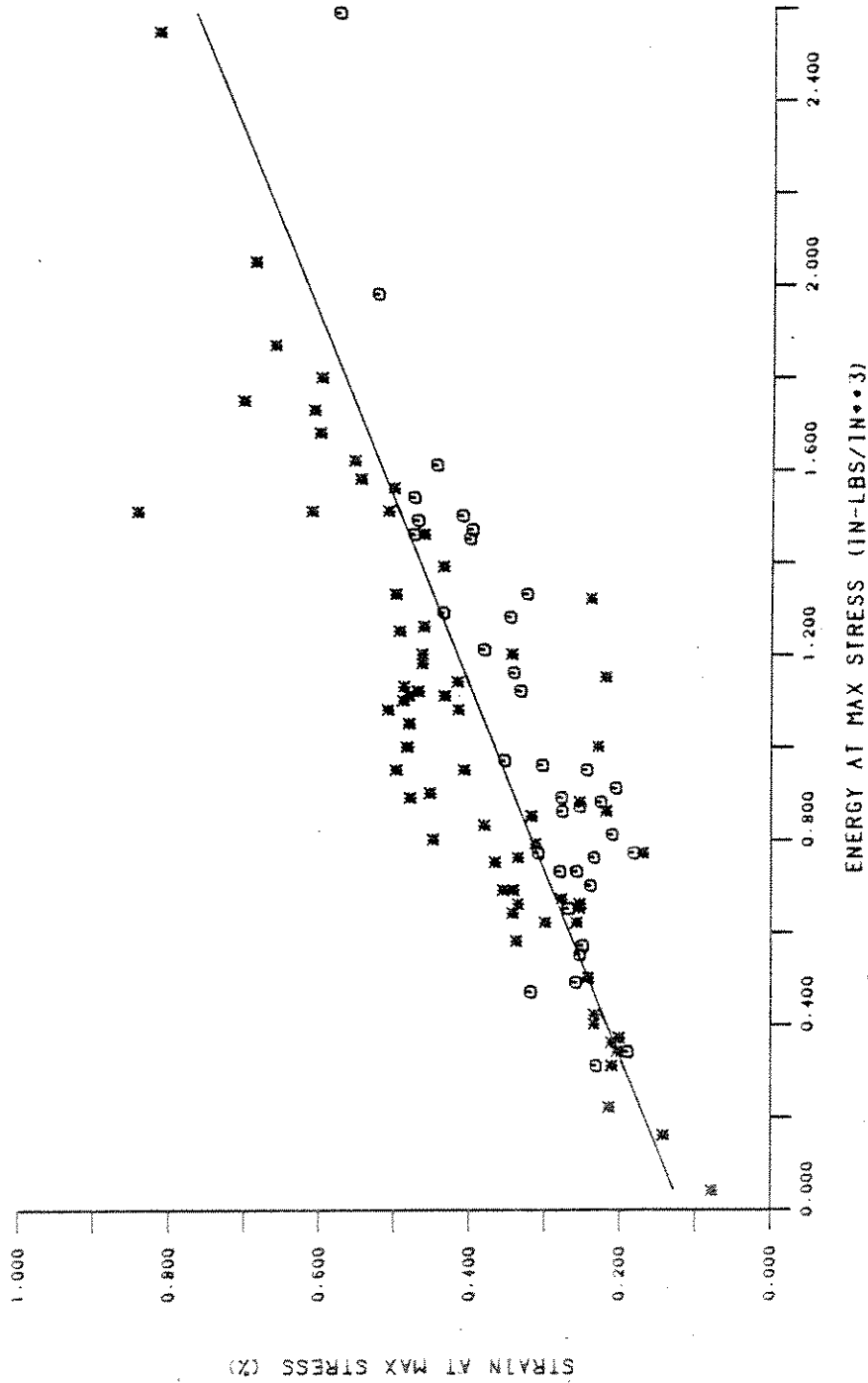


Fig. 15 - Strain at maximum stress as a function of the energy dissipated at maximum stress for $\dot{\epsilon} = 10^{-5}/\text{sec}$.

MPSI PHASE1: UNIAXIAL COMPRESSION
STRAIN RATE = $(10E-3)/\text{SEC}$

* TEMPERATURE = -5 DEG C
O TEMPERATURE = -20 DEG C
— COMMON LINEAR REGRESSION LINE

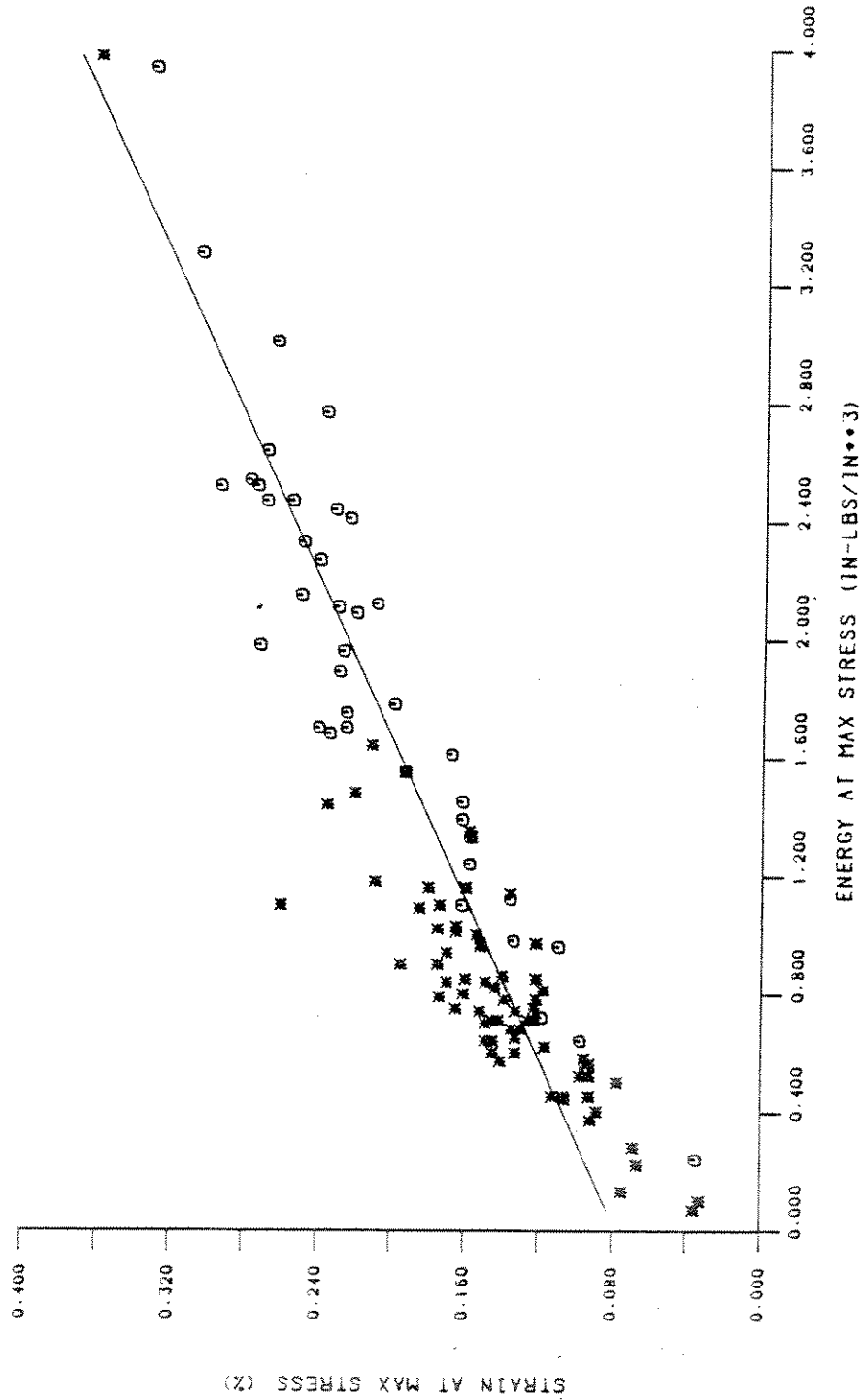


Fig. 16 - Strain at maximum stress as a function of the energy dissipated at maximum stress for $\dot{\epsilon} = 10^{-3}/\text{sec}$.

The effects of temperature and strain rate on I_p are again investigated by conducting t-tests for the two levels of constant temperature and strain rate. The results are summarized in Table 21. This summary shows that at all four test conditions except for C320, the mean values of I_p are similar. If the mean value for C320 was similar to the other mean values, then we could hypothesize that the peak value for the stress-strain curve is associated with a critical value of energy independent of temperature and strain rate. This is a very attractive hypothesis and should not be abandoned without a closer examination of why the mean value of C320 is different from the others. One possibility for the difference is due to the fact that all tests are included in each sample population of a given test condition when calculating I_p . Selective editing of the tests according to ice type or failure mode could significantly change the mean values in Table 21 and hence change the conclusions of the pairwise t-tests. If editing of the data set proves fruitless, then a failure criteria based on I_p over a more restrictive temperature, strain rate regime should be investigated.

IDEALIZED STRESS-STRAIN RESPONSE

When discussing the mechanical response of a material, all mechanical properties should be taken into account before a general impression of the material's behavior can be made. The stress-strain curve for multi-year ridge ice is a nonmonotonic curve which has a peak stress at approximately .1-.4% strain and decreases to a fairly constant value at strains greater than 4% (see Mellor⁸ for a detailed account of the stress-strain behavior of ice). This type of curve can be characterized by the initial tangent modulus, the peak value of stress and the constant stress at large strains. We will attempt to define a single parameter which depends on these properties. This parameter would then provide a useful basis for comparing different stress-strain curves and discussing changes in the mechanical response with temperature and strain rate.

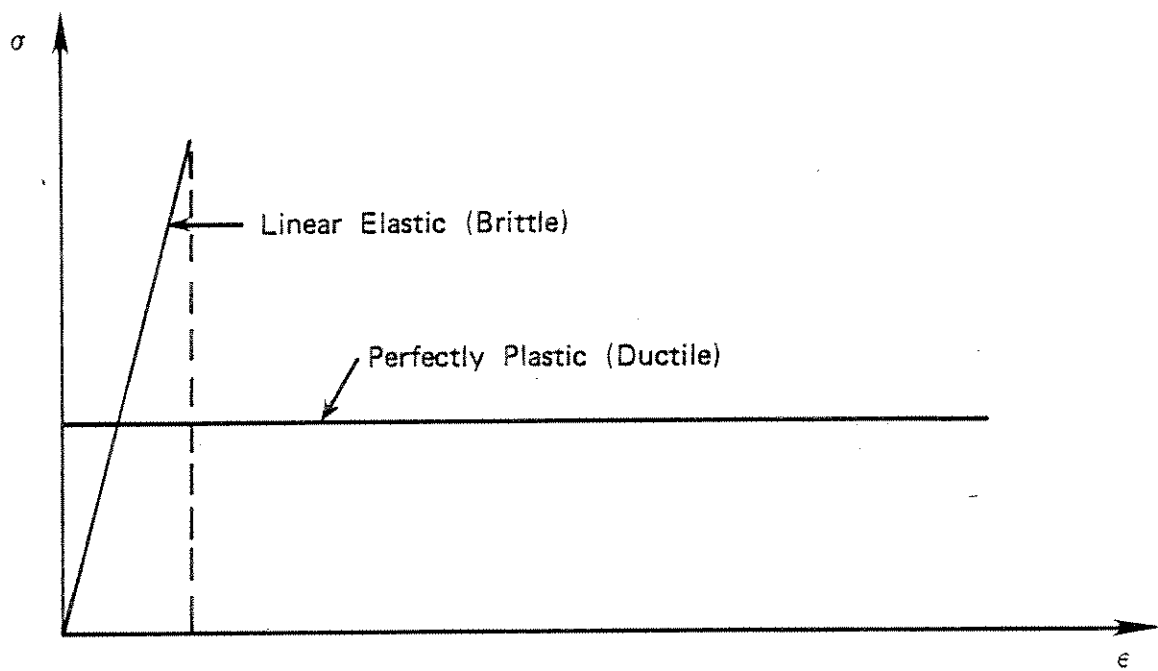
Engineers commonly characterize the mechanical response of materials in qualitative terms as being either brittle or ductile. This terminology is useful here, but the usual definitions of these terms must be modified before being applied to multi-year ridge ice. A ductile material is usually defined as a material that undergoes appreciable deformation before rupture (failure), whereas a brittle material undergoes very little deformation prior to rupture.

These definitions are not very suitable for ice since an ice sample tested at supposedly brittle conditions (e.g., 10^{-3} /sec strain rate) can still support loads at large strains.

More suitable definitions arise by considering the idealized response of a ductile and brittle material. A truly ductile material is often modeled as a perfectly plastic material whose characteristic stress-strain shape is a rectangle elongated along the strain axis. This model allows the material to flow indefinitely under a constant yield stress. A truly brittle material is often modeled as a linear elastic material whose stress-strain shape is a sharp ramp. This model allows the material to attain high stresses very rapidly and unloads instantaneously when the failure stress is reached. These two models, illustrated in Figure 17, are consistent with the usual definitions of ductile and brittle since plastic strains are usually quite large when compared to elastic strains. However, it is the shape of these models that should be kept in mind when classifying the response of multi-year ridge ice. A flat stress-strain curve with a fairly constant post-peak behavior is defined as a ductile response, and a sharp stress-strain curve with rapid unloading after the peak stress is defined as a brittle response. The notions of "flat" and "sharp" stress-strain curves will be quantified in the following sections.

ENERGY COMPONENTS

Perhaps the most appropriate mechanical property to describe mechanical response is the total dissipated energy since its calculation takes into account all aspects of the stress-strain curve. However, this quantity is not very useful in describing the shape of the stress-strain curve since no information is provided about its distribution in the stress-strain plane. The observation in a previous section that the residual stress appears to be rate independent suggests a useful decomposition of the total energy which would permit a quantitative measure of the shape of the stress-strain curve. If the residual stress is indeed independent of strain rate, then its contribution to the calculation of the total energy would also be rate independent. We define this rate independent contribution as the flow energy. This quantity is estimated by calculating the area of the trapezoid bound by the initial tangent modulus, the constant residual stress, the constant strain of 0.045, and the strain axis. Thus, the flow energy is given by the equation,



84/411/07

Fig. 17 - Schematic diagram of idealized material models.

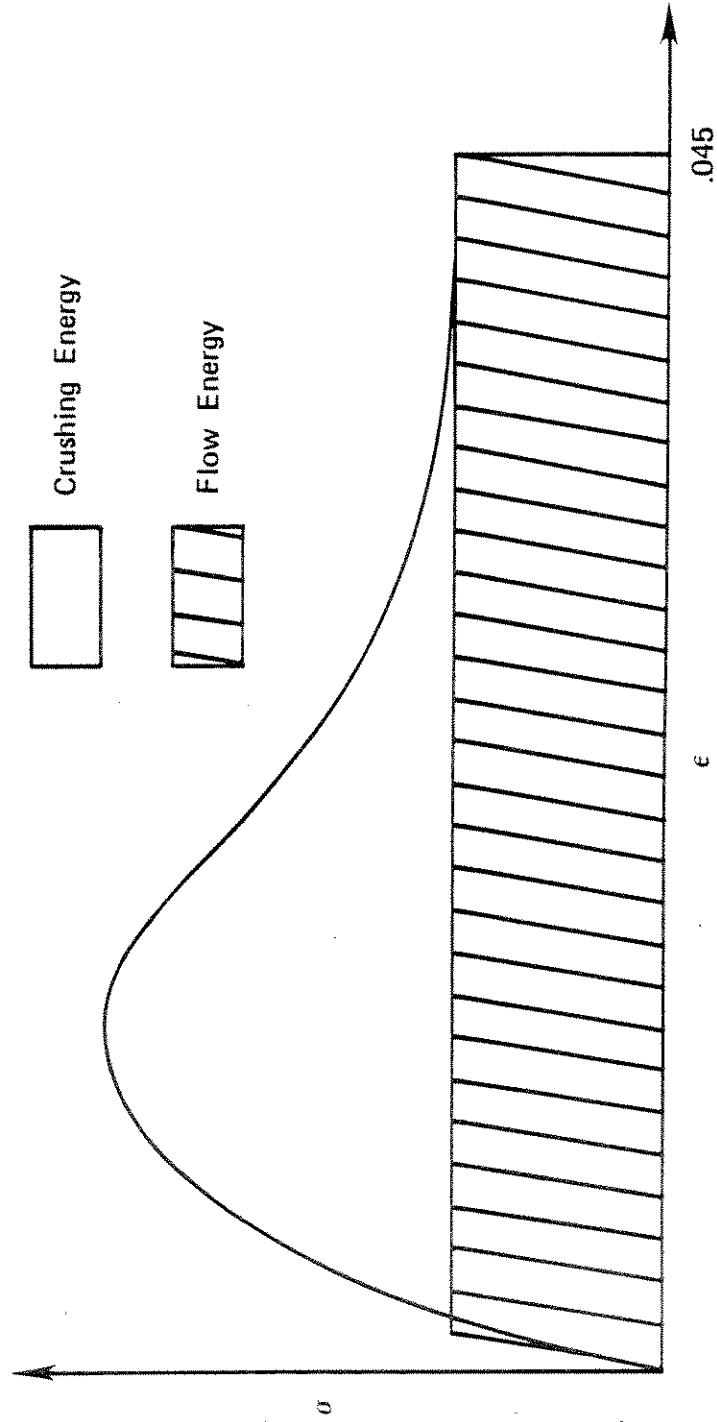
$$I_F = \frac{1}{2} \left(0.09 - \frac{\sigma_R}{E_T} \right) \sigma_R \quad .$$

The difference between the total energy (I_T) and the flow energy (I_F) would be the rate dependent contribution and is defined as the crushing energy (I_C). In some cases, it is possible that our estimation of the flow energy is greater than the total energy which would result in a negative crushing energy. In this event, the flow energy is set equal to the total energy, and the crushing energy is set equal to zero. Figure 18 is a schematic representation of the decomposition of the total energy. Similar to the summaries for the primary mechanical properties, the effects of temperature and strain rate on the mean values of flow energy and crushing energy are summarized in Tables 22 and 23. As expected, Table 22 shows the flow energy to be independent of strain rate, and Table 23 shows the crushing energy to increase with increasing strain rate.

STRESS-ENERGY PAIRS

Earlier, we saw that the two stress quantities, σ_M and σ_R , are related to the total energy, and that relationship depends on temperature and strain rate. In the previous section, the total energy has been decomposed into rate dependent and rate independent parts via the quantities I_C and I_F . With this decomposition, we can now create two conjugate stress-energy pairs which provide correlations independent of strain rate.

The first conjugate pair is formed from the rate dependent stress and energy quantities. In Figures 19 and 20, we plot σ_M as a function of I_C for the two levels of temperature. Figure 19 shows that there is a correlation between σ_M and I_C and that the correlation is independent of strain rate. A linear regression line is calculated for all points in Figure 19 and is found to be statistically significant with a R^2 value of 0.946. Figure 20 does not present such a strong argument for a σ_M vs I_C relationship independent of strain rate. The data points in this figure form two widely separated clusters of points according to strain rate. In this situation, we are guaranteed a good fit between the two clusters, but this does not necessarily mean that the clusters are correlated. Despite this fact, a regression line is calculated for the combined points in Figure 20, and, as expected, the regression line is statistically significant with a R^2 value of 0.929.



84/411/08

Fig. 18 - Schematic representation of flow energy and crushing energy.

Table 22

SUMMARY OF MEAN VALUES FOR I_F (in-lbf)/in³

$\dot{\epsilon}$ \ T	-5°C	-20°C
$10^{-5}/\text{sec}$	8.92±1.97 61	11.12±3.16 29
$10^{-3}/\text{sec}$	42 7.96±2.56	18 11.46±3.39

Table 23

SUMMARY OF MEAN VALUES FOR I_C (in-lbf)/in³

$\dot{\epsilon}$ \ T	-5°C	-20°C
$10^{-5}/\text{sec}$	1.27±0.89 61	1.59±0.82 29
$10^{-3}/\text{sec}$	42 5.78±1.50	18 10.89±2.13

MPSI PHASE1: UNIAXIAL COMPRESSION

TEMPERATURE = -5 DEG C

* STRAIN RATE = (10E-5)/SEC
 O STRAIN RATE = (10E-3)/SEC
 — LINEAR REGRESSION LINE

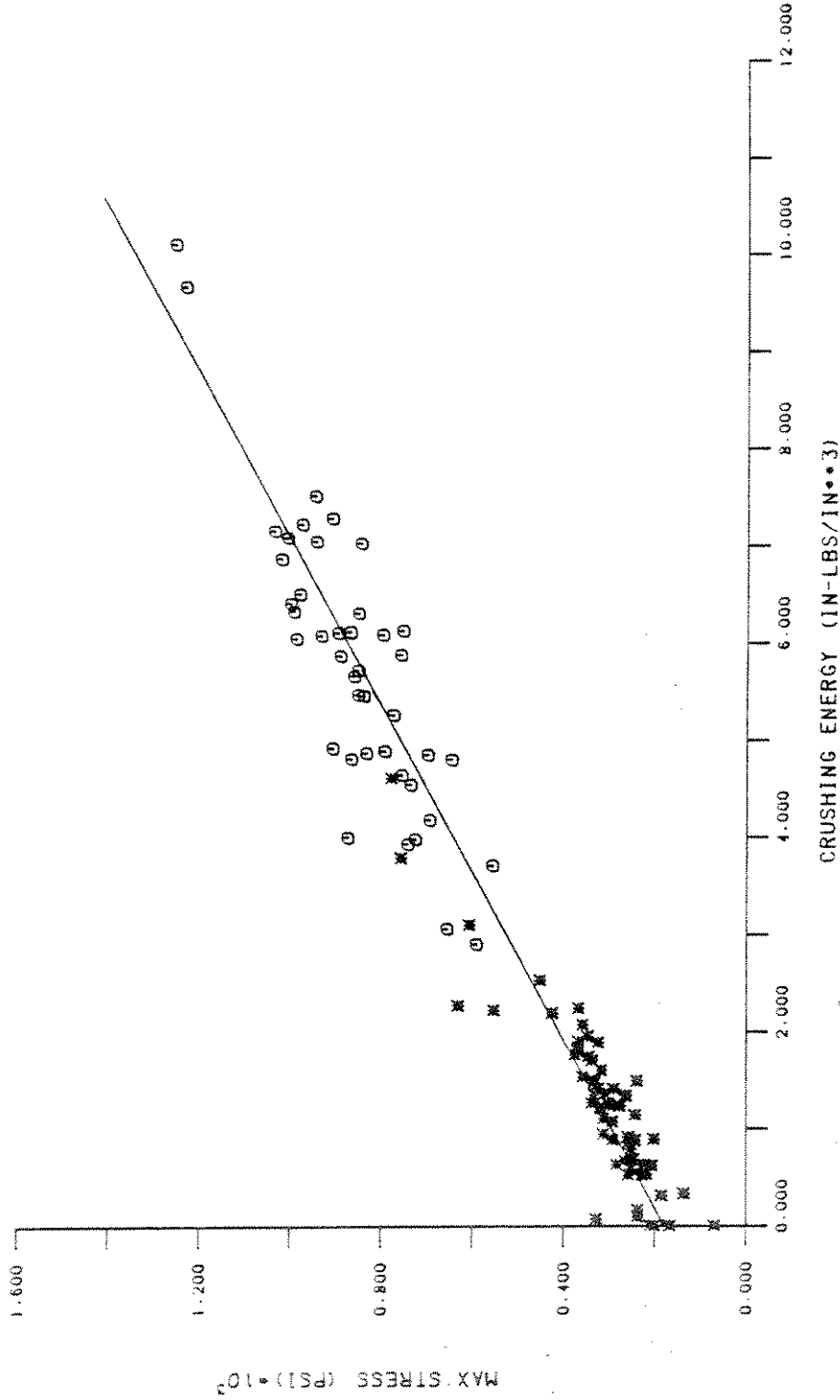


Fig. 19 - Maximum stress as a function of the crushing energy for $T = -5^\circ\text{C}$.

MPSI PHASE1: UNIAXIAL COMPRESSION
TEMPERATURE = -20 DEG C

* STRAIN RATE = (1.0E-5)/SEC
O STRAIN RATE = (1.0E-3)/SEC
— LINEAR REGRESSION LINE

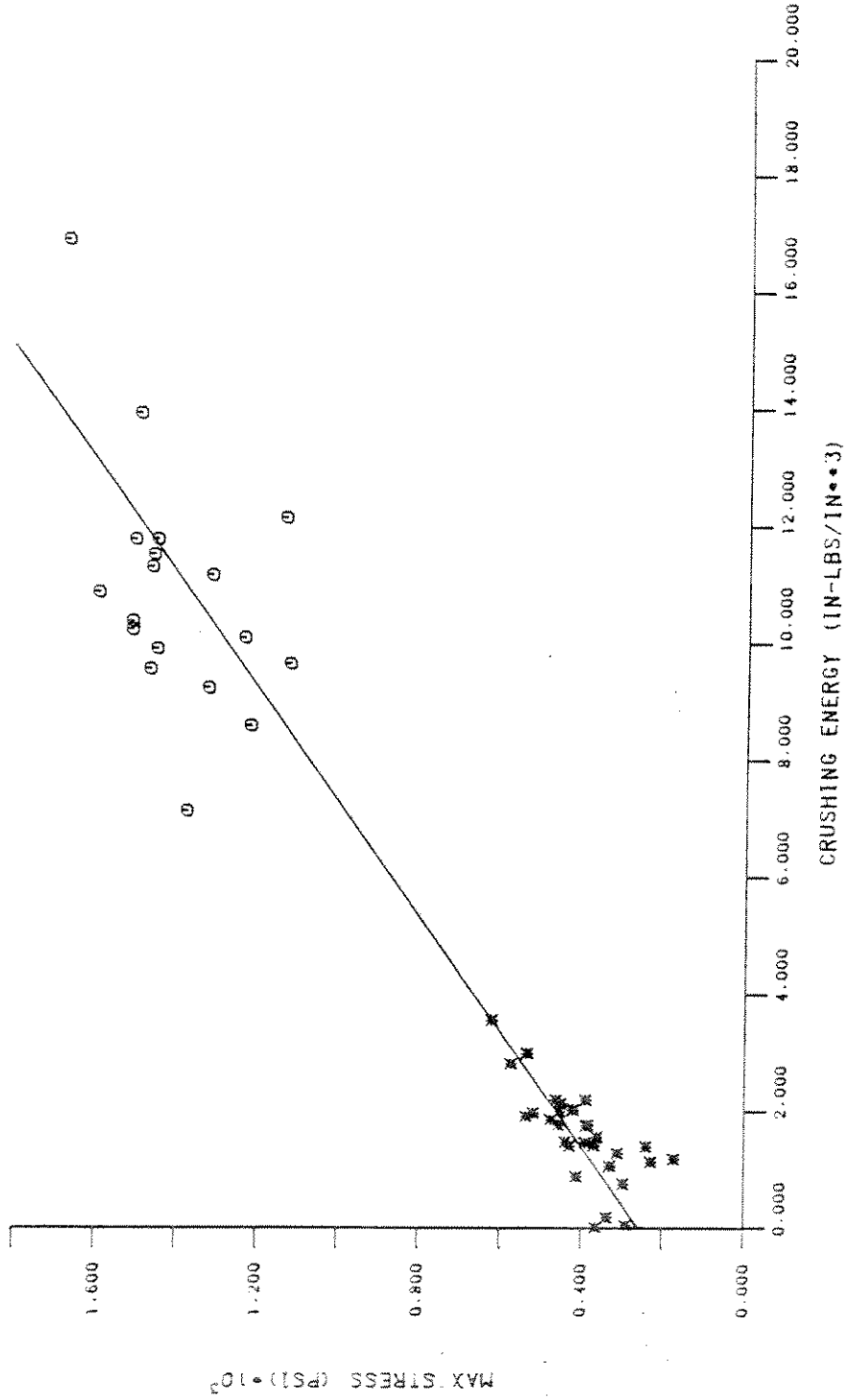


Fig. 20 - Maximum stress as a function of the crushing energy for T = -20°C.

The parameters for the regression lines in Figures 19 and 20 are summarized in Table 24. It is interesting to note that the intercepts for each line correspond closely to the mean residual stress for that temperature. This suggests that at a given temperature, the ratio $(\sigma_M - \sigma_R)/I_C$ is independent of strain rate. A comparison of the linear coefficients of the regression lines in Table 24 shows that they are in close agreement. This suggests that the only effect temperature has on the σ_M vs I_C relationship is to translate the regression line up or down by changing the temperature dependent value of the intercept σ_R . Comparison of Figures 19 and 20 with Figures 7 and 8 shows that the subtraction of the rate independent flow energy from the total energy eliminates the translation of regression lines in Figures 7 and 8. This results in a single relationship between I_C and σ_M independent of strain rate.

The second conjugate pair is formed from the rate independent stress and energy quantities. In Figures 21 and 22, we plot σ_R as a function of I_F for each temperature. The resulting, almost exact correlation between σ_R and I_F in both figures is to be expected from our definition of the flow energy. The important point to note is that the data points for each strain rate have very similar distributions along the σ_R vs I_F line lending further support for the rate independence of σ_R and I_F . The strain rate dependent translations for the regression lines seen in Figures 9 and 10 are again eliminated from Figures 21 and 22 by subtracting the rate dependent crushing energy from the total energy.

The equation defining the flow energy can be considered a regression line relating σ_R and I_F with a R^2 value of 1.0. The parameters for this line are summarized in Table 24. This table serves the same purpose as Table 19 by relating stress and energy quantities. However, in Table 19, σ_M and σ_R are functions of the total energy whereas in Table 24, the dependent and independent variables are rate dependent and rate independent conjugate pairs of stress and energy. The number of regression lines in Table 24 have been reduced by a factor of two since the dependence on strain rate has been eliminated. Comparison of the R^2 values in both tables indicates that the decomposition of the independent variable, I_T , into rate dependent and rate independent components significantly reduces the scatter in the dependent variables σ_M and σ_R .

Table 24

LINEAR REGRESSION MODELS BASED ON
CRUSHING ENERGY AND FLOW ENERGY

Independent Variable	Dependent Variable	Test Conditions	Linear Coefficient	Intercept	R ²
I _C	σ _M	C55, C35	114.97	179.84	.95
I _C	σ _M	C520, C320	102.03	260.63	.93
I _F	σ _R	C55, C35	$1/2 \left(.09 - \frac{\sigma_R}{E_T} \right) \sigma_R$	0.0	1.0
I _F	σ _R	C520, C320	$1/2 \left(.09 - \frac{\sigma_R}{E_T} \right) \sigma_R$	0.0	1.0

Table 25

SUMMARY OF MEAN VALUES FOR I_C/I_F

$\frac{\epsilon}{T}$	-5°C	-20°C
10 ⁻⁵ /Sec	.138±.089 61	.157±.093 29
10 ⁻³ /sec	.822±.400 42	1.088±.571 18

MPSI PHASE1: UNIAXIAL COMPRESSION

TEMPERATURE = -5 DEG C

* STRAIN RATE = (10E-3)/SEC
O STRAIN RATE = (10E-3)/SEC

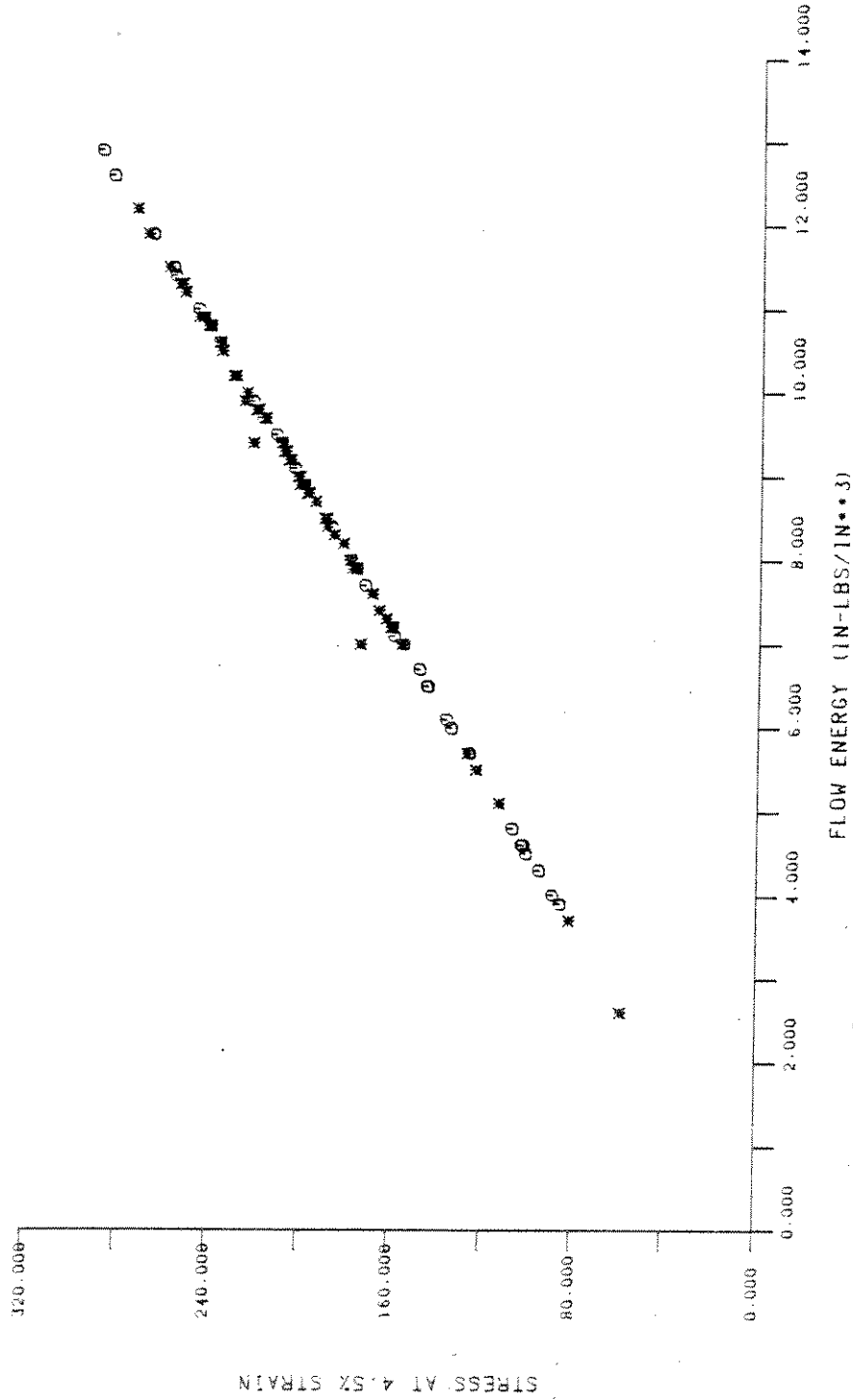


Fig. 21 - Stress at 4.5% strain as a function of the flow energy for T = -5°C.

MPSI PHASE1: UNIAXIAL COMPRESSION
TEMPERATURE = -20 DEG C

* STRAIN RATE = 0.0E-51/SEC
O STRAIN RATE = 0.0E-31/SEC

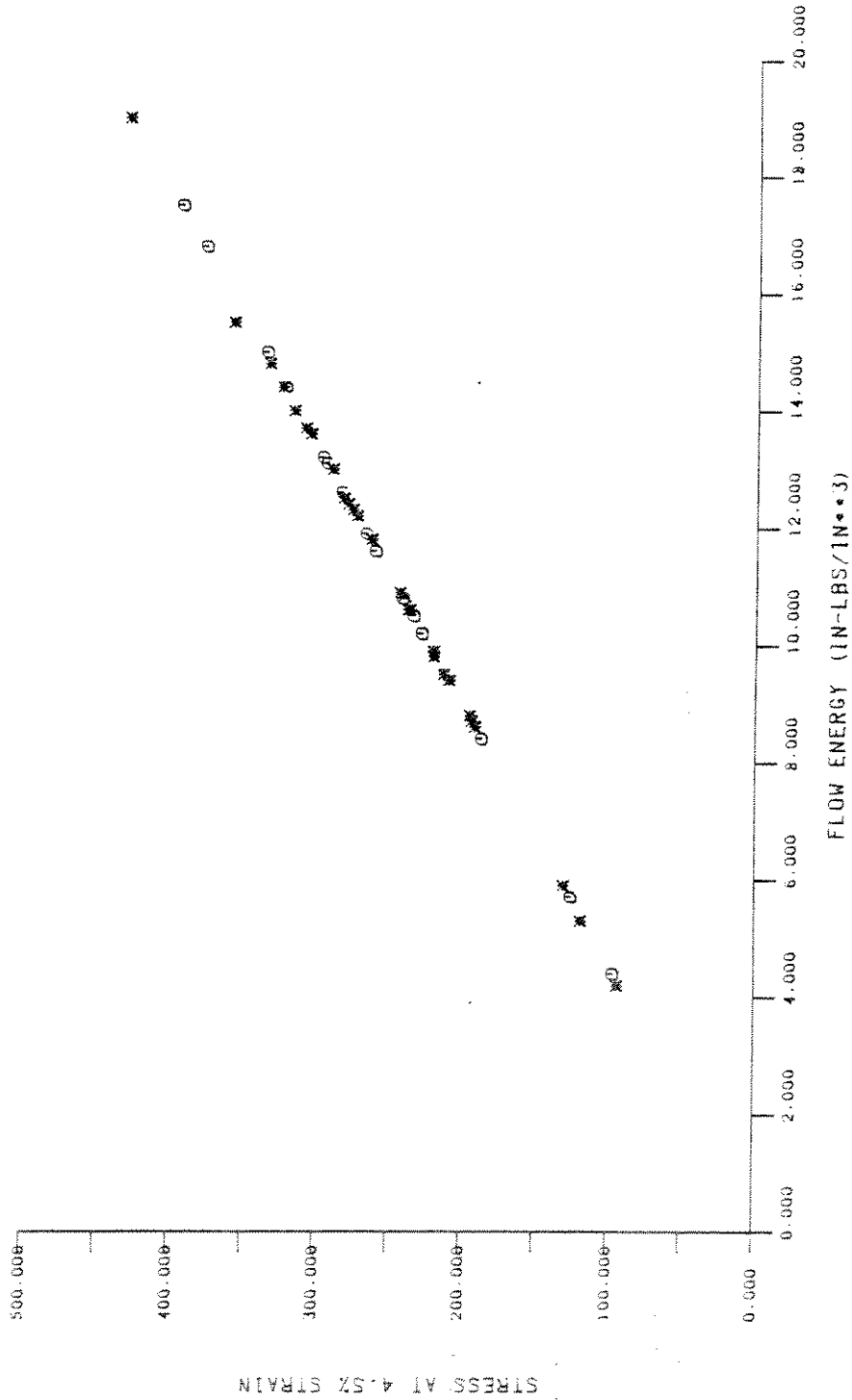


Fig. 22 - Stress at 4.5% strain as a function of the flow energy for
T = -20°C.

A PARAMETER FOR CHARACTERIZING THE STRESS-STRAIN
RESPONSE OF MULTI-YEAR RIDGE ICE

The quantities I_C and I_F can now be combined to yield a parameter which describes quantitatively the ductility or brittleness of a given stress-strain curve. From Figure 18 we see that the "hump" of the stress-strain curve is described by the crushing energy which measures the amount of energy in excess of the flow energy. By calculating the ratio, I_C/I_F , we can identify with each stress-strain curve a number which represents its shape. A stress-strain curve with a low crushing energy relative to its flow energy would have a low I_C/I_F value and would be classified as ductile. A curve with a high crushing energy relative to its flow energy would have a high I_C/I_F value and would be classified as brittle.

In practice it is not very practical to calculate the quantity I_C/I_F . A quantity easier to calculate and serving the same purpose as I_C/I_F would be desirable. From Figures 19 and 20 we see that the crushing energy is proportional to $(\sigma_M - \sigma_R)$ and by definition the flow energy is proportional to σ_R . Thus, the ratio $(\sigma_M - \sigma_R)/\sigma_R$ would be proportional to I_C/I_F and would provide another quantitative measure of ductility or brittleness. Figures 23 and 24 illustrate the relation between I_C/I_F and $(\sigma_M - \sigma_R)/\sigma_R$ for each temperature.

By taking the limiting values of I_C/I_F and $(\sigma_M - \sigma_R)/\sigma_R$, we see that in the limit these ratios represent the stress-strain curves of the material models shown in Figure 17. When I_C/I_F and $(\sigma_M - \sigma_R)/\sigma_R$ equals zero, we have $I_C = 0$ and $\sigma_M = \sigma_R$. In this case the stress-strain curve would resemble a perfectly plastic material. When I_C/I_F and $(\sigma_M - \sigma_R)/\sigma_R$ become unbounded, we have $I_F = \sigma_R = 0$ and the stress-strain curve would resemble a brittle elastic material.

The mean values of the ratio, I_C/I_F , are summarized for each test condition in Table 25. This table shows that the ratio increases with increasing strain rate and is independent of temperature. The temperature independence is due to the proportional increases in the values of σ_M and σ_R with the decrease in temperature resulting in a relatively constant value of I_C/I_F . Thus, a change in temperature causes a proportional change in the shape of the stress-strain curve whereas a change in strain rate will distort the shape of the stress-strain curve. To illustrate the effects of temperature and strain rate on the mechanical response and the variability of

MPSI PHASE1: UNIAXIAL COMPRESSION

TEMPERATURE = -5 DEG C

* STRAIN RATE ~ (10E-5)/SEC
 O STRAIN RATE ~ (10E-3)/SEC
 ——— LINEAR REGRESSION LINE

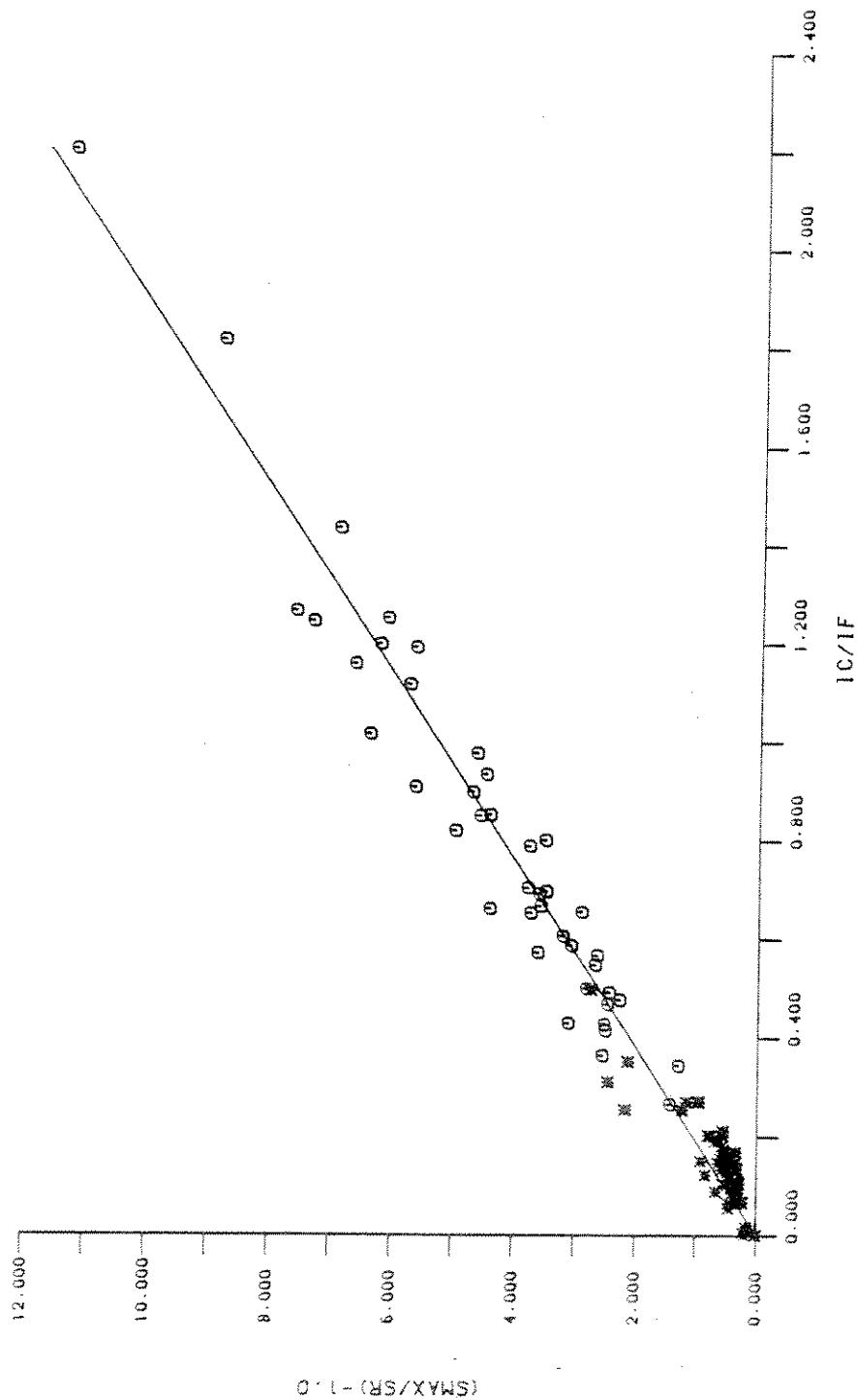


Fig. 23 - $\frac{\sigma_M - \sigma_R}{\sigma_R}$ as a function of I_C/I_F for $T = -5^\circ C$.

MPSI PHASE1: UNIAXIAL COMPRESSION
TEMPERATURE = -20 DEG C

W STRAIN RATE = (10E-3)/SEC
O STRAIN RATE = (10E-3)/SEC
— LINEAR REGRESSION LINE

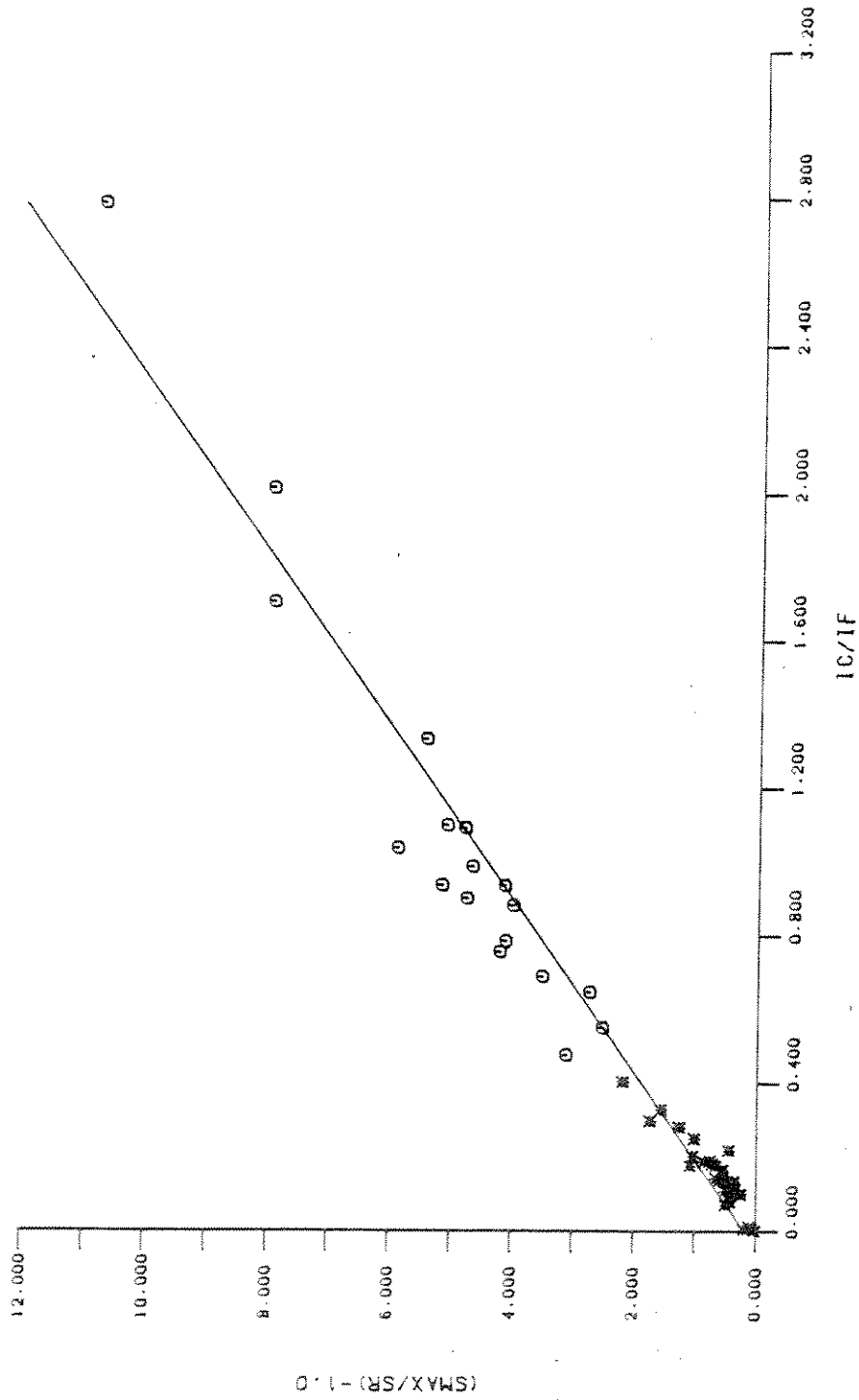


Fig. 24 - $\frac{\sigma_M - \sigma_R}{\sigma_R}$ as a function of I_C/I_F for $T = -20^\circ\text{C}$.

the response within a given test condition, we choose the tests with maximum, minimum, and mean values of I_C/I_F at each test condition. The stress-strain curves for these tests are shown in Figures 25-28 according to test condition. The remaining stress-strain curves can be found in Appendix C according to test conditions. The splines for each force-time history are listed in Appendix B.

"AVERAGE" STRESS-STRAIN CURVES

Finally, we would like to establish a method of defining a stress-strain curve which in some sense represents the average response of multi-year ice at each test condition. The most obvious method of doing this would be to calculate point by point averages of all stress-strain curves within each test condition and then plot those average values to obtain an average stress-strain curve. This was done for each test condition, and the resulting curves are shown in Figures 29 and 30 for $T = -5^\circ\text{C}$ and $T = -20^\circ\text{C}$, respectively.

A much easier method of selecting an average curve would be to compare the primary mechanical properties of each test with the corresponding mean values. The "error" associated with each property is its difference from the mean. In order to compare the errors associated with the different properties, each error should be normalized with respect to the mean value. If the errors of each property are to be summed for each test, then each normalized error should be squared. Thus, we can calculate a residual error from the mean for each test from the equation,

$$E^2 = \sum_{j=1}^5 \left(\frac{x_j - \bar{x}_j}{\bar{x}_j} \right)^2$$

Here j denotes each of the five primary properties and the quantities x_j and \bar{x}_j denote the actual and mean values, respectively, of the j th property. The residual errors for each test are summarized in Tables 26-29. The "average" stress-strain curve can now be chosen to be the curve with the minimum or least square of the residual error. The "average" curves chosen by the least squares method are shown in Figures 31 and 32.

A residual error for each curve obtained by pointwise averaging can also be calculated. These errors are listed in Table 30 along with the least

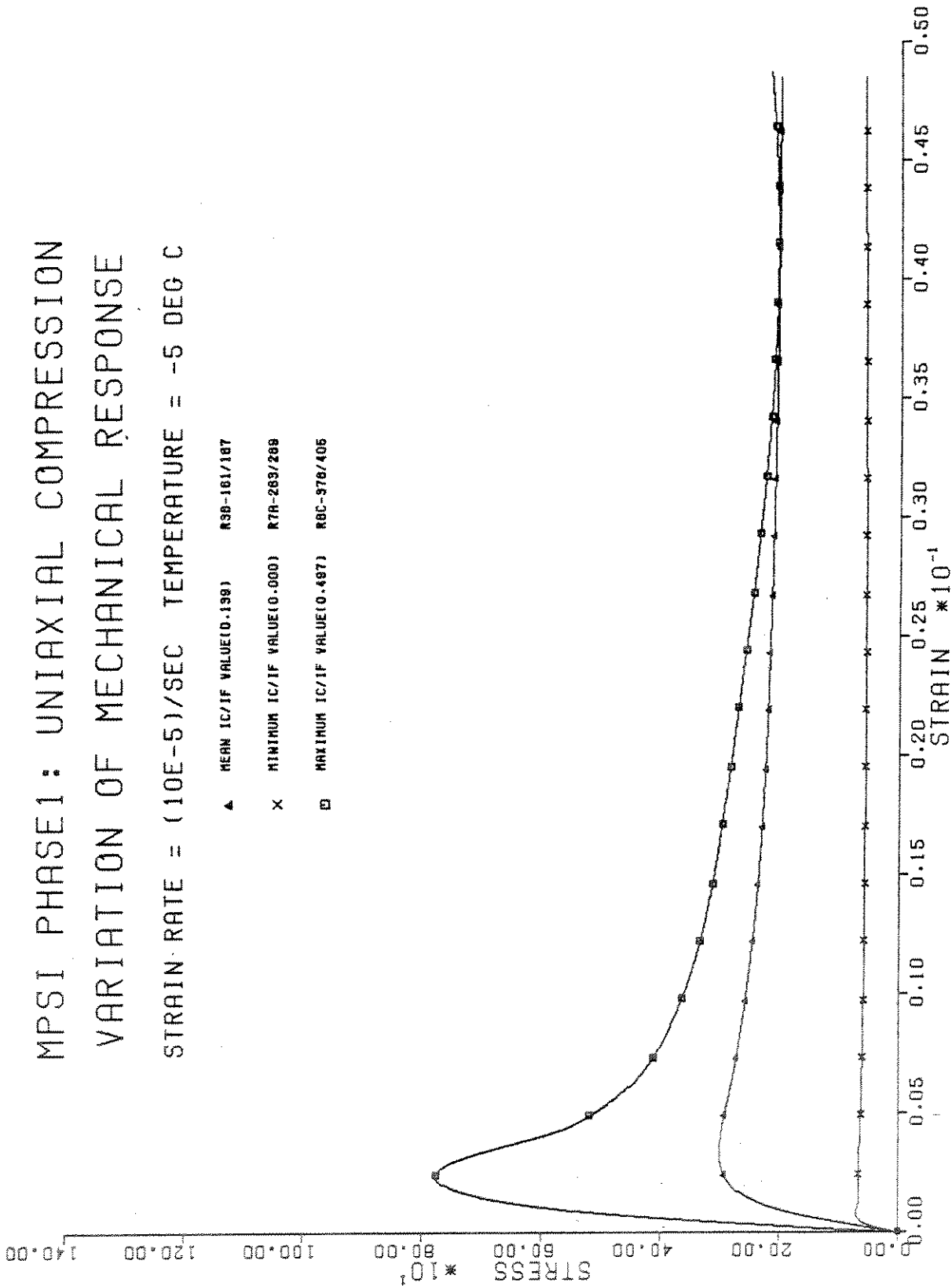


Fig. 25 - Variation of the mechanical response of multi-year ridge ice for $\dot{\epsilon} = 10^{-5}/\text{sec}$ and $T = -5^{\circ}\text{C}$.

MPSI PHASE1: UNIAXIAL COMPRESSION VARIATION OF MECHANICAL RESPONSE

STRAIN RATE = $(10E-5)/\text{SEC}$ TEMPERATURE = -20 DEG C

▲ MEAN IC/IF VALUE(0.185) R9C-385/422
X MINIMUM IC/IF VALUE(0.000) R9A-125/162
□ MAXIMUM IC/IF VALUE(0.404) R10-071/098

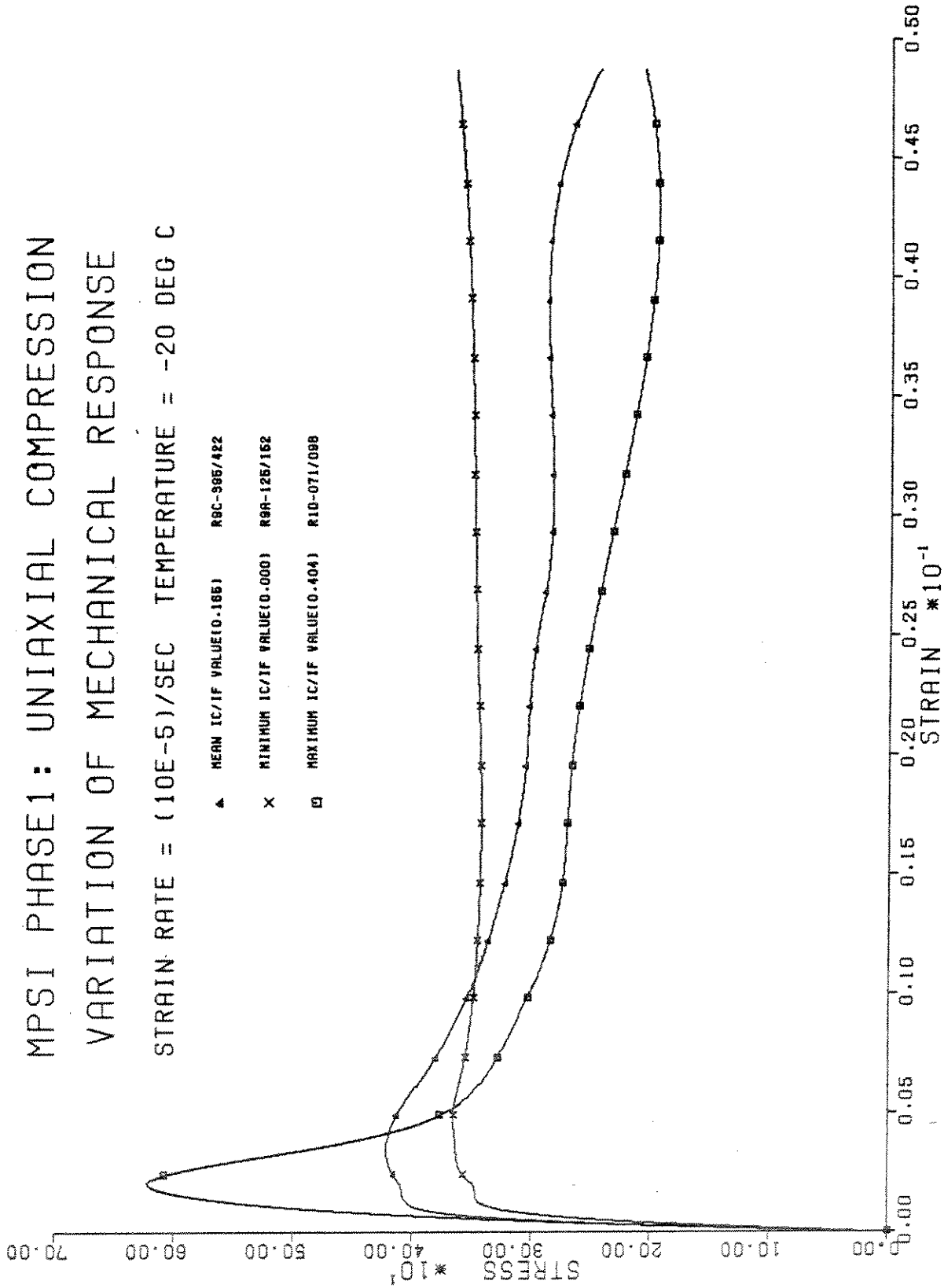


Fig. 26 - Variation of the mechanical response of multi-year ridge ice for $\dot{\epsilon} = 10^{-5}/\text{sec}$ and $T = -20^\circ\text{C}$.

MPSI PHASE1: UNIAXIAL COMPRESSION VARIATION OF MECHANICAL RESPONSE

STRAIN RATE = $(10E-3)/\text{SEC}$ TEMPERATURE = -5 DEG C

▲ MEAN IC/IF VALUE(0.822) R2D-394/371
× MINIMUM IC/IF VALUE(0.288) R6R-305/391
□ MAXIMUM IC/IF VALUE(2.208) R2A-285/310

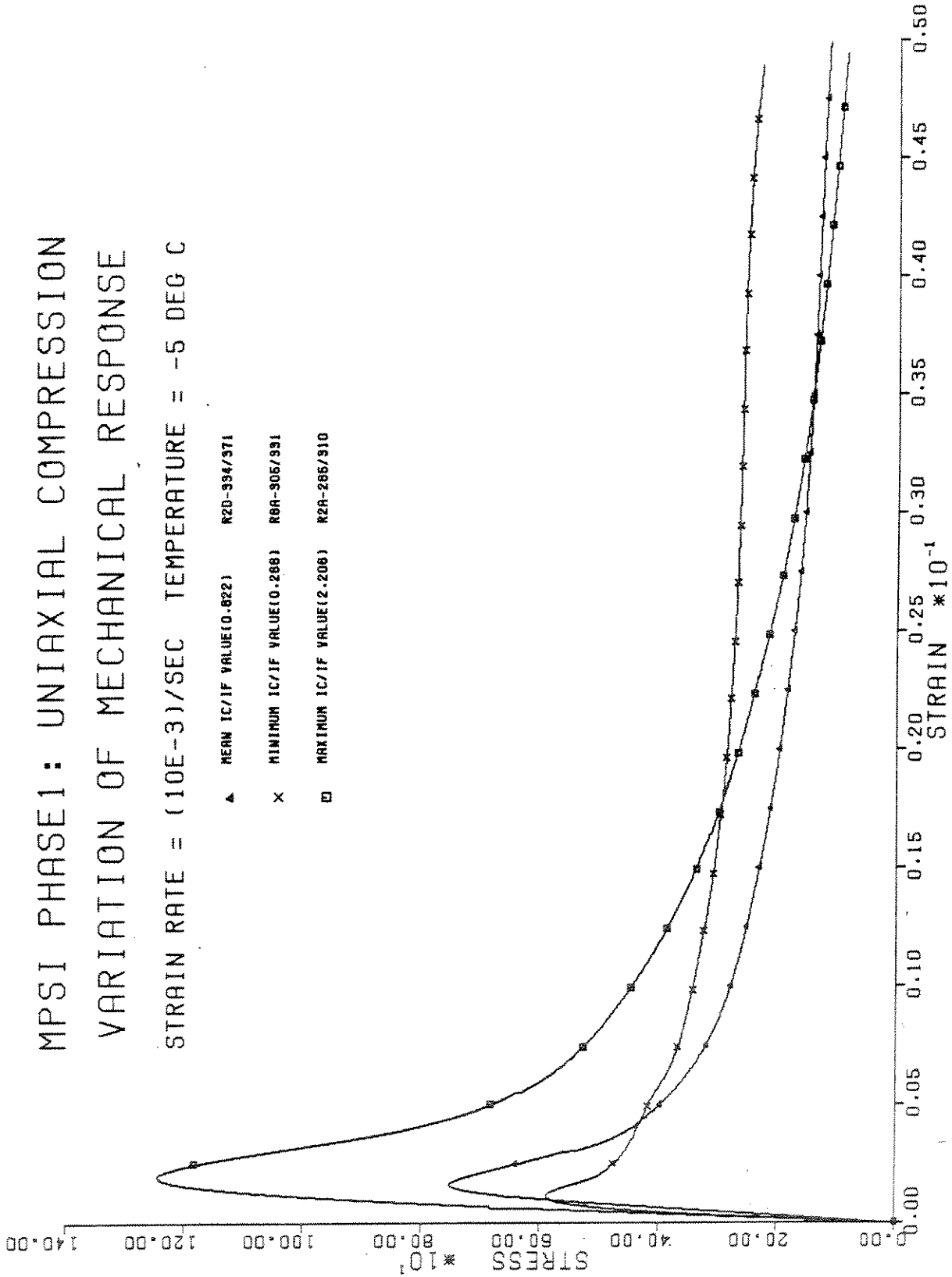


Fig. 27 - Variation of the mechanical response of multi-year ridge ice for $\dot{\epsilon} = 10^{-3}/\text{sec}$ and $T = -5^\circ\text{C}$.

MPSI PHASE1: UNIAXIAL COMPRESSION

VARIATION OF MECHANICAL RESPONSE

STRAIN RATE = $(10E-3)/\text{SEC}$ TEMPERATURE = -20 DEG C

▲ MEAN IC/IF VALUE(1.090) R100-608/636
 X MINIMUM IC/IF VALUE(0.476) R9C-607/634
 □ MAXIMUM IC/IF VALUE(2.766) R9B-076/103

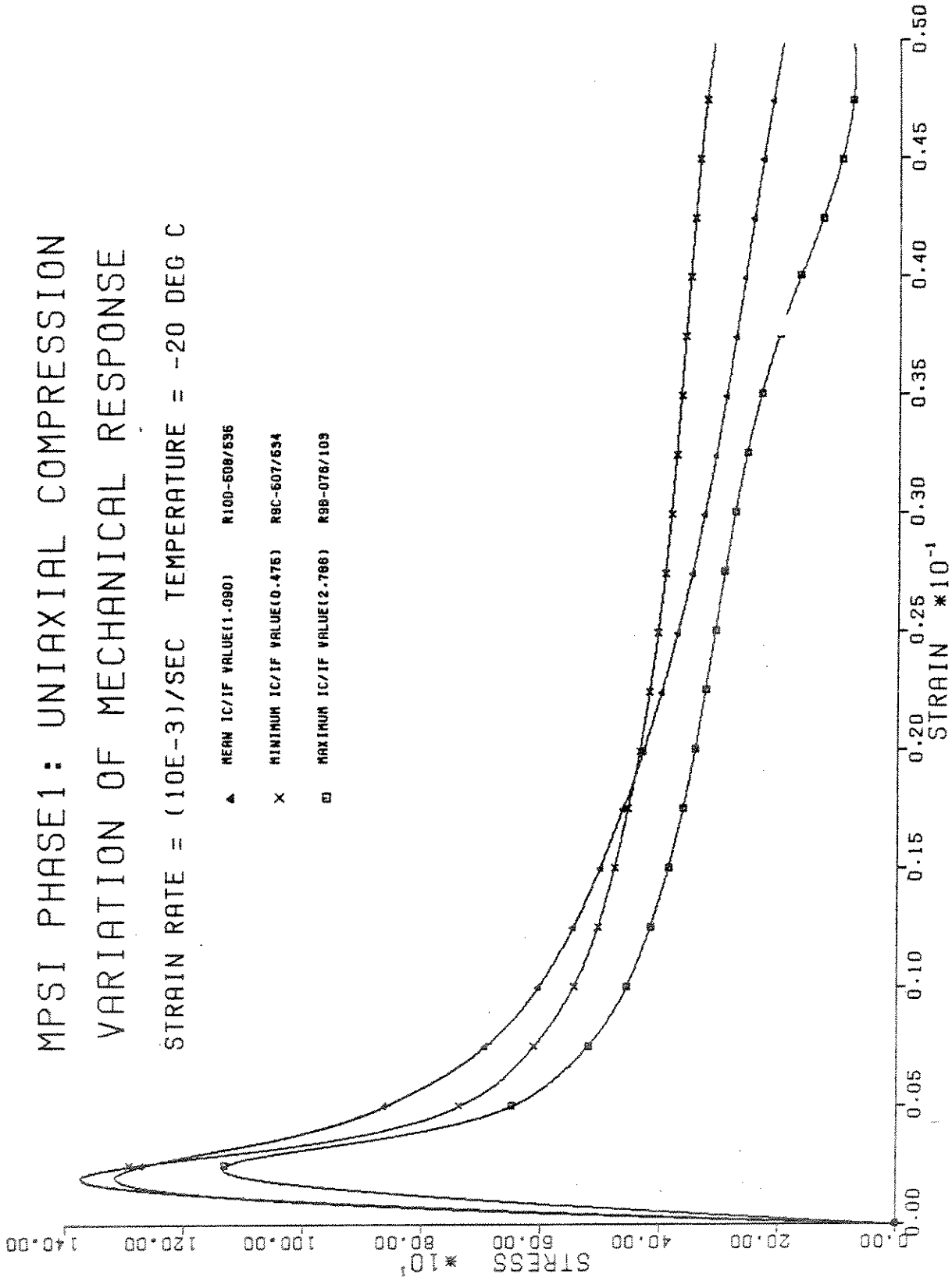


Fig. 28 - Variation of the mechanical response of multi-year ridge ice for $\dot{\epsilon} = 10^{-3}/\text{sec}$ and $T = -20^\circ\text{C}$.

POINT BY POINT 'AVERAGE' CURVE

TEMPERATURE = -5 DEG C

* STRAIN RATE = 1.0×10^{-5} /SEC
 □ STRAIN RATE = 1.0×10^{-3} /SEC

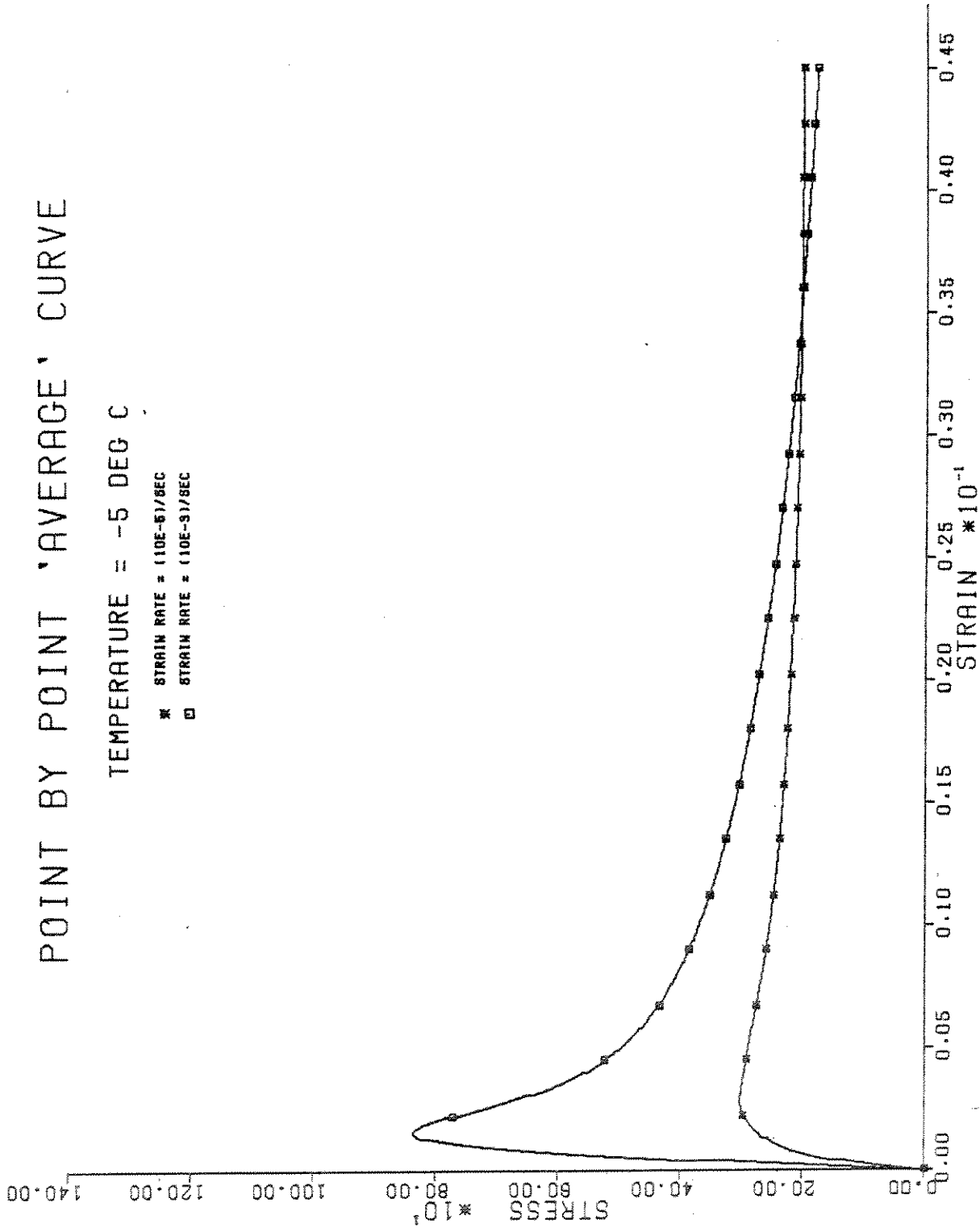


Fig. 29 - Point by point "average" stress-strain curve of multi-year ridge ice for $\dot{\epsilon} = 10^{-5}$ /sec and $\dot{\epsilon} = 10^{-3}$ /sec at $T = -5^\circ\text{C}$.

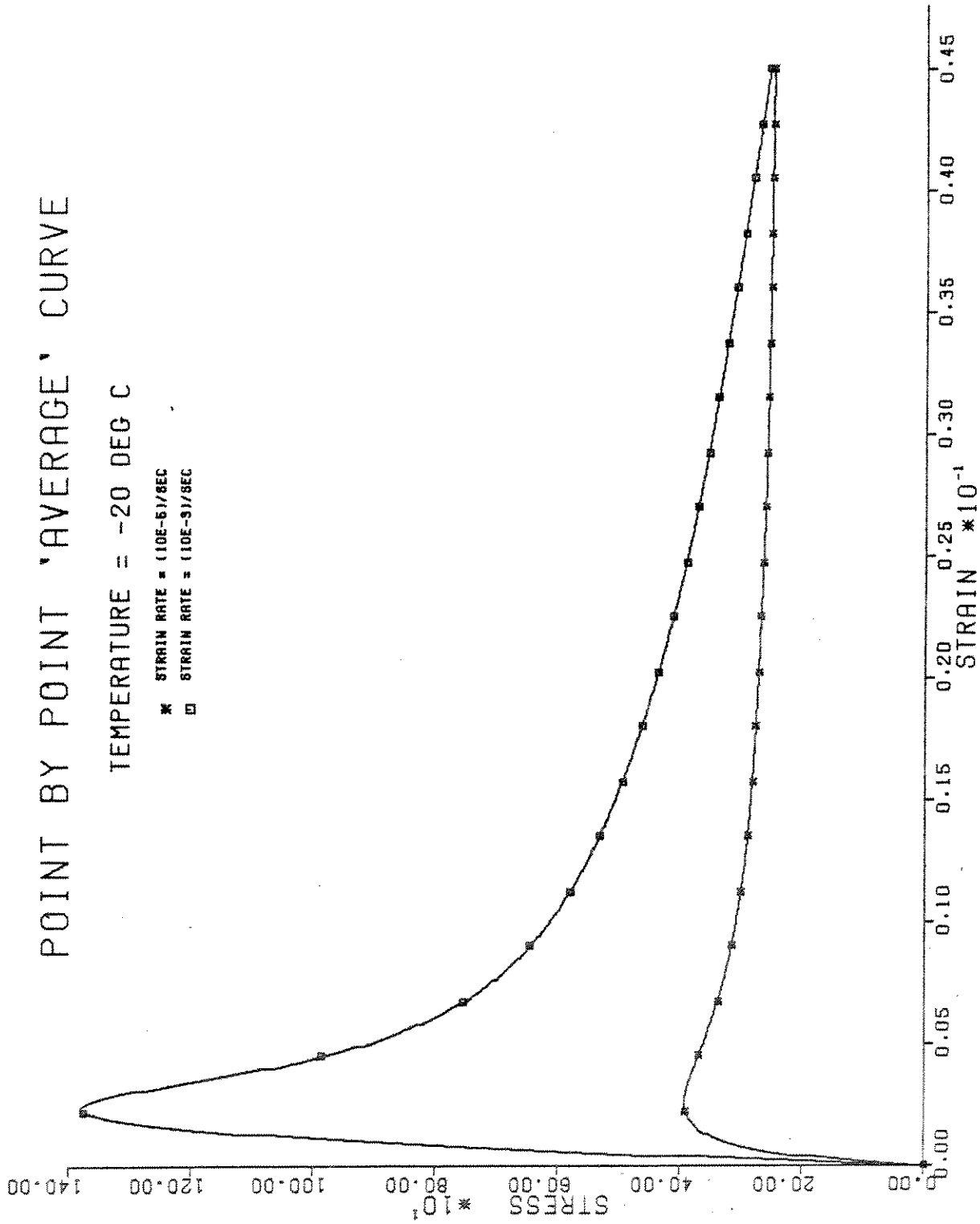


Fig. 30 - Point by point "average" stress-strain curve of multi-year ridge ice for $\dot{\epsilon} = 10^{-5}/\text{sec}$ and $\dot{\epsilon} = 10^{-3}/\text{sec}$ at $T = -20^\circ\text{C}$.

Table 26

NORMALIZED ERRORS
STRAIN RATE = (10E-5)/SEC TEMPERATURE = -5°C

Ridge ID	I_C/I_F	σ_M	Norm σ_M	ϵ_M	Norm ϵ_M	σ_R	Norm σ_R	E_T	Norm E_T	I_T	Norm I_T	Total Res
R1A-062/089	0.202	425.	1.344	0.344	0.860	241.	1.205	0.965	1.896	13.0	1.276	1.059
R1B-062/089	0.133	321.	1.015	0.463	1.157	205.	1.025	0.467	0.917	10.4	1.021	0.033
R2A-140/165	0.212	368.	1.164	0.597	1.492	236.	1.180	0.493	0.969	12.8	1.257	0.369
R2B-094/121	0.000	167.	0.528	0.142	0.355	174.	0.870	0.201	0.395	7.0	0.687	1.119
R3A-106/131	0.134	333.	1.053	0.461	1.152	245.	1.226	0.330	0.648	12.4	1.217	0.248
R3B-161/187	0.139	300.	0.949	0.335	0.837	201.	1.005	0.231	0.454	10.2	1.001	0.327
R4A-312/338	0.145	277.	0.876	0.481	1.202	189.	0.945	0.482	0.947	9.7	0.952	0.064
R4B-328/354	0.163	244.	0.772	0.497	1.242	156.	0.780	0.211	0.415	8.1	0.795	0.544
R5A-165/191	0.254	606.	1.917	0.229	0.572	272.	1.361	1.041	2.045	15.3	1.502	2.498
R5B-075/101	0.351	755.	2.388	0.219	0.547	241.	1.205	0.797	1.566	14.6	1.433	2.682
R7A-059/085	0.135	359.	1.136	0.545	1.362	252.	1.261	0.488	0.959	12.8	1.257	0.285
R7B-126/152	0.010	239.	0.756	0.452	1.130	206.	1.030	0.327	0.642	9.3	0.913	0.213
R8A-133/159	0.017	238.	0.753	0.335	0.837	202.	1.010	0.450	0.884	9.2	0.903	0.110
R8B-162/189	0.141	324.	1.025	0.433	1.082	224.	1.120	0.294	0.578	11.4	1.119	0.215
R3C-095/122	0.075	265.	0.838	0.483	1.207	201.	1.005	0.177	0.348	9.6	0.942	0.498
R3D-159/186	0.000	201.	0.636	0.841	2.102	198.	0.990	0.268	0.527	8.8	0.864	1.591
R5C-039/066	0.155	376.	1.189	0.435	1.087	253.	1.266	0.689	1.354	13.1	1.286	0.321
R5D-159/186	0.203	359.	1.136	0.599	1.497	230.	1.150	0.212	0.417	12.3	1.207	0.672
R6C-166/193	0.000	211.	0.667	0.337	0.843	221.	1.105	0.314	0.617	9.4	0.923	0.299
R8C-048/075	0.069	228.	0.721	0.234	0.585	169.	0.845	0.500	0.982	8.1	0.795	0.316
R8D-236/263	0.006	329.	1.041	0.254	0.635	267.	1.336	0.441	0.866	12.0	1.178	0.297
R1A-226/252	0.122	208.	0.658	0.204	0.510	113.	0.565	1.286	2.527	5.7	0.560	3.070
R1A-399/425	0.156	203.	0.642	0.234	0.585	127.	0.635	1.056	2.075	6.6	0.648	1.712
R2A-314/339	0.150	313.	0.990	0.257	0.643	163.	0.815	0.432	0.849	8.4	0.825	0.216
R2B-408/434	0.109	339.	1.072	0.607	1.517	258.	1.291	0.466	0.916	12.8	1.257	0.430
R2B-468/494	0.104	259.	0.819	0.380	0.950	194.	0.970	0.534	1.049	9.6	0.942	0.042
R3A-220/245	0.085	248.	0.784	0.342	0.855	178.	0.890	0.183	0.360	8.6	0.844	0.514

Table 26 (Cont'd.)

Ridge ID	I_C/I_F	σ_M	Norm σ_M	ϵ_M	Norm ϵ_M	σ_R	Norm σ_R	E_T	Norm E_T	I_T	Norm I_T	Total Res
R3A-430/456	0.135	301.	0.952	0.463	1.157	208.	1.040	1.045	2.053	10.6	1.041	1.139
R3B-363/389	0.168	369.	1.167	0.501	1.252	243.	1.215	0.499	0.980	12.7	1.247	0.199
R4A-426/452	0.203	318.	1.006	0.312	0.780	176.	0.880	0.661	1.299	9.5	0.933	0.156
R4B-391/417	0.103	293.	0.927	0.277	0.693	190.	0.950	0.708	1.391	9.4	0.923	0.261
R4B-449/475	0.118	244.	0.772	0.355	0.888	166.	0.830	0.282	0.554	8.3	0.815	0.327
R5A-397/423	0.137	309.	0.977	0.480	1.200	225.	1.125	0.135	0.265	11.3	1.109	0.608
R5A-442/468	0.270	451.	1.427	0.253	0.633	209.	1.045	0.624	1.226	11.9	1.168	0.398
R5A-504/530	0.123	319.	1.009	0.493	1.232	220.	1.100	0.232	0.456	11.0	1.080	0.367
R5B-398/423	0.105	294.	0.930	0.407	1.017	229.	1.145	0.344	0.676	11.3	1.109	0.143
R7A-263/289	0.000	71.	0.225	0.078	0.195	59.	0.295	0.234	0.460	2.6	0.255	2.593
R7A-342/368	0.310	553.	1.749	0.218	0.545	160.	0.800	0.542	1.065	9.4	0.923	0.818
R7B-241/267	0.087	226.	0.715	0.448	1.120	161.	0.805	0.185	0.363	7.8	0.766	0.594
R8A-164/190	0.066	259.	0.819	0.242	0.605	176.	0.880	0.387	0.760	8.4	0.825	0.291
R8A-432/458	0.254	631.	1.996	0.169	0.423	199.	0.995	0.866	1.701	11.2	1.099	1.827
R8B-333/359	0.146	335.	1.060	0.253	0.633	206.	1.030	0.936	1.839	10.6	1.041	0.845
R8B-515/541	0.173	338.	1.069	0.416	1.040	219.	1.095	0.449	0.882	11.5	1.129	0.046
R3C-380/407	0.055	186.	0.588	0.210	0.525	127.	0.635	0.278	0.546	6.0	0.589	0.903
R3D-219/246	0.070	252.	0.797	0.341	0.853	186.	0.930	0.316	0.621	8.9	0.874	0.227
R3D-287/314	0.134	334.	1.057	0.659	1.648	251.	1.256	0.328	0.644	12.7	1.247	0.675
R5C-219/246	0.161	290.	0.917	0.487	1.217	197.	0.985	0.248	0.487	10.2	1.001	0.317
R5C-282/309	0.101	257.	0.813	0.508	1.270	189.	0.945	0.295	0.580	9.3	0.913	0.295
R5D-225/252	0.181	368.	1.164	0.508	1.270	235.	1.175	0.387	0.760	12.4	1.217	0.235
R5D-294/321	0.203	325.	1.028	0.498	1.245	208.	1.040	0.461	0.906	11.2	1.099	0.081
R6A-562/589	0.067	219.	0.693	0.479	1.197	176.	0.880	0.327	0.642	8.4	0.825	0.306
R6C-529/556	0.147	368.	1.164	0.811	2.027	272.	1.361	1.039	2.041	14.0	1.374	2.437
R8C-378/405	0.497	775.	2.451	0.239	0.598	207.	1.035	0.762	1.497	13.9	1.364	2.650
R8C-476/503	0.089	137.	0.433	0.214	0.535	82.	0.410	0.190	0.373	4.0	0.393	1.647

Table 26 (Cont'd.)

Ridge ID	I_C/I_F	σ_M	Norm σ_M	ϵ_M	Norm ϵ_M	σ_R	Norm σ_R	E_T	Norm E_T	I_T	Norm I_T	Total Res
R8D-534/561	0.270	241.	0.762	0.200	0.500	123.	0.615	0.312	0.613	7.0	0.687	0.702
R9A-341/368	0.164	265.	0.838	0.488	1.220	182.	0.910	0.645	1.267	9.5	0.933	0.159
R9B-385/412	0.000	289.	0.914	0.701	1.752	0.	0.000	0.380	0.747	0.0	0.000	0.638
R9C-426/453	0.065	284.	0.898	0.468	1.170	216.	1.080	0.446	0.876	10.3	1.011	0.061
R10A-351/378	0.169	348.	1.101	0.685	1.712	258.	1.291	0.539	1.059	13.5	1.325	0.711
R10B-351/378	0.088	313.	0.990	0.415	1.037	240.	1.200	0.658	1.293	11.7	1.149	0.149
R10C-316/343	0.099	253.	0.800	0.366	0.915	179.	0.895	0.346	0.680	8.8	0.864	0.179
R10D-325/352	0.190	346.	1.094	0.317	0.792	205.	1.025	0.341	0.670	10.9	1.070	0.166

Table 27

NORMALIZED ERRORS
STRAIN RATE = (10E-5)/SEC TEMPERATURE = -20°C

Ridge ID	I_C/I_F	σ_M	Norm σ_M	ϵ_M	Norm ϵ_M	σ_R	Norm σ_R	E_T	Norm E_T	I_T	Norm I_T	Total Res
R1C-065/092	0.298	574.	1.459	0.181	0.562	209.	0.840	2.364	3.426	12.2	0.961	6.316
R1D-071/098	0.404	622.	1.581	0.205	0.637	195.	0.784	1.164	1.687	12.3	0.969	0.990
R3C-128/155	0.101	429.	1.091	0.332	1.031	307.	1.234	0.457	0.662	15.1	1.189	0.214
R3D-129/156	0.004	291.	0.740	0.249	0.773	243.	0.977	0.392	0.568	10.9	0.858	0.326
R5D-121/148	0.071	412.	1.047	0.234	0.727	275.	1.105	0.848	1.229	13.2	1.039	0.142
R6A-461/488	0.107	330.	0.839	0.279	0.866	220.	0.884	0.447	0.648	10.9	0.858	0.201
R8C-165/192	0.135	518.	1.317	0.324	1.006	323.	1.298	0.568	0.823	16.4	1.291	0.306
R8D-192/219	0.142	475.	1.208	0.244	0.758	289.	1.161	0.909	1.317	14.8	1.165	0.256
R9A-125/152	0.000	365.	0.928	0.474	1.472	356.	1.431	0.564	0.817	15.5	1.220	0.495
R9B-043/070	0.012	338.	0.859	0.435	1.351	304.	1.222	0.966	1.400	13.8	1.087	0.360
R10A-195/222	0.133	312.	0.793	0.268	0.832	213.	0.856	0.400	0.580	10.8	0.850	0.291
R10D-157/184	0.114	369.	0.938	0.474	1.472	275.	1.105	0.493	0.714	13.7	1.079	0.325
R1C-210/236	0.187	385.	0.979	0.257	0.798	209.	0.840	0.408	0.591	11.1	0.874	0.250
R1C-240/266	0.180	451.	1.147	0.225	0.699	262.	1.053	2.312	3.351	13.9	1.094	5.650
R1D-209/236	0.281	534.	1.358	0.210	0.652	237.	0.952	0.633	0.917	13.6	1.071	0.263
R1D-315/342	0.191	229.	0.582	0.258	0.801	131.	0.526	0.521	0.755	7.0	0.551	0.700
R3D-250/277	0.104	440.	1.119	0.341	1.059	315.	1.266	0.381	0.552	15.5	1.220	0.337
R3D-318/345	0.134	454.	1.154	0.522	1.621	332.	1.334	0.442	0.641	16.8	1.323	0.755
R5C-328/355	0.250	390.	0.992	0.303	0.941	194.	0.780	2.768	4.012	10.9	0.858	9.142
R5D-255/282	0.116	390.	0.992	0.469	1.457	281.	1.129	0.397	0.575	14.0	1.102	0.416
R5D-325/352	0.175	462.	1.175	0.410	1.273	278.	1.117	0.436	0.632	14.6	1.150	0.277
R8C-508/535	0.328	241.	0.613	0.189	0.587	94.	0.378	0.347	0.503	5.6	0.441	1.267
R8D-477/504	0.219	173.	0.440	0.318	0.988	119.	0.478	0.331	0.480	6.5	0.512	1.095
R8D-565/592	0.203	389.	0.989	0.239	0.742	191.	0.768	0.610	0.884	10.3	0.811	0.170
R9B-449/476	0.080	297.	0.755	0.308	0.957	209.	0.840	0.440	0.638	10.1	0.795	0.261
R9C-395/422	0.165	421.	1.070	0.346	1.075	272.	1.093	0.735	1.065	14.2	1.118	0.037
R9D-317/344	0.145	362.	0.920	0.381	1.183	236.	0.948	0.504	0.730	12.1	0.953	0.117
R10A-320/347	0.177	457.	1.162	0.253	0.786	220.	0.884	0.533	0.772	11.6	0.913	0.145
R10B-418/445	0.100	536.	1.363	0.573	1.780	427.	1.716	0.423	0.613	20.9	1.646	1.819

Table 28

NORMALIZED ERRORS
STRAIN RATE = (10E-3)/SEC TEMPERATURE = -5°C

Ridge ID	I_C/I_F	σ_M	Norm σ_M	ϵ_M	Norm ϵ_M	σ_R	Norm σ_R	E_T	Norm E_T	I_T	Norm I_T	Total Res
R1B-131/157	1.253	1222.	1.389	0.211	1.476	172.	0.970	0.883	0.874	17.4	1.267	0.465
R3A-188/213	0.667	927.	1.054	0.140	0.979	203.	1.144	1.089	1.078	15.2	1.106	0.042
R3B-130/155	0.364	870.	0.989	0.123	0.860	245.	1.381	1.140	1.129	15.0	1.092	0.190
R4B-299/325	1.268	885.	1.006	0.126	0.881	103.	0.581	1.016	1.006	10.5	0.764	0.246
R2C-049/076	0.430	654.	0.743	0.145	1.014	159.	0.896	0.643	0.637	10.2	0.742	0.275
R2D-134/161	0.653	733.	0.833	0.149	1.042	155.	0.874	0.708	0.701	11.5	0.837	0.162
R4C-309/336	0.587	847.	0.963	0.209	1.462	208.	1.172	0.670	0.663	14.8	1.077	0.363
R6A-398/425	1.017	789.	0.897	0.135	0.944	107.	0.603	0.929	0.920	9.7	0.706	0.264
R6A-504/531	0.500	829.	0.942	0.175	1.224	217.	1.223	0.717	0.710	14.6	1.063	0.191
R7D-088/114	0.692	1014.	1.152	0.160	1.119	221.	1.246	1.772	1.754	16.8	1.223	0.717
R9C-080/107	0.428	902.	1.025	0.185	1.294	256.	1.443	0.833	0.825	16.4	1.194	0.351
R9D-082/109	1.247	847.	0.963	0.160	1.119	102.	0.575	0.791	0.783	10.3	0.750	0.306
R1B-216/241	0.704	856.	0.973	0.149	1.042	179.	1.009	0.953	0.944	13.7	0.997	0.006
R1B-243/268	0.909	982.	1.116	0.122	0.853	148.	0.834	1.257	1.245	12.7	0.924	0.128
R2A-285/310	2.206	1244.	1.414	0.193	1.350	102.	0.575	1.008	0.998	14.7	1.070	0.479
R2B-438/464	1.118	969.	1.101	0.152	1.063	144.	0.812	1.024	1.014	13.7	0.997	0.050
R3A-401/427	0.850	890.	1.012	0.123	0.860	160.	0.902	1.248	1.236	13.3	0.968	0.086
R3B-239/265	0.477	834.	0.948	0.133	0.930	255.	1.437	1.007	0.997	16.9	1.230	0.252
R3B-331/357	0.801	940.	1.068	0.152	1.063	209.	1.178	1.073	1.062	16.9	1.230	0.097
R4A-398/423	0.977	754.	0.857	0.161	1.126	134.	0.755	0.734	0.727	11.9	0.866	0.189
R4B-358/384	1.436	750.	0.852	0.142	0.993	95.	0.535	0.859	0.850	10.4	0.757	0.319
R5A-473/499	0.789	846.	0.962	0.144	1.007	178.	1.003	0.953	0.944	14.3	1.041	0.006
R5B-370/396	0.934	793.	0.901	0.130	0.909	145.	0.817	0.976	0.966	12.6	0.917	0.059
R7A-232/258	0.662	723.	0.822	0.145	1.014	134.	0.755	0.656	0.650	10.0	0.728	0.289
R8A-305/331	0.266	590.	0.671	0.113	0.790	243.	1.370	0.916	0.907	13.8	1.005	0.298
R8B-300/326	0.344	554.	0.630	0.260	1.818	241.	1.358	0.531	0.526	14.5	1.055	1.163
R2C-196/223	0.573	862.	0.980	0.145	1.014	187.	1.054	0.804	0.796	13.2	0.961	0.047

Table 28 (Cont'd.)

Ridge ID	I_C/I_F	σ_M	Norm σ_M	ϵ_M	Norm ϵ_M	σ_R	Norm σ_R	E_T	Norm E_T	I_T	Norm I_T	Total Res
R2C-278/305	0.468	691.	0.785	0.174	1.217	199.	1.122	0.618	0.612	13.1	0.954	0.261
R2D-334/371	0.820	752.	0.855	0.165	1.154	126.	0.710	0.657	0.650	10.3	0.750	0.314
R4C-414/441	0.415	740.	0.841	0.152	1.063	211.	1.189	0.854	0.846	13.4	0.975	0.090
R4C-512/539	1.819	841.	0.956	0.139	0.972	86.	0.485	1.011	1.001	10.9	0.793	0.311
R4D-495/522	0.000	631.	0.717	0.141	0.986	0.	0.000	0.704	0.697	0.0	0.000	0.172
R7C-143/170	0.567	1029.	1.170	0.220	1.538	282.	1.590	0.749	0.742	19.8	1.441	0.928
R7C-541/568	0.898	1001.	1.138	0.154	1.077	176.	0.992	1.035	1.025	15.0	1.092	0.034
R7D-223/250	0.655	938.	1.066	0.235	1.643	240.	1.353	0.632	0.626	17.8	1.296	0.770
R7D-312/339	0.606	994.	1.130	0.165	1.154	236.	1.330	0.867	0.858	17.0	1.237	0.226
R9A-445/482	1.200	643.	0.731	0.149	1.042	89.	0.502	0.685	0.678	8.8	0.641	0.555
R9C-332/359	0.697	695.	0.790	0.195	1.364	155.	0.874	0.584	0.578	11.8	0.859	0.390
R9D-249/276	1.160	770.	0.875	0.170	1.189	101.	0.569	0.687	0.680	9.8	0.713	0.421
R10A-269/296	0.492	987.	1.122	0.180	1.259	287.	1.618	0.947	0.938	19.2	1.398	0.625
R10B-274/301	0.548	974.	1.107	0.174	1.217	265.	1.494	0.932	0.923	18.4	1.339	0.423
R10D-231/258	1.193	903.	1.026	0.175	1.224	136.	0.767	0.874	0.865	13.4	0.975	0.124

Table 29

NORMALIZED ERRORS
STRAIN RATE = (10E-3)/SEC TEMPERATURE = -20°C

Ridge ID	I _C /I _F	σ _M	Norm σ _M	ε _M	Norm ε _M	σ _R	Norm σ _R	E _T	Norm E _T	I _T	Norm I _T	Total Res
R6A-531/558	0.900	1217.	0.863	0.158	0.756	212.	0.830	1.489	1.312	18.1	0.810	0.241
R9B-076/103	2.786	1134.	0.804	0.240	1.148	97.	0.380	0.751	0.662	16.5	0.738	0.628
R9C-049/076	0.784	1509.	1.070	0.269	1.287	295.	1.155	0.925	0.815	23.6	1.056	0.149
R9D-150/177	0.935	1592.	1.129	0.224	1.072	259.	1.014	1.310	1.154	22.5	1.007	0.046
R10B-084/111	1.331	1493.	1.058	0.209	1.000	233.	0.912	1.392	1.226	24.4	1.092	0.071
R2C-226/253	1.036	1510.	1.071	0.249	1.191	220.	0.861	0.844	0.744	20.1	0.899	0.137
R2D-406/433	1.704	1122.	0.795	0.234	1.120	126.	0.493	0.719	0.633	15.3	0.685	0.547
R4C-482/509	0.688	1449.	1.027	0.220	1.053	321.	1.257	1.068	0.941	24.3	1.087	0.080
R4D-382/409	0.880	1457.	1.033	0.274	1.311	292.	1.143	0.803	0.707	24.6	1.101	0.214
R6C-559/586	1.097	1449.	1.027	0.255	1.220	239.	0.936	1.043	0.919	22.5	1.007	0.060
R7C-457/484	2.014	1669.	1.183	0.305	1.459	187.	0.732	0.848	0.747	25.3	1.132	0.398
R7D-254/281	0.550	1323.	0.938	0.294	1.407	375.	1.468	0.702	0.619	26.0	1.163	0.561
R7D-546/573	0.986	1503.	1.066	0.240	1.148	266.	1.041	0.959	0.845	23.7	1.060	0.056
R9C-507/534	0.475	1374.	0.974	0.199	0.952	334.	1.308	1.129	0.995	22.1	0.989	0.098
R10A-407/434	0.646	1462.	1.037	0.269	1.287	391.	1.531	0.797	0.702	28.8	1.289	0.537
R10B-449/476	0.755	1466.	1.039	0.230	1.100	282.	1.104	0.919	0.810	22.2	0.993	0.059
R10C-506/533	0.934	1235.	0.876	0.225	1.077	241.	0.943	0.758	0.668	20.9	0.935	0.139
R10D-508/535	1.090	1315.	0.932	0.199	0.952	228.	0.893	1.249	1.100	21.4	0.957	0.030

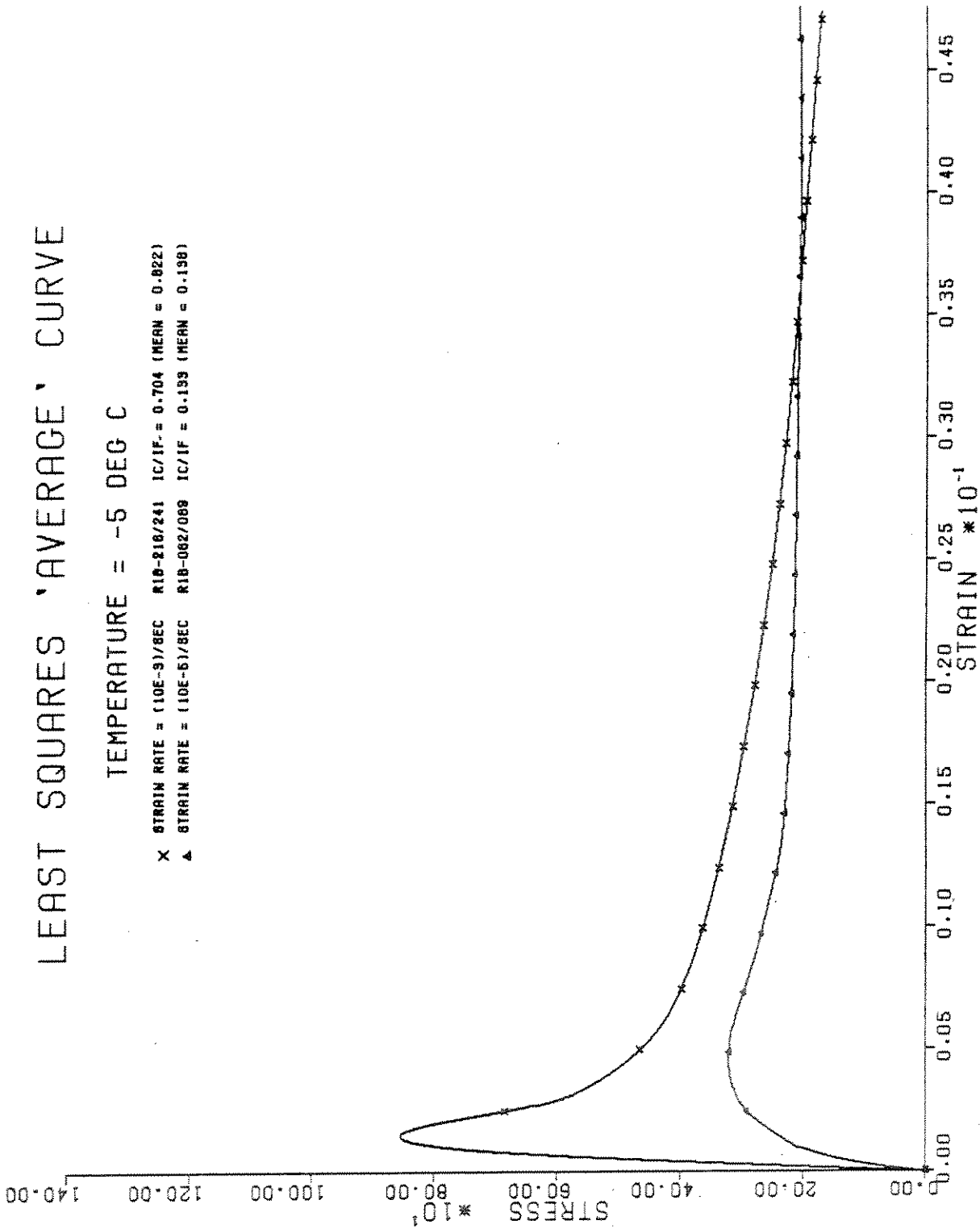


Fig. 31 - Least squares "average" stress-strain curve of multi-year ridge ice for $\dot{\epsilon} = 10^{-5}/\text{sec}$ and $\dot{\epsilon} = 10^{-3}/\text{sec}$ at $T = -5^\circ\text{C}$.

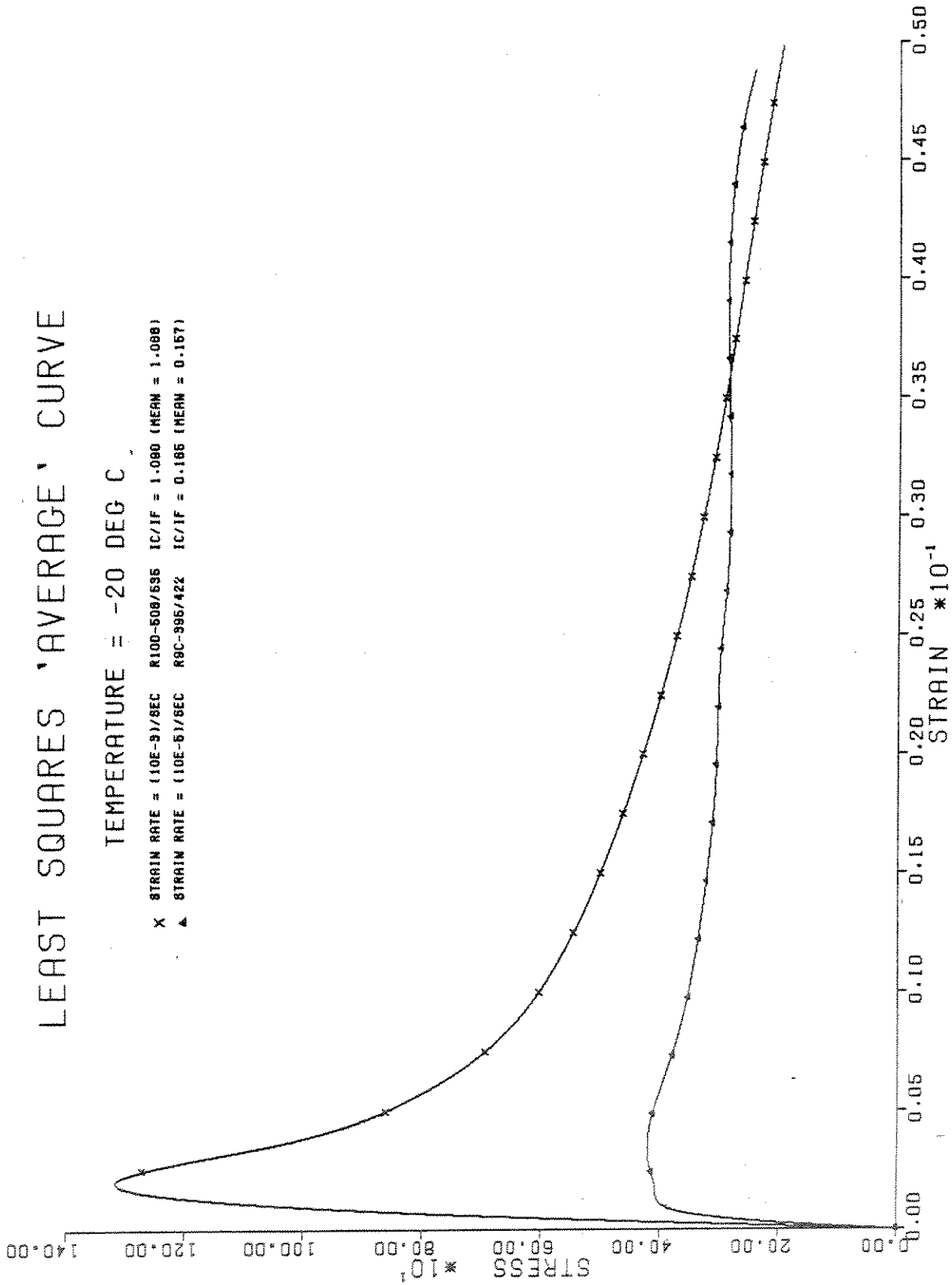


Fig. 32 - Least squares "average" stress-strain curve of multi-year ridge ice for $\dot{\epsilon} = 10^{-5}$ /sec and $\dot{\epsilon} = 10^{-3}$ /sec at $T = -20^{\circ}\text{C}$.

Table 30

COMPARISON OF RESIDUAL ERROR
FOR THE TWO AVERAGING TECHNIQUES

Test Condition	Point by Point Averaging	Least Square Averaging
C55	.100	.033
C520	.060	.037
C35	.083	.006
C320	.046	.030

Table 31

STRUCTURAL CLASSIFICATION SCHEME FOR
MULTI-YEAR PRESSURE RIDGE ICE SAMPLES

Ice Type	Code	Structural Characteristics
Granular	1	Isotropic, equiaxed crystals
Columnar	2	Elongated, columnar grains
	2A	Columnar sea ice with c-axes normal to growth direction. Axes may not be aligned
	2B	Columnar sea ice having random c-axis orientation (Transition ice)
	2C	Columnar freshwater ice. May be either anisotropic or isotropic
Mixed	3	Combination of Types I and II
	3A	Largely Type II with granular veins
	3B	Largely Type I with inclusions of Type I or II ice (brecciated ice).

square error for each test condition. Comparison of the errors for each test condition shows that the least square method of selecting an average curve provides a better "average" since this method yields a curve which better reflects the average primary mechanical properties.

Tables 26-29 contain the values of I_C/I_F for each test in addition to the residual errors. These tables suggest that the quantity I_C/I_F provides another possible method of choosing an average stress-strain curve. Tests with low residual errors have values of I_C/I_F very close to the mean value of I_C/I_F .

PHYSICAL PROPERTIES

It is well documented in the literature (e.g., see Weeks and Ackley⁹) that the physical properties of ice significantly affect its mechanical response. The six physical properties most commonly recorded to characterize an ice sample are salinity, density, brine volume, air volume, total porosity, and crystal structure. The crystal structure of an ice sample depends greatly on the temperature and other environmental conditions at the time of crystallization. However, once the structure is formed, it can exist over a wide range of temperatures and can be considered independent of temperature. The other five properties are governed by the phase diagrams for solid seawater and consequently are functions of temperature. Frankenstein and Garner¹⁰ have derived an equation relating salinity and brine volume in the temperature range from -2°C to -30°C . Over this same temperature range, Cox and Weeks⁶ have derived equations to calculate the air volume if the salinity and density are known. Once the air volume is known, the total porosity can be calculated as the sum of the air and brine volumes. Thus, we see that of the five temperature dependent physical properties, only two are independent. Any two of these properties along with the crystal structure are sufficient to describe the effects of physical properties on the mechanical response of ice.

Given the temperature, it is easy to specify the temperature dependent physical properties from a few simple laboratory measurements and application of the equations referred to above. Specifying the crystal structure is not as straightforward since a classification scheme has to be developed which accounts for crystal shape (e.g., columnar, granular), c-axis orientation, and grain size. Previously, Cherepanov¹¹ and Michel¹² have devised

classification schemes for undeformed ice, but these are not suitable for multi-year ridge ice. In addition to continuous regions of granular and columnar ice types, multi-year ridge ice can contain regions of discontinuous structure such as snow filled voids, block interfaces, and healed cracks. Richter and Cox³ have developed a classification scheme to encompass all possible ice types in multi-year pressure ridges. Their scheme is summarized in Table 31 and is applied to high, intermediate, and low strength samples from test conditions C55 and C35 in Tables 32 and 33, respectively.

The salinity, density, brine volume, air volume, and porosity are listed for each test in Tables 34-37 according to test conditions. Since these properties depend on temperature, the data from the two pairs of test conditions with the same temperature can be combined into a single data file. Descriptive statistics are calculated for each of the combined data files and are summarized in Tables 38 and 39 for -5°C and -20°C , respectively. These two tables also contain a similar statistical summary of the properties of the samples tested at each strain rate. Comparison of the combined statistics with the statistics for each strain rate indicates that, on the average, the ice tested at different test conditions has the same temperature dependent physical properties.

To demonstrate the effect of physical properties on the mechanical properties, the maximum stress and initial tangent modulus are plotted as functions of the total porosity for each test condition in Figures 33-40. In each figure, a line is drawn to approximate an upper bound for the given mechanical property and test condition. These upper bounds show the maximum stress and initial tangent modulus to decrease with increasing porosity as one would expect. Since strength and the tangent modulus are known to decrease with increasing brine volume, the test samples with a brine volume of less than 5% are distinguished from the others to investigate the possibility of those samples being the upper bound for those properties. The upper bound is determined by low brine volume samples in Figures 34 and 36, but brine volume alone does not determine the upper bound since low brine volume samples are also associated with lower bound values of strength and tangent modulus. Consideration of ice structure would probably explain the lower values of strength and tangent modulus associated with the low brine volume samples.

To demonstrate the effects of crystal structure, the data points having a crystallographic classification are identified in Figures 33, 35, 37,

Table 32

STRENGTH, STRUCTURE, AND POROSITY OF SELECTED RIDGE ICE SAMPLES*
TESTED AT $\dot{\epsilon} = 10^{-5}$ /SEC AND T = -5°C

Ridge ID	Strength (lbf/in ²)	Ice Type	Grain Size (mm)	Porosity (%/°°)
<u>High Strength</u>				
R1B-320/346	1090	2A-Aligned 0° Elongation	55 × 10	25.3
R5B-075/101	774	2A-Aligned 5° Elongation	17 × 6	72.3
R1B-429/455	696	2A 5° Elongation	15 × 10	23.7
R8A-432/458	657	2A-Aligned 5° Elongation	30 × 5	24.5
R5A-165/191	619	2A 0° Elongation	15 × 3	16.9
R7A-342/368	607	2C 0° Elongation	2 to 20	24.4
<u>Intermediate Strength</u>				
R3B-363/387	394	3B	< 1	15.3
R2A-140/165	388	1	2	10.1
R5B-341/367	368	1	< 1	56.1
R7A-059/082	361	1	< 1	69.5
R8B-515/541	348	2B	20 × 5	23.8
<u>Low Strength</u>				
R7B-241/267	229	3	5	77.8
R1A-226/252	214	2A 40° Elongation	25 × 15	19.4
R1A-399/425	214	3	-	38.9
R2B-094/121	171	3B	< 1	143
R7A-263/286	68	3A 40° Elongation	35	154

* From Cox, et al.¹

Table 33

STRENGTH, STRUCTURE, AND POROSITY OF SELECTED RIDGE ICE SAMPLES*
TESTED AT $\dot{\epsilon} = 10^{-3}/\text{SEC}$ AND $T = -5^{\circ}\text{C}$

Ridge ID	Strength (lbf/in ²)	Ice Type	Grain Size (mm)	Porosity (°/%)
<u>High Strength</u>				
R1A-300/326	1580	2A-Aligned 0° Elongation	55 × 10	20.3
R7B-440/466	1540	2A-Aligned 5° Elongation	45 × 10	32.0
R8B-483/509	1440	2A-Aligned 15° Elongation	50 × 15	25.6
R8A-384/410	1297	2A 0° Elongation	40 × 10	24.2
R2A-285/310	1270	2A 10° Elongation	25 × 15	22.3
R1A-175/201	1270	2A 80° Elongation	-	16.2
R5B-141/167	1270	2A 0° Elongation	45 × 25	21.1
<u>Intermediate Strength</u>				
R3B-331/357	971	3B	< 1	31.4
R3A-188/213	970	3	5	23.5
R3A-401/427	925	3	< 1	21.0
R1B-216/241	915	2A 40° Elongation	35 × 20	16.3
R4B-299/325	910	3	2 to 10	56.2
R4B-420/466	910	3A	35 × 10	53.0
<u>Low Strength</u>				
R8B-300/326	587	3	-	15.1
R7B-175/201	557	2C 50° Elongation	5	23.3
R7B-072/098	487	3	-	53.4
R2A-110/135	408	1	< 1	86.9
R8A-033/059	346	3	-	75.2

* From Cox, et al.¹

Table 34

PHYSICAL PROPERTIES
STRAIN RATE = (10E-5)/SEC TEMPERATURE = -5°C

Ridge ID	Salinity Test SX (0/00)	Density Test SX (lb/ft ³)	Brine Volume (0/00)	Air Volume (0/00)	Porosity (0/00)	Ice Type
R1A-062/089	1.80	55.05	17.1	41.9	59.0	
R1B-062/089	0.30	54.54	2.8	48.4	51.3	
R2A-140/165	0.10	56.77	1.0	9.1	10.1	1
R2B-094/121	0.44	49.35	3.7	139.2	143.0	3B
R3A-106/131	0.60	55.61	5.8	30.1	35.9	
R3B-161/187	1.13	56.92	11.1	8.1	19.2	
R4A-312/338	1.60	53.92	14.9	61.2	76.1	
R4B-328/354	1.57	56.11	15.2	22.9	38.1	
R5A-165/191	0.41	56.58	4.0	12.9	16.9	2A
R5B-075/101	1.80	54.26	16.9	55.5	72.3	2A
R7A-059/085	1.70	54.37	15.9	53.6	69.5	1
R7B-126/152	0.40	51.90	3.6	94.6	98.2	
R8A-133/159	1.00	55.95	9.7	24.8	34.5	
R8B-162/189	0.82	56.36	8.0	17.4	25.4	
R3C-095/122	0.54	54.87	5.1	42.9	48.0	
R3D-159/186	0.26	49.39	2.2	138.2	140.5	
R5C-039/066	1.27	53.10	11.6	75.0	86.6	
R5D-159/186	0.58	56.15	5.6	20.7	26.3	
R6C-166/193	0.45	50.74	3.9	114.8	118.8	
R8C-048/075	0.56	54.28	5.2	53.4	58.6	
R8D-236/263	0.50	54.74	4.7	45.1	49.8	
R1A-226/252	1.26	57.00	12.4	7.0	19.4	2A
R1A-399/425	2.40	56.62	23.4	15.4	38.9	3
R2A-205/230	0.38	55.32	3.6	35.0	38.6	
R2A-314/339	2.10	56.79	20.6	12.0	32.5	
R2B-408/434	0.80	55.82	7.7	26.9	34.6	
R2B-468/494	0.70	55.91	6.8	25.2	32.0	
R3A-220/245	1.61	57.06	15.8	6.5	22.3	
R3A-430/456	2.18	56.21	21.1	22.2	43.3	
R3B-363/389	0.89	56.99	8.7	6.5	15.3	3B
R4A-426/452	1.30	55.79	12.5	28.2	40.8	
R4B-391/417	2.27	56.42	22.1	18.7	40.8	
R4B-449/475	1.83	56.51	17.8	16.4	34.2	
R5A-397/423	0.80	56.44	7.8	16.0	23.8	
R5A-442/468	1.09	56.73	10.7	11.4	22.1	
R5A-504/530	1.23	56.47	12.0	16.1	28.1	
R5B-341/367	0.79	54.57	7.4	48.7	56.1	1
R5B-398/423	1.13	56.37	11.0	17.7	28.7	
R7A-263/289	3.03	50.22	26.3	127.6	153.9	3A
R7A-342/368	1.05	56.57	10.2	14.1	24.4	2C
R7B-241/267	1.30	53.63	12.0	65.8	77.8	3
R8A-164/190	1.20	56.45	11.7	16.4	28.1	
R8A-432/458	1.80	57.06	17.1	6.8	24.5	2A
R8B-333/359	1.50	57.04	14.8	6.7	21.4	

Table 34 (cont'd)

Ridge ID	Salinity Test SX (0/00)	Density Test SX (lb/ft ³)	Brine Volume (0/00)	Air Volume (0/00)	Porosity (0/00)	Ice Type
R8B-515/541	1.80	57.10	17.7	6.1	23.8	2B
R3C-296/323	1.62	55.91	15.6	26.5	42.2	
R3C-380/407	1.28	55.33	12.2	36.1	48.3	
R3D-219/246	1.28	53.43	11.8	69.3	81.1	
R3D-287/314	1.36	56.05	13.1	23.7	36.8	
R5C-219/246	1.29	55.67	12.4	30.2	42.6	
R5C-282/309	3.64	56.14	35.3	25.8	61.0	
R5D-225/252	1.37	56.35	13.3	18.5	31.8	
R5D-294/321	1.73	56.72	16.9	12.7	29.6	
R6A-562/589	2.38	54.01	22.2	60.9	83.1	
R6C-529/556	0.86	56.14	8.3	21.3	29.7	
R8C-378/405	1.44	56.77	14.1	11.3	25.4	
R8C-476/503	1.86	57.20	18.4	4.5	22.9	
R8D-446/473	1.95	56.62	19.0	14.7	33.8	
R8D-534/561	1.96	56.80	19.2	11.6	30.8	
R9A-341/368	0.65	53.71	6.0	63.5	69.5	
R9B-385/412	0.72	54.65	6.8	47.2	54.0	
R9C-426/453	1.08	56.31	10.5	18.7	29.2	
R9D-181/208	1.39	56.67	13.6	13.0	26.6	
R10A-351/378	0.27	56.75	2.6	9.8	12.4	
R10B-351/378	0.89	56.85	8.7	9.0	17.8	
R10C-316/343	2.89	56.58	28.2	17.0	45.2	
R10D-325/352	1.61	56.56	15.7	15.2	30.9	

Table 35

PHYSICAL PROPERTIES
STRAIN RATE = (10E-5)/SEC TEMPERATURE = -20°C

Ridge ID	Salinity Test SX (0/00)	Density Test SX (lb/ft ³)	Brine Volume (0/00)	Air Volume (0/00)	Porosity (0/00)	Ice Type
R1C-065/092	0.27	55.94	0.9	25.9	26.8	
R1D-071/098	0.61	56.61	2.0	14.6	16.6	
R3C-128/155	0.74	56.13	2.4	23.1	25.6	
R3D-129/156	0.14	49.65	0.4	135.4	135.8	
R5C-097/124	0.28	53.38	0.9	70.6	71.4	
R5D-121/148	0.53	55.91	1.7	26.7	28.5	
R6A-461/488	1.05	54.67	3.4	48.8	52.2	
R8C-165/192	0.88	54.44	2.8	52.7	55.5	
R8D-192/219	0.83	54.72	2.7	47.7	50.4	
R9A-125/152	0.04	50.96	0.1	112.5	112.6	
R9B-043/070	0.02	51.65	0.1	100.4	100.5	
R10A-195/222	0.53	56.20	1.7	21.7	23.4	
R10D-157/184	0.69	56.76	2.3	12.1	14.4	
R1C-210/236	1.10	55.40	3.6	36.1	39.7	
R1C-240/266	1.55	55.88	5.1	28.2	33.3	
R1D-209/236	0.99	56.01	3.2	25.4	28.6	
R1D-315/342	2.21	56.53	7.3	17.6	24.9	
R3C-329/359	1.69	55.94	5.5	27.4	32.9	
R3C-411/438	1.36	56.55	4.5	16.4	20.9	
R3D-250/277	1.59	55.85	5.2	28.8	34.0	
R3D-318/345	1.45	56.60	4.8	15.6	20.4	
R5C-250/277	1.55	56.55	5.1	16.6	21.7	
R5C-328/355	3.88	57.00	12.9	11.1	24.0	
R5D-255/282	1.69	56.22	5.5	22.5	28.5	
R5D-325/352	1.44	56.83	4.8	11.6	16.4	
R6A-661/688	2.83	54.39	9.0	55.4	64.4	
R6C-589/616	1.63	56.52	5.4	12.0	17.4	
R8C-444/471	1.48	56.56	4.9	16.4	21.3	
R8C-508/535	2.61	56.84	8.7	12.6	21.3	
R8D-477/504	1.95	57.10	6.5	7.4	14.0	
R8D-565/592	1.45	56.81	4.8	12.0	16.8	
R9A-523/550	0.81	55.83	2.6	28.4	31.1	
R9B-449/476	1.57	55.09	5.1	42.0	47.1	
R9C-395/422	1.09	55.77	3.6	29.7	33.3	
R9D-317/344	1.11	55.35	3.6	37.1	40.6	
R10A-320/347	1.23	56.92	4.1	9.9	14.0	
R10B-418/445	0.28	56.62	0.9	14.1	15.1	

Table 36

PHYSICAL PROPERTIES

STRAIN RATE = (10E-3)/SEC TEMPERATURE = -5°C

Ridge ID	Salinity Test SX (0/00)	Density Test SX (lb/ft ³)	Brine Volume (0/00)	Air Volume (0/00)	Porosity (0/00)	Ice Type
R1A-175/201	0.70	56.81	6.9	9.4	16.2	2A
R1B-131/157	0.37	56.82	3.6	8.7	12.3	
R2A-110/135	0.20	52.43	1.8	85.0	86.9	1
R2B-135/161	0.10	55.81	1.0	25.8	26.8	
R3A-188/213	1.40	56.85	13.7	9.8	23.5	3
R3B-130/155	1.13	56.28	11.0	19.3	30.3	
R4A-283/309	1.30	53.58	12.0	66.7	78.7	
R4B-299/325	1.30	54.89	12.3	43.9	56.2	3
R5A-135/161	0.20	56.10	1.9	20.9	22.9	
R5B-141/167	0.20	56.20	1.9	19.2	21.1	2A
R7A-005/031	0.02	52.92	0.2	76.2	76.4	
R7B-072/098	0.48	54.53	4.5	48.9	53.4	3
R8A-033/059	0.30	53.16	2.8	72.5	75.2	3A
R8B-011/037	0.10	52.48	0.9	84.0	84.9	
R2C-049/076	0.17	49.93	1.5	130.6	132.1	
R2D-134/161	0.37	52.64	3.4	81.5	84.8	
R4C-244/271	2.58	56.13	25.0	24.3	49.2	
R4C-309/336	0.88	55.43	8.4	33.7	42.1	
R4D-228/255	2.51	55.90	24.2	28.1	52.3	
R7C-007/034	0.10	54.27	0.9	52.9	53.8	
R6A-398/425	0.88	52.18	7.9	90.4	98.3	
R6A-504/531	0.81	53.47	7.5	67.9	75.3	
R7D-088/114	0.64	55.33	6.1	35.1	41.2	
R9C-080/107	0.46	54.67	4.3	46.1	50.4	
R9D-082/109	0.41	53.72	3.8	62.9	66.7	
R1A-300/326	1.00	56.77	9.8	10.5	20.3	2A
R1B-216/241	1.20	57.14	11.8	4.4	16.3	2A
R1B-243/268	1.56	57.14	15.4	5.0	20.4	
R2A-285/310	0.70	56.46	6.8	15.5	22.3	2A
R2A-383/408	2.00	56.81	19.6	11.5	31.1	
R2B-351/377	2.46	56.37	23.9	19.8	43.8	
R2B-438/464	2.70	56.48	26.3	18.3	44.6	
R3A-401/427	1.45	57.03	14.3	6.8	21.0	3
R3B-239/265	2.00	57.13	19.7	5.9	25.6	
R3B-331/357	2.00	56.79	19.6	11.8	31.4	3B
R4A-398/423	1.30	56.03	12.6	23.2	36.5	
R4B-358/384	1.96	56.00	18.9	25.5	44.4	
R4B-420/446	3.30	56.39	32.2	20.8	53.0	3A
R5A-473/499	0.91	55.75	8.8	28.3	37.1	
R5B-287/313	4.00	56.96	39.4	12.1	51.4	
R5B-370/396	1.26	55.09	12.0	40.4	52.3	
R7A-232/258	3.40	49.76	29.2	136.1	165.3	

Table 36 (cont'd)

Ridge ID	Salinity Test SX (0/00)	Density Test SX (lb/ft ³)	Brine Volume (0/00)	Air Volume (0/00)	Porosity (0/00)	Ice Type
R7A-295/321	0.95	54.09	8.9	57.3	66.1	
R7B-175/201	0.13	56.03	1.3	22.0	23.3	2C
R7B-440/466	2.48	57.08	24.4	7.6	32.0	2A
R8A-305/331	1.50	56.70	14.7	12.6	27.2	
R8A-384/410	1.70	57.01	16.7	7.5	24.2	2A
R8B-300/326	0.30	56.61	2.9	12.2	15.1	3
R8B-483/509	2.10	57.0	20.7	4.9	25.6	2A
R2C-196/223	1.04	55.35	9.9	35.4	45.3	
R2C-278/305	2.33	54.66	22.0	49.5	71.5	
R2D-220/247	0.37	54.65	3.5	46.7	50.1	
R2D-334/371	1.90	54.58	17.9	50.3	68.1	
R4C-414/441	3.03	56.76	29.7	14.1	43.7	
R4C-512/539	1.03	55.85	9.9	26.6	36.6	
R4D-495/522	2.92	57.16	28.8	6.9	35.7	
R6C-476/503	0.93	54.44	8.7	51.2	59.9	
R7C-143/170	0.77	56.27	7.5	18.9	26.4	
R7C-541/568	1.15	56.75	11.3	11.2	22.5	
R7D-223/250	2.04	55.49	19.5	34.5	54.0	
R7D-312/339	1.12	54.82	10.6	44.7	55.3	
R9A-445/482	1.05	54.01	9.8	58.8	68.6	
R9B-329/356	0.78	55.00	7.4	41.0	48.4	
R9C-332/359	0.83	54.98	7.9	41.5	49.3	
R9D-249/276	0.96	53.81	8.9	62.2	71.1	
R10A-269/296	0.81	56.39	7.9	16.9	24.8	
R10B-274/301	1.09	56.44	10.6	16.5	27.1	
R10C-445/472	1.99	56.71	19.5	13.2	32.7	
R10D-231/258	1.03	56.61	10.1	13.4	23.5	

Table 37

PHYSICAL PROPERTIES
STRAIN RATE = (10E-3)/SEC TEMPERATURE = -20°C

Ridge ID	Salinity Test SX (0/00)	Density Test SX (lb/ft ³)	Brine Volume (0/00)	Air Volume (0/00)	Porosity (0/00)	Ice Type
R1C-127/154	0.31	56.08	1.0	22.8	23.8	
R1D-153/178	1.00	56.20	3.3	22.1	25.4	
R2C-129/156	0.63	54.62	2.0	50.5	52.5	
R2D-095/122	0.20	53.22	0.6	73.3	73.9	
R4D-198/225	2.31	54.72	7.4	49.2	56.5	
R6A-531/558	1.22	54.37	3.9	54.2	58.1	
R6C-134/161	0.29	52.48	0.9	86.2	87.1	
R7C-092/119	0.82	55.89	2.7	27.4	30.1	
R7D-036/063	0.19	55.16	0.6	39.5	40.1	
R9A-071/098	0.04	50.93	0.1	113.0	113.1	
R9B-076/103	0.03	50.68	0.1	117.4	117.4	
R9C-049/076	0.38	54.81	1.2	45.8	47.0	
R9D-150/177	1.22	55.68	4.0	31.4	35.4	
R10A-238/265	0.81	56.58	2.7	15.4	18.0	
R10B-084/111	0.61	56.33	2.0	19.5	21.5	
R1C-349/375	3.42	56.71	11.3	15.6	27.0	
R1C-384/410	1.94	54.65	6.2	50.0	56.2	
R1D-179/206	1.03	56.63	3.4	14.7	18.1	
R1D-285/312	2.48	57.29	8.3	4.6	12.9	
R2C-226/253	0.89	54.80	2.8	46.4	49.3	
R2C-310/337	2.63	55.15	8.5	42.0	50.5	
R2D-265/292	3.01	55.25	9.7	40.6	50.3	
R2D-406/433	1.61	55.13	5.2	41.4	46.5	
R4C-482/509	1.28	55.92	4.2	27.3	31.5	
R4C-543/570	1.87	56.16	6.1	23.7	29.8	
R4D-382/409	1.15	56.45	3.8	18.0	21.8	
R4D-414/441	0.90	55.25	2.9	38.6	41.5	
R4D-525/552	0.88	56.19	2.9	22.2	25.1	
R6C-559/586	1.70	55.92	5.6	27.7	33.3	
R7C-457/484	1.32	57.04	4.4	7.9	12.3	
R7C-572/599	1.33	56.73	4.4	13.3	17.7	
R7D-254/281	1.21	55.62	3.9	32.5	36.4	
R7D-546/573	1.09	56.72	3.6	13.2	16.8	
R9A-424/451	0.68	54.00	2.1	60.1	62.3	
R9B-417/444	0.62	54.37	2.0	53.6	55.6	
R9C-507/534	1.86	56.77	6.2	13.1	19.3	
R9D-348/375	1.14	55.39	3.7	36.4	40.1	
R10A-407/434	0.22	56.68	0.7	13.0	13.8	
R10B-449/476	0.36	56.70	1.2	12.8	14.0	
R10C-506/533	3.65	57.02	12.2	10.5	22.7	
R10D-508/535	2.35	57.00	7.8	9.6	17.4	

Table 38

STATISTICAL SUMMARY OF PHYSICAL PROPERTIES OF ICE SAMPLES TESTED AT -5°C

Combined Strain Rates										
Variable	N	Mean	Standard Deviation	Minimum Value	Maximum Value	Sum	Kurtosis	Skewness	Variance	C.V.
Salinity	136	1.272	0.818	0.020	4.000	172.930	0.593	0.850	0.669	64.347
Density	136	55.436	1.742	49.350	57.200	7539.350	2.659	-1.638	3.033	3.141
Brine	136	12.224	7.899	0.200	39.400	1662.500	0.573	0.827	62.394	64.617
Airvol	136	34.272	30.095	4.400	139.200	4661.000	2.846	1.681	905.693	87.811
Porosity	136	46.501	29.020	10.100	165.300	6324.100	3.843	1.777	842.155	62.407

Strain Rate = (10E-5)/Sec										
Variable	N	Mean	Standard Deviation	Minimum Value	Maximum Value	Sum	Kurtosis	Skewness	Variance	C.V.
Salinity	67	1.280	0.710	0.100	3.640	85.790	0.980	0.803	0.504	55.441
Density	67	55.482	1.823	49.350	57.200	3717.270	3.476	-1.897	3.324	3.286
Brine	67	12.294	6.825	1.000	35.300	823.700	0.884	0.743	46.578	55.513
Airvol	67	33.488	31.584	4.500	139.200	2243.700	3.490	1.904	997.527	94.313
Porosity	67	45.794	30.837	10.100	153.900	3068.200	3.488	1.849	950.912	67.338

Strain Rate = (10E-3)/Sec										
Variable	N	Mean	Standard Deviation	Minimum Value	Maximum Value	Sum	Kurtosis	Skewness	Variance	C.V.
Salinity	69	1.263	0.916	0.020	4.000	87.140	0.271	0.868	0.840	72.563
Density	69	55.392	1.670	49.760	57.200	3822.080	1.915	-1.362	2.790	3.016
Brine	69	12.157	8.869	0.200	39.400	838.800	0.265	0.859	78.654	72.954
Airvol	69	35.033	28.787	4.400	136.100	2417.300	2.323	1.447	828.686	82.170
Porosity	69	47.187	27.350	12.300	165.300	3255.900	4.749	1.727	748.012	57.961

Table 39

STATISTICAL SUMMARY OF PHYSICAL PROPERTIES OF ICE SAMPLES TESTED AT -20°C

Combined Strain Rates										
Variable	N	Mean	Standard Deviation	Minimum Value	Maximum Value	Sum	Kurtosis	Skewness	Variance	C.V.
Salinity	78	1.229	0.856	0.020	3.880	95.830	1.004	0.990	0.733	69.683
Density	78	55.506	1.594	49.650	57.290	4329.470	3.473	-1.842	2.541	2.872
Brine	78	4.022	2.828	0.100	12.900	313.700	1.101	1.009	7.996	70.309
Airvol	78	34.397	27.448	4.600	135.400	2683.000	3.445	1.838	753.374	79.796
Porosity	78	38.429	26.298	12.300	135.800	2997.500	3.359	1.810	691.605	68.433

Strain Rate = (10E-5)/Sec										
Variable	N	Mean	Standard Deviation	Minimum Value	Maximum Value	Sum	Kurtosis	Skewness	Variance	C.V.
Salinity	37	1.220	0.808	0.020	3.880	45.150	2.158	1.059	0.653	66.220
Density	37	55.572	1.694	49.650	57.100	2056.180	4.618	-2.150	2.869	3.048
Brine	37	4.003	2.671	0.100	12.900	148.100	2.258	1.075	7.132	66.722
Airvol	37	33.149	29.217	7.400	135.400	1226.500	4.594	2.146	853.608	88.138
Porosity	37	37.173	28.036	14.000	135.800	1375.400	4.565	2.134	786.043	75.422

Strain Rate = (10E-3)/Sec										
Variable	N	Mean	Standard Deviation	Minimum Value	Maximum Value	Sum	Kurtosis	Skewness	Variance	C.V.
Salinity	41	1.236	0.907	0.030	3.650	50.680	0.497	0.965	0.823	73.398
Density	41	55.446	1.517	50.680	57.290	2273.290	2.762	-1.566	2.302	2.736
Brine	41	4.039	2.995	0.100	12.200	165.600	0.601	0.988	8.972	74.159
Airvol	41	35.524	26.062	4.600	117.400	1456.500	2.727	1.562	679.254	73.365
Porosity	41	39.563	24.922	12.300	117.400	1622.100	2.549	1.511	621.124	62.993

MPSI PHASE1: UNIAXIAL COMPRESSION
STRAIN RATE = (10E-5/SEC) TEMPERATURE = -5 DEG C

* BRINE VOLUME < 5.0
○ BRINE VOLUME > 5.0

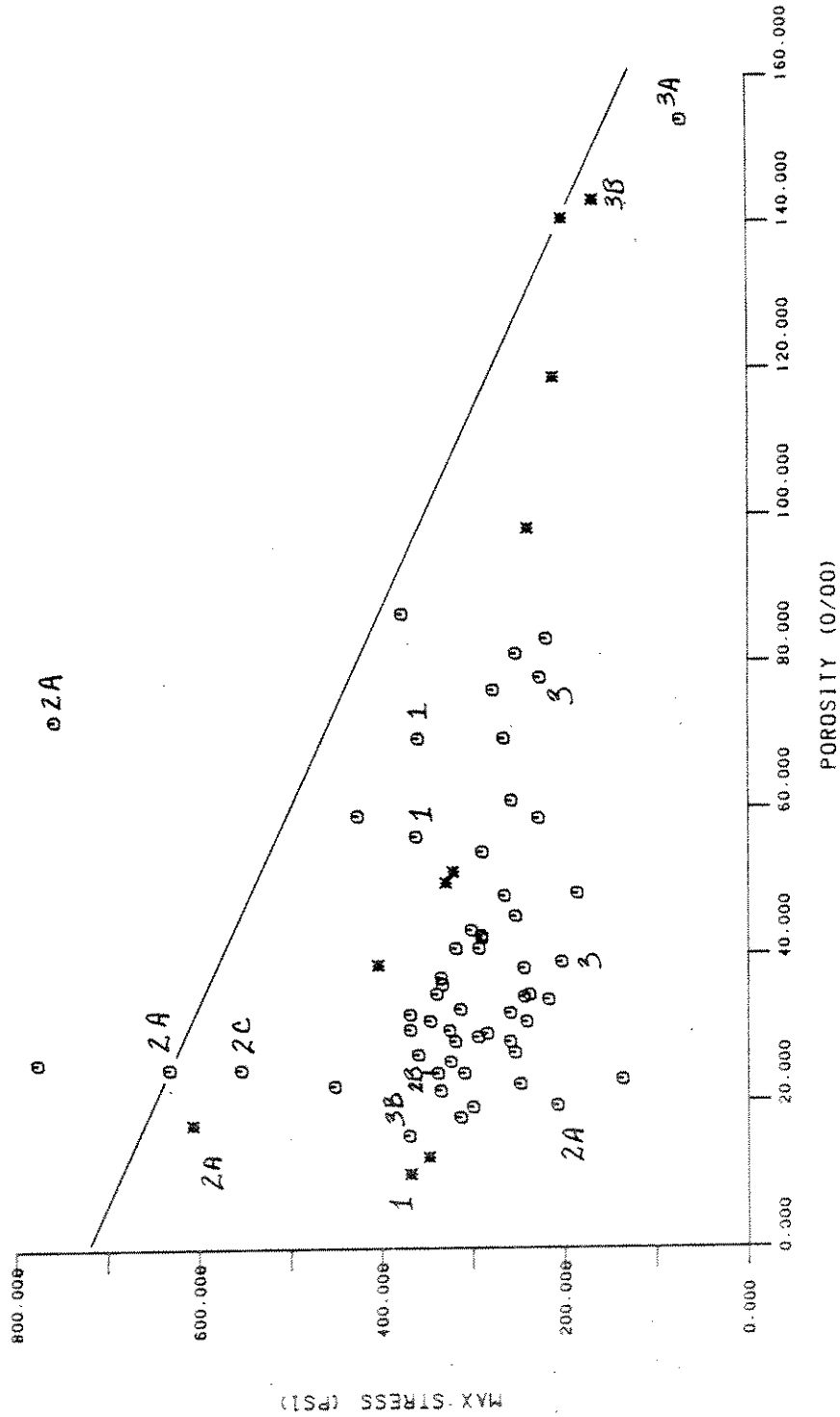


Fig. 33 - Maximum stress as a function of porosity for $\dot{\epsilon} = 10^{-5}/\text{sec}$ and $T = -5^{\circ}\text{C}$.

MPSI PHASE1: UNIAXIAL COMPRESSION
STRAIN RATE = (10E-5/SEC) TEMPERATURE = -20 DEG C

■ BRINE VOLUME < 5.0
○ BRINE VOLUME > 5.0

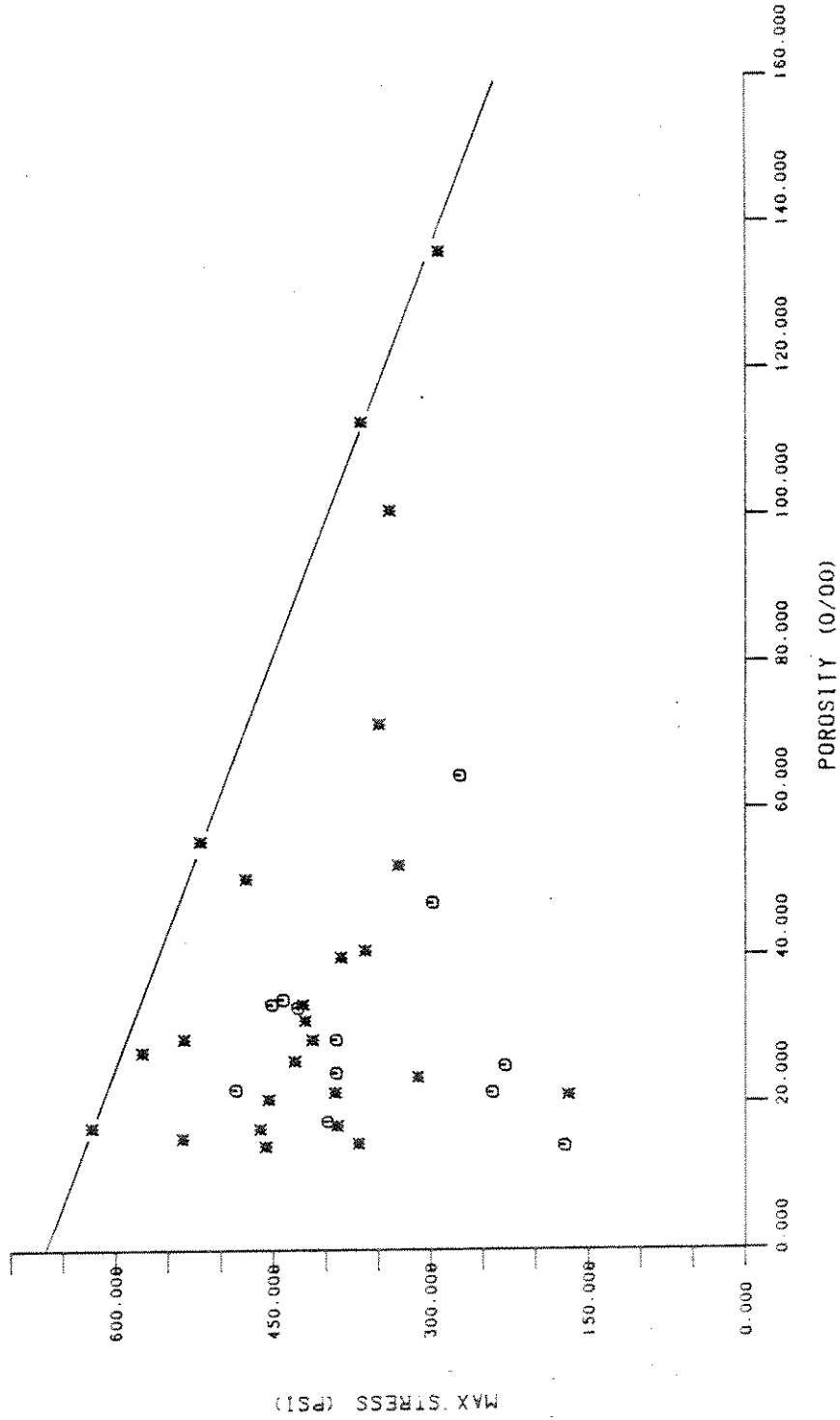


Fig. 34 - Maximum stress as a function of porosity for $\dot{\epsilon} = 10^{-5}/\text{sec}$ and $T = -20^{\circ}\text{C}$.

MPSI PHASE1: UNIAXIAL COMPRESSION
STRAIN RATE = (10E-3/SEC) TEMPERATURE = -5 DEG C

* BRINE VOLUME < 5.0
O BRINE VOLUME > 5.0

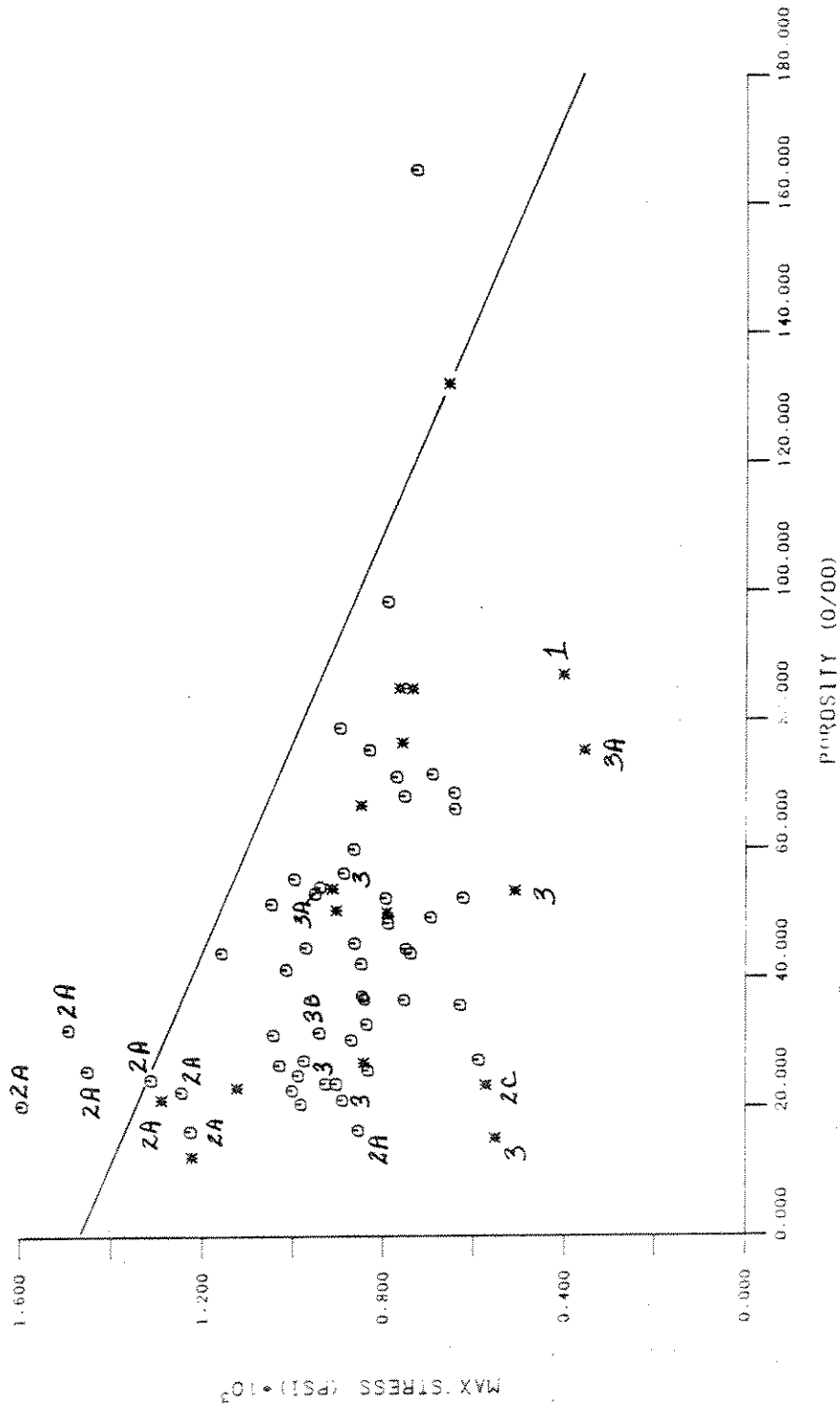


Fig. 35 - Maximum stress as a function of porosity for $\dot{\epsilon} = 10^{-3}/\text{sec}$ and $T = -5^{\circ}\text{C}$.

MPSI PHASE1: UNIAXIAL COMPRESSION
STRAIN RATE=(10E-3)/SEC TEMPERATURE=-20 DEG C

✱ BRINE VOLUME < 5.0
○ BRINE VOLUME > 5.0

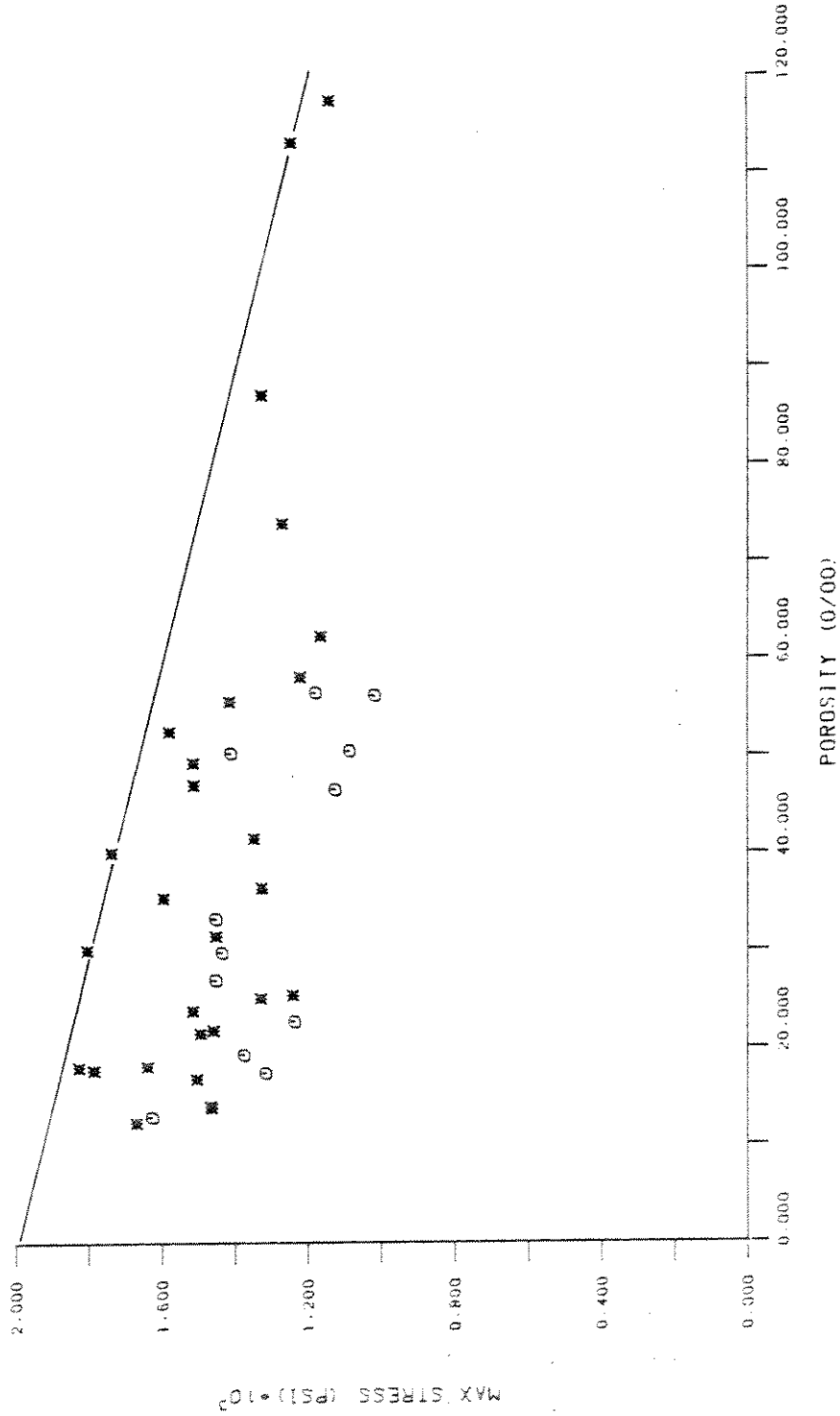


Fig. 36 - Maximum stress as a function of porosity for $\dot{\epsilon} = 10^{-3}/\text{sec}$ and $T = -20^\circ\text{C}$.

MPSI PHASE1: UNIAXIAL COMPRESSION
STRAIN RATE = (10E-5/SEC) TEMPERATURE = -5 DEG C

* BRINE VOLUME < 5.0
o BRINE VOLUME > 5.0

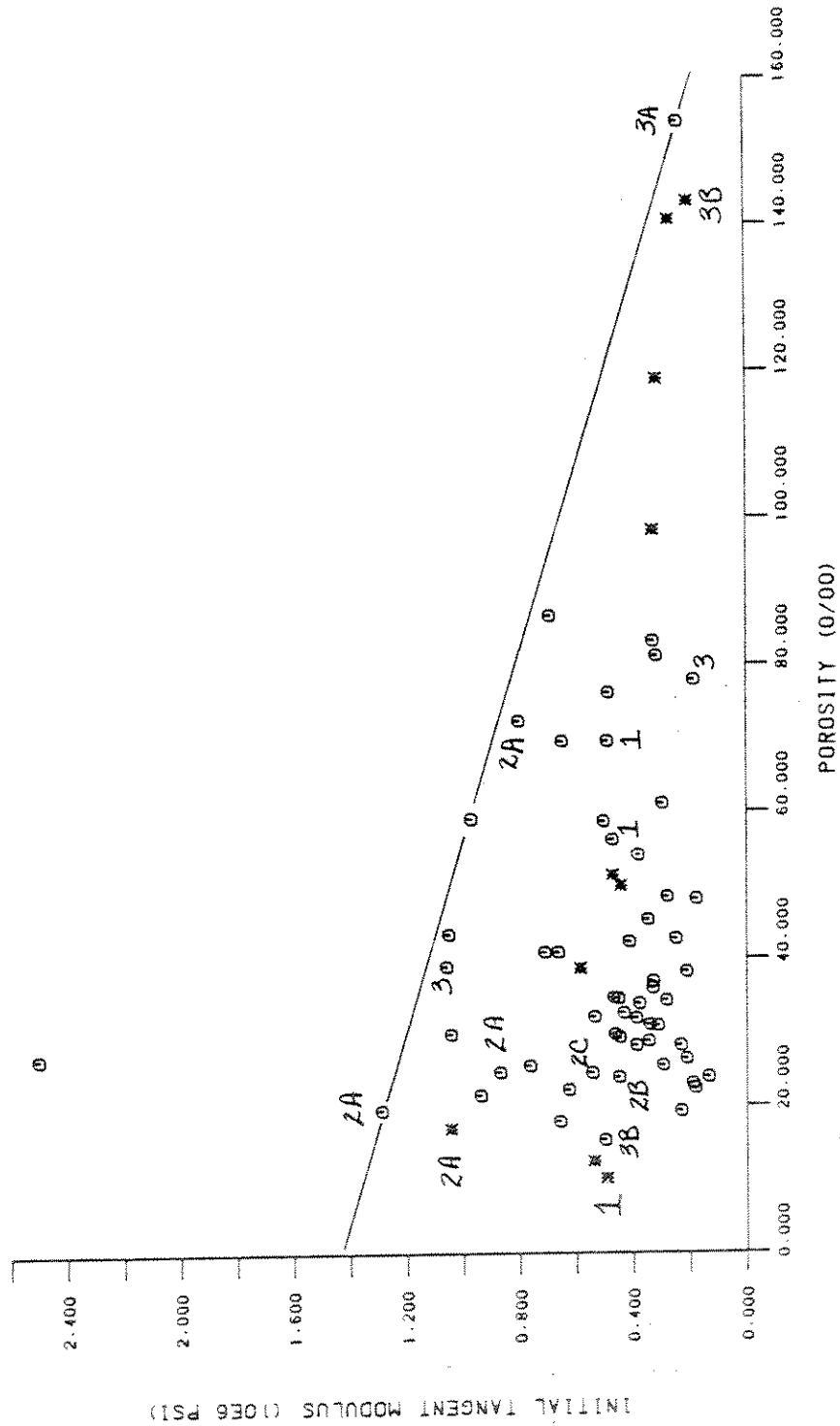
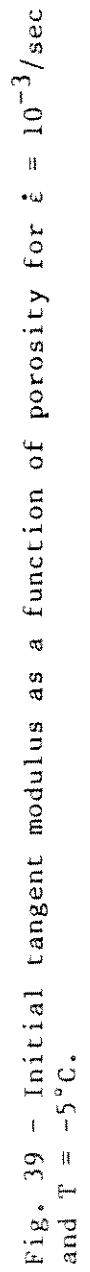


Fig. 37 - Initial tangent modulus as a function of porosity for $\dot{\epsilon} = 10^{-5}/\text{sec}$ and $T = -5^{\circ}\text{C}$.

Graph showing Initial Tangent Modulus (10⁶ PSI) versus Porosity (0/100) for 2019-T3 Aluminum. The data points (represented by asterisks and circles) show a linear relationship, fitted by a straight line.

Porosity (0/100)	Initial Tangent Modulus (10 ⁶ PSI)
0.000	3.200
20.000	2.400
40.000	1.600
60.000	0.800
80.000	0.000
100.000	0.800
120.000	1.600
140.000	2.400
160.000	3.200

Fig. 38 - Initial tangent modulus as a function of porosity for $\dot{\epsilon} = 10^{-5}/\text{sec}$ and $T = -20^\circ\text{C}$.



MPSI PHASE1: UNIAXIAL COMPRESSION
STRAIN RATE=(10E-3)/SEC TEMPERATURE=-20 DEG C

* BRINE VOLUME < 5.0
O BRINE VOLUME >= 5.0

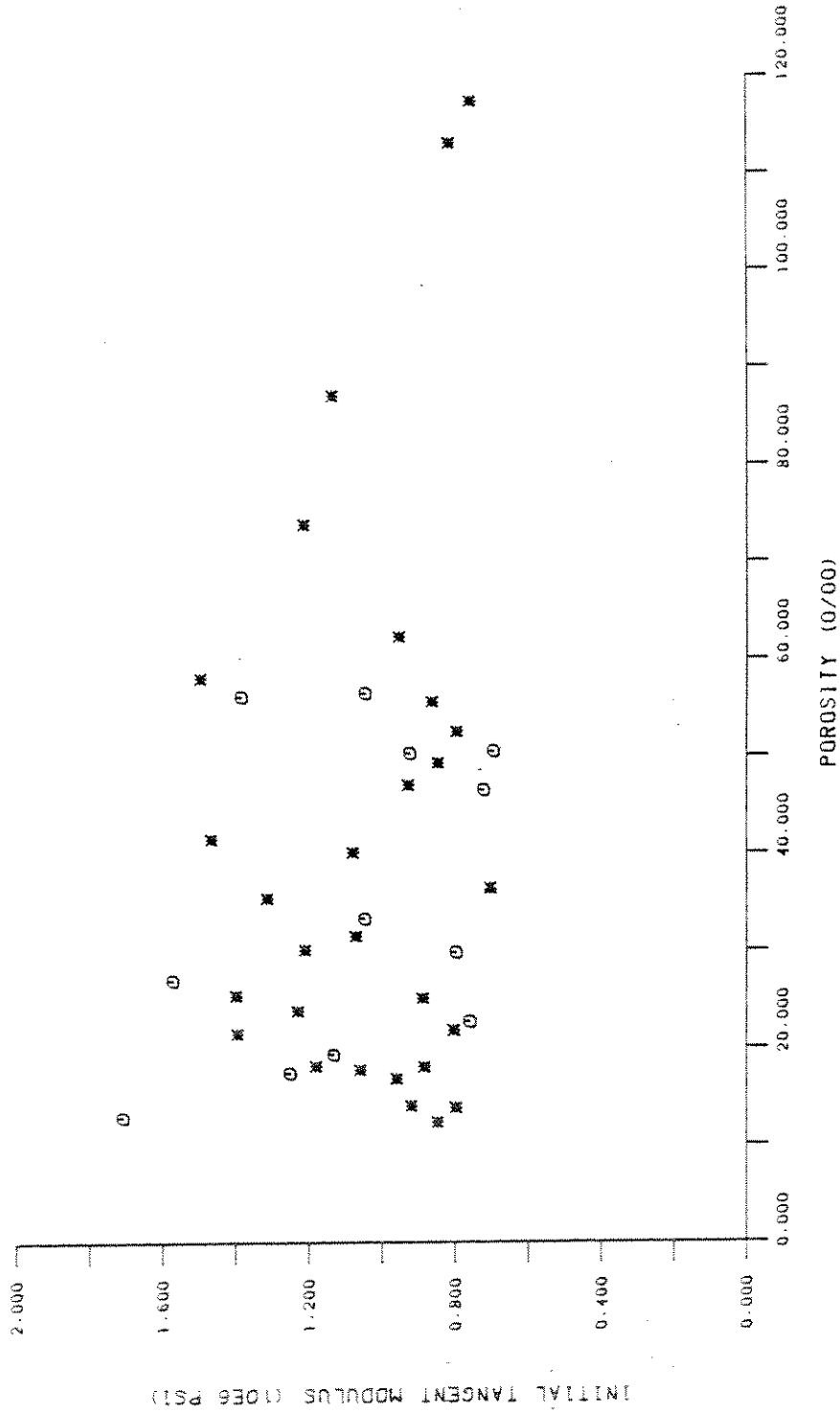


Fig. 40 - Initial tangent modulus as a function of porosity for $\dot{\epsilon} = 10^{-3}/\text{sec}$ and $T = -20^{\circ}\text{C}$.

and 39. In these figures, the columnar ice types (i.e., 2A, 2B, and 2C) appear to be more closely clustered than the granular or mixed ice types (i.e., 1, 3, 3A, and 3B). This is due to the generally low porosity of the columnar samples and the wide range of porosities found in the granular and mixed ice types. The columnar samples, however, do show much scatter in the maximum stress since crystal orientation plays an important role in these samples. The columnar ice types loaded in the hard fail direction (i.e., small angle between the load direction and axis of elongation) generally determine the upper bound on strengths, while the granular, mixed, and columnar loaded in the soft fail direction ice types fall into the intermediate and low strength ranges.

SUMMARY

Current methods of calculating ice loads depend on a knowledge of the mechanical properties of the ice feature being considered. Prior to the completion of MPSI-1 limited data were available describing the uniaxial compressive response of multi-year ridge ice. The results presented here summarize the mechanical properties of approximately 220 uniaxial compression tests conducted at two temperatures and two strain rates in MPSI-1. The effects of temperatures and strain rate on the mechanical properties are investigated by conducting pairwise t-tests on the mean values for the two levels of constant temperature and constant strain rate.

As expected, the t-tests show that the maximum stress and the total dissipated energy increase with increasing strain rate and decreasing temperature. The tangent modulus increases with increasing strain rate but is independent of temperature. The residual stress is independent of strain rate but increases with decreasing temperature. The strain at maximum stress increases with decreasing strain rate, but the t-tests on temperature effects are inconclusive.

An energy based failure criterion was investigated by calculating the energy dissipated to peak strength. The results from the t-tests conducted on this energy quantity show that at all test conditions except for one (i.e., C320), the mean value of the energy dissipated at peak strength is the same. This observation offers some promise for an energy based failure criterion, but further investigations need to be made to understand why the energy dissipated at C320 is different. Even if these investigations prove

fruitless, an energy based failure criterion could possibly be hypothesized on a restricted temperature strain-rate regime where the mean values of the energy dissipated to peak strength are the same.

Improved techniques for calculating ice loads will depend on more than a knowledge of a single mechanical property such as the compressive strength. Numerical modeling techniques, such as the finite element method for example, can take advantage of the entire stress-strain curve to describe the material behavior. Given the large variations observed in the mechanical properties, a means of classifying the stress-strain curves was sought to allow a comparison of different curves at a particular test condition and to investigate the effects of temperature and strain rate on the stress-strain response.

The total energy dissipated (I_T) by an ice sample seems to be a logical choice as a parameter for discussing the stress-strain response since all important mechanical properties contribute to its calculation. Material response is typically described in qualitative terms as being either brittle or ductile. However, this familiar terminology is of no use in connection with I_T unless its spatial distribution in the stress-strain plane is somehow brought into play.

A measure of the spatial distribution of I_T can be derived by decomposing I_T into a rate independent and a rate dependent part. The rate independent component of the total energy dissipated is defined as the flow energy (I_F) and the rate dependent component is defined as the crushing energy (I_C). The ratio, I_C/I_F , can now be used to provide a quantitative measure of ductility or brittleness. An ice sample with a low I_C/I_F value has a flat stress-strain curve and hence represents a ductile response. On the other hand, a high I_C/I_F value indicates a sharp stress-strain curve. Rate independent correlations between stress and energy components can be obtained by pairing the flow energy with the residual stress (σ_R) and the crushing energy with the maximum stress (σ_M). From these correlations, we find the quantity

$$\left(\frac{\sigma_M - \sigma_R}{\sigma_R} \right)$$

is proportional to I_C/I_F and hence provides another measure of brittleness or ductility.

Pairwise t-tests were conducted for the ratio I_C/I_F for the two levels of constant temperature and strain rate. Results show that the mean value of I_C/I_F does not change with temperature but increases with increasing strain rate. Thus, changes in temperature cause a proportional change in the shape of the stress-strain curve. This is due to approximately proportional increases in maximum stress and residual stress with decreasing temperature. Changes in strain rate cause a distortion in the shape of the stress-strain curve as one would expect.

A comparison of the I_C/I_F value within a particular test condition shows large variation of the mechanical response. If the entire stress-strain response is to be incorporated into an improved design methodology, then a method needs to be chosen to somehow suitably average the wide range of responses observed at a particular test condition. Two methods were investigated. The first method is simply a point by point averaging of each curve. The second method is to minimize the least square "error" from the mean of all important mechanical properties. Of the two methods investigated, the second is the easier method to apply and provides a means of choosing a real stress-strain curve which is more faithful to the observed average mechanical properties.

The effects of the physical properties on the mechanical properties were briefly investigated. Similar to other ice types, the maximum stress and tangent modulus of multi-year ridge ice decrease with increasing porosity. The possibility that the samples with low brine volumes form an upper bound on the strength vs porosity and tangent modulus vs porosity plots was also investigated but no such upper bound was found. The limited amount of crystallographic information showed that columnar samples had smaller variations in porosity than other ice types, but still had large variations in strengths due to variations in the orientations of the axis of elongation of the crystal with respect to loading direction. The larger variations in mechanical properties of the mixed and granular ice types are due primarily to large variations in porosity.

RECOMMENDATIONS FOR FUTURE WORK

Although the effects of temperature and strain rate on the uniaxial response of multi-year ridge ice have been investigated, our understanding of the material's behavior is by no means complete. In ice-structure interaction

problems, the ice will be subjected to three dimensional states of stress. Consequently, a knowledge of the effects of confining pressure on the mechanical response of multi-year ridge ice is needed. Phase II of the program (MPSI-2) includes approximately 60 conventional triaxial tests which will provide information on the pressure dependence of the mechanical response.

It is expected that a simple linear interpolation of the mechanical properties between the two MPSI-1 test temperatures (i.e., -5°C and -20°C) will be adequate to define the temperature dependence of the properties over that temperature range. However, there are situations such as summer floe impacts and the local contact between a ridge keel and conical structure where the temperature of the ice would be warmer than -5°C . At warm temperatures, the mechanical behavior of ice becomes highly nonlinear, and extrapolation of the MPSI-1 temperature data would probably over-predict ice strengths near the melting point. Clearly, warm temperature strength data are needed. A test program independent of the MPSI program has been initiated to obtain these data.

With the completion of the program to obtain warm temperature strength data, we will have a comprehensive view of the small scale mechanical response of multi-year ridge ice. Emphasis should then be shifted from the laboratory to the field. In particular, investigations need to be made on the internal structure of multi-year ridges. The small scale data show large variations in the mechanical properties which are attributed to the wide variety of ice types found in multi-year ridges. Very little is known about the spatial distribution of these ice types within a ridge. Structural trends observed in a ridge could play an important role in the calculation of ice loads. It was observed, for example, that the keel region of the continuous core sampled in MPSI-1 contained predominantly vertically oriented columnar ice. If this is in general true for all keels, then the design methodology and geometry could be modified to take advantage of this feature.

REFERENCES

1. Cox, G. F. N., Richter-Menge, J. A., Weeks, W. F., Mellor, M., and Bosworth, H. W. (1983), The Mechanical Properties of Multi-Year Sea Ice, Phase I: Test Results, Report 84-9, Cold Regions Res. and Eng. Lab., U.S. Army, Hanover, New Hampshire.
2. Cox, G. F. N., Richter, J. A., Weeks, W. F., and Mellor, M. (1984), A Summary of the Strength and Modulus of Ice Samples from Multi-Year Pressure Ridges, presented at the Third Int. Offshore Mech. and Arctic Symposium, Am. Soc. Mech. Eng., New Orleans, February.
3. Richter, J. A. and Cox, G. F. N. (1984), A Preliminary Examination of the Effect of Structure on the Compressive Strength of Ice Samples from Multi-Year Pressure Ridges, presented at the Third Int. Offshore Mech. and Arctic Symposium, Am. Soc. Mech. Eng., New Orleans, February.
4. Weeks, W. F. (1984), The Variation of Ice Strength Within and Between Multi-Year Pressure Ridges in the Beaufort Sea, presented at the Third Int. Offshore Mech. and Arctic Symposium, Am. Soc. Mech. Eng., New Orleans, February.
5. Mellor, M., Cox, G. F. N., and Bosworth, H. W. (1984), The Mechanical Properties of Multi-Year Sea Ice, Phase I: Techniques for Measuring the Mechanical Properties of Ice, Report 84-8, Cold Regions Res. and Eng. Lab., U.S. Army, Hanover, New Hampshire.
6. Cox, G. F. N. and Weeks, W. F. (1982), Equations for Determining the Gas and Brine Volumes in Sea Ice Samples, Report 82-30, Cold Regions Res. and Eng. Lab., U.S. Army, Hanover, New Hampshire.
7. Dorris, J. F. (1985), Classification of Failure Modes for Unconfined Compression Tests of Multi-Year Ridge Ice, Technical Information Record BRC-1285, Shell Development Bellaire Research Center, Houston.
8. Mellor, M. (1983), Mechanical Behavior of Sea Ice, Mon. 83-1, Cold Regions Res. and Eng. Lab., U.S. Army, Hanover, New Hampshire.
9. Weeks, W. F. (1982), The Growth, Structure, and Properties of Sea Ice, Mon. 82-1, Cold Regions Res. and Eng. Lab., U.S. Army, Hanover, New Hampshire.
10. Cherepanov, N. V. (1974), Classification of Ice of Natural Water Bodies, Proc. Int. Conf. Eng. Ocean Environ., Ocean 74, Inst. Electr. Electron. Eng., Halifax, Nova Scotia.
11. Michel, B. (1978), Ice Mechanics, Les Presses de l'Université Laval, Quebec, Canada.
12. IMSL Reference Manual, Edition 7 (1979), International Mathematical and Statistical Libraries, Inc., Houston.

TECHNICAL PROGRESS REPORT - BRC 45-85

DISTRIBUTION

Shell Development Company

- 6 - Information Services, WRC, Houston (w/2 sets of Appen.)
- 1 - Patents and Licensing Division, Houston (w/1 set of Appen.)

Shell Oil Company

- 1 - Vice President, Exploration, Head Office, Houston (w/1 set of Appen.)
- 1 - General Manager, Drilling & Producing Operations, Head Office, Houston
(w/1 set of Appen.)
- 6 - General Manager, Engineering, Head Office, Houston (w/1 set of Appen.)

Appendices A, B and C of this TPR are bound separately and are of limited interest. The number of sets of Appendices being distributed with TPR are indicated for each location.

